FN-568

Conceptual Design Report: Kaons At The Main Injector

Physics Goals, Technical Components, and Civil Construction

Fermi National Accelerator Laboratory
Batavia, Illinois

Operated by Universities Research Association Inc.
Under Contract with the United States Department of Energy

KAMI CONCEPTUAL DESIGN REPORT

June 7, 1991

K. Arisaka[4], *G. Bock*[1], *S. Childress*[1], *S. Cihangir*[1], *R. Coleman*[1], *M. Crisler*[1], *R. Currier*[1], *T. Diehl*[1], *R. Fast*[1], *R. Ford*[1], *G. Gollin*[2], *Y.B. Hsiung*[1], *D. Jensen*[1], *G. Koizumi*[1], *A. Malensek*[1], *W. Molzon*[3], *S. Pordes*[1], *R. Rameika*[1], *W. Slater*[4], *S. Somalwar*[5], *E. Swallow*[5,6], *G. Thomson*[7], *R. Tschirhart*[1], *J. Volk*[1], *Y. Wah*[5], *B. Wands*[1], *B. Winstein*[1,5], *H. Yamamoto*[5], *T. Yamanaka*[1]

We would like to thank the following people for many useful suggestions, contributions and discussions:

A. Barker[5], *J. Flynn*[1], *I. Gaines*[1], *G. Gutierrez*[1], *S. Holmes*[1], *V. Jacobsen*[1], *L. Kula*[1], *J. Lach*[1], *A. Lee*[1], *F. Markley*[1], *H. Montgomery*[1], *C. Moore*[1], *S. Schnetzer*[7], *E. Villegas*[1], *A. Visser*[1], *Y. Zou*[7]

Special thanks to Kristen Ford for her considerable effort in the preparation of this report and cover design.

1 Fermilab
2 Univ. of Illinois
3 Univ. of California at Irvine
4 Univ. of California at Los Angeles
5 Univ. of Chicago
6 Elmhurst College
7 Rutgers University

TABLE OF CONTENTS

INTRODUCTION 1

1. PHYSICS MOTIVATION 3

2. SITING AND STAGING 19

3. FACILITY LAYOUT 27

4. TECHNICAL DESIGN OF THE FACILITY 33
   4.1 Primary Beam 33
      4.1.1 Rates 33
      4.1.2 Debunched Beam in the Main Injector 36
      4.1.3 Primary Beam Transport 37
      4.1.4 Target Focus 42
      4.1.5 Beam Stability 45
      4.1.6 Beam Halo 49
      4.1.7 Instrumentation 51

   4.2 Secondary Beam 52
      4.2.1 Layout 53
      4.2.2 Secondary Particle Yields 55
      4.2.3 The Kaon Target 63
      4.2.4 Magnet Design 66
      4.2.5 The K_L Neutral Channel 72
      4.2.6 The Kaon Beam Dump 77
      4.2.7 Vacuum System 81
      4.2.8 Muon Flux Calculation 85
      4.2.9 K_S Beam 90

   4.3 Analysis Magnets 91
      4.3.1 Introduction 91
      4.3.2 Magnetostatic Analysis 92

TABLE OF CONTENTS

4.3.3 Preliminary Cost Estimate - Magnets with Conventional Coils 95
4.3.4 Using CCM for KAMI 96

5. THE DETECTOR 101
5.1 Tracking Chambers 101
5.1.1 General Specifications 101
5.1.2 System Design 103

5.2 Electromagnetic Calorimeter 106
5.2.1 ε'/ε 107
5.2.2 Rare Decay Searches 110
5.2.3 Candidate Materials 111
5.2.4 Calibration 113

5.3 Particle Identification 114
5.3.1 Electron Identification by Transition Radiation 114
5.3.2 Muon Identification 117

5.4 Gamma Veto 119
5.4.1 Design Considerations 119
5.4.1.1 Photonuclear Inefficiencies 119
5.4.1.2 Proton Detection 120
5.4.1.3 Pion Detection 120
5.4.1.4 Neutron Detection 121
5.4.2 Chosen Configuration 123

5.5 Triggers 125
5.5.1 ε'/ε Experiment 125
5.5.2 High Rate Experiments 127

TABLE OF CONTENTS

5.6 The DAQ System and Off-line Computing 130
5.6.1 Introduction 130
5.6.2 Detector Channels 131
5.6.3 Event Sizes 131
5.6.4 The Readout System 132
5.6.5 "Tape" 133
5.6.6 Off-line Computing 134

5.7 Radiation Damage 135
5.7.1 E731 Simulation 136
5.7.2 KAMI Simulation 138
5.7.3 Ongoing CsI Tests 140

6. COSTS 141
6.1 Civil Construction Costs 141
6.2 Primary Beam (Technical) Costs 143
6.3 Secondary Beam Costs 144
6.4 Analysis Magnet Costs 148
6.5 Detector Costs 149
6.6 Cost Estimate Summary 156

7. SCHEDULING 159

8. RESEARCH and DEVELOPMENT 163
8.1 Primary Beam 163
8.2 Target Area 164
8.3 Spectrometer Magnets 164
8.4 Detector R&D 165
8.4.1 Vacuum and Veto System 165
8.4.2 Tracking Chambers 166
8.4.3 TRD 166

TABLE OF CONTENTS

8.4.4 Electromagnetic Calorimetry 166
8.4.5 DAQ 166

9. SUMMARY 169

APPENDIX A 171
A.1 KAMI Charged Kaon Beam 171
A.2 Charged Kaon Physics and Sensitivity 175
A.2.1 Search for $K^+ \rightarrow \pi^+$ + "nothing" 175
A.2.2 Search for $K^+ \rightarrow \pi^+ \mu^+ e^-$ 176
A.2.3 Direct CP violation in
$K^+ \rightarrow \pi^+ \pi^+ \pi^-$ and $K^- \rightarrow \pi^- \pi^- \pi^+$ 176

INTRODUCTION

With the advent of the Main Injector, there is the possibility of doing a whole new generation of experiments in neutral kaon physics. Although the energy of the Main Injector is not as high as the Tevatron, the average number of protons deliverable per hour is about two orders of magnitude greater! This high flux of protons allows for the construction of neutral Kaon beams that are small and well defined while at the same time of high enough intensity to saturate the best detectors we know how to build at the present time. With these beams, it is possible to probe with ever greater precision and sensitivity the fundamental questions of CP violation and rare decays.

We present here the Conceptual Design Report for the Kaons at the Main Injector (KAMI) program. This is not an experiment proposal, so the physics goals, detector design and backgrounds are presented in general terms. However, the facility needs are outlined in more detail to provide a scale (in time and money) for this program.

The general physics background and goals are presented in Section 1. Four classes of experiments are outlined. Each class has somewhat different running configurations. It will be necessary to support those differing configurations in the overall program. The siting and staging are discussed in Section 2. The design of the Facility is laid out in Section 3.

The technical details of the primary beam, the secondary beam and the spectrometer magnets are presented in Section 4, the Technical Design part of the report. The detector, including electronics and data acquisition, is discussed in Section 5.

Cost and Scheduling are discussed in Sections 6 and 7. It is of course the goal of this program to be ready to start working on physics as soon as the Main Injector can deliver beam.

In Section 8, we outline general areas of research and development that have been or must be started to meet the goals outlined above. We would like to emphasize that excellent and timely physics results from this program depend on a continuing and vital development program directed toward the very high intensity running of high precision experiments anticipated with the Main Injector. Section 9 contains a brief summary.

1. PHYSICS MOTIVATION

For high precision and high sensitivity studies of the physics of kaon decays, the important characteristics of the new Main Injector are its high energy (relative to other "factories") and its high intensity. Experiments of this kind are becoming increasingly important in the study of CP violation and for searches for new interactions. An extracted beam of 120 GeV will produce a source of high energy kaons that will not be surpassed in intensity by any facility now under consideration world-wide[1].

The attention at Fermilab[2] in kaon physics has recently been concentrated on precision studies of the $K_L \rightarrow 2\pi^0$ decay (ε'/ε), on a search for the mode $K_S \rightarrow \pi^+\pi^+\pi^0$ (η_{+-0}), and on a search for $K_L \rightarrow \pi^0 e^+ e^-$ which, in the Standard Model model, has a large direct CP violating component. At present, the Fermilab experiments at the Tevatron have superb sensitivity for these modes even in comparison to the dedicated rare kaon decay program at BNL where the proton intensity is significantly higher. The

---

1 The possibility of using the Main Injector for Kaon Physics was discussed by B. Winstein, G. Bock, and R. Coleman, EFI-89, which was published in New Directions in Neutrino Physics at Fermilab, Sept. 14-16, 1988. A workshop was held at Fermilab in May, 1989, on Kaon and Neutrino physics at the Main Injector, proceedings edited by S. Holmes and B. Winstein. Further discussion can be found in the proceedings of the Breckenridge conference, Physics at Fermilab in the 1990's, edited by D. Green and H. Lubatti, 1989. A letter of intent to pursue high precision, high sensitivity kaon decay physics at the Main Injector was submitted by a collaboration from Chicago, Elmhurst, Fermilab, Irvine, Illinois, Rutgers, and Saclay, P804. Recent work has been written up for the Snowmass workshop on Physics in the 1990's, edited by E. Berger.

2 These experiments include E731 a collaboration between Chicago, Elmhurst, Fermilab, Illinois and Saclay; E773, a collaboration between Chicago, Elmhurst, Fermilab, Illinois, and Rutgers; E799 and P832, a collaboration between Chicago, Elmhurst, Fermilab, Illinois, Rutgers and UCLA; and E621, a collaboration between Michigan, Rutgers and Minnesota.

advantage for these and other modes arises primarily from the higher energy of the decay products. However, to make substantial progress, much more flux than is available at the Tevatron is required.

Let's consider the likely evolution of this field in the years prior to the Main Injector. If we look broadly at the field of rare and CP violating kaon decay physics, we note that the best searches for the lepton number violating decays $K_L \rightarrow \mu e$ and $K^+ \rightarrow \pi^+\mu^+e^-$ come from BNL experiments[3] and the sensitivities for these are nearing the 10^{-11} level. These results might be improved[4] by another order of magnitude there. The interesting mode $K^+ \rightarrow \pi^+ +$ "nothing" seems to be best done with a stopped charged kaon beam and there BNL has the best experiment[5]. This effort could probably be upgraded[6] to better than 10^{-10} sensitivity; both these upgrades make use of the BNL Booster.

We now consider the CP violating modes. The $K_L \rightarrow \pi^0e^+e^-$ sensitivity is now in the 10^{-9} range as a result of a combination of BNL845[7] and FNAL731[8] and it will be pushed to nearly the 10^{-11} level in E799 at the Tevatron. There is also a dedicated experiment[9] at KEK pursuing the $K_L \rightarrow \pi^0e^+e^-$ mode. The sensitivity to ε'/ε is now at the level[10] of 6×10^{-4}, with all of the E731 data, and it is similar for NA31 at CERN; it is proposed to improve the sensitivity to about 1.5×10^{-4} in a future Tevatron experiment (P832).

For the proper execution of both E799 and P832 at the Tevatron, the detector and beam need substantial upgrades. The required upgrades will

---

3 BNL E791 collaboration; BNL E777 collaboration.

4 Upgrade proposals presented to BNL.

5 BNL E787.

6 Upgrade proposal to BNL.

7 K.E. Ohl, *et al.*, *Phys. Rev. Lett.* **64**, 2755 (1990).

8 *New Limit on $K_L \rightarrow \pi^0e^+e^-$*, A. Barker, *et al.*, *Phys. Rev.* **D41**, 3546 (1990).

9 KEK E162.

10 J.R. Patterson, *et al.*, *Phys. Rev. Lett.* **64**, 1491 (1990).

be important for the subsequent utilization of the much higher intensity kaon beam using the Main Injector.

When the Main Injector first delivers a high intensity kaon beam in five to six years, what issues should be confronted? The answer will, of course, depend very much of the results in the intervening years. In all likelihood, a new generation of ε'/ε experiment will be needed. Of course, if the results of the previous generation experiment still leave in doubt the issue of a non-zero signal, the case for motivating a new effort is quite clear.

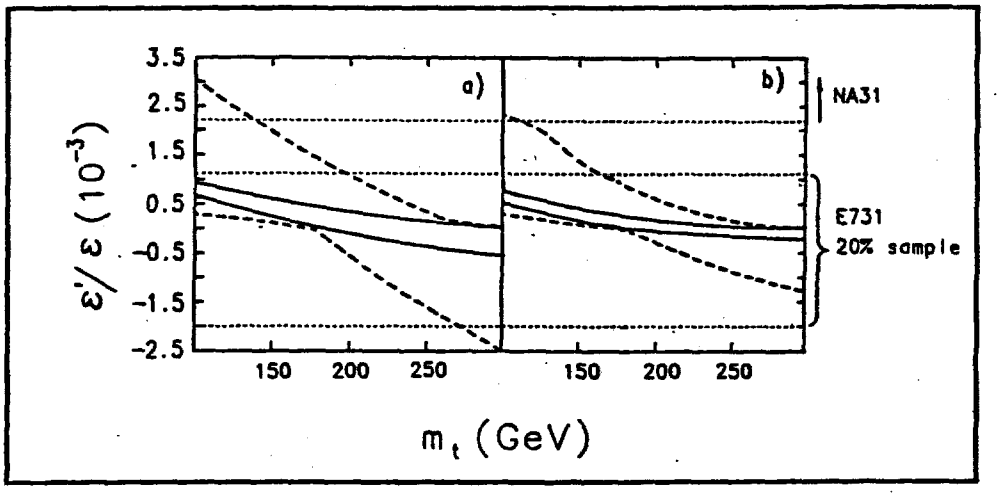

Fig. 1.1: ε'/ε vs. M_t from Buchalla, Buras, and Harlander. The solid curves represent the "standard" range of ε'/ε values while the dashed curves represent the allowed range when all parameters ($\bar{R}$, s_{23}, Λ_{QCD}, B_K, and M_s) take their extreme values. It should be noted that the allowed range could be even greater than that shown because of other assumptions inherent in the methods of Ref. 11. Also shown are the measurements by E731, and NA31. a) (b)) is for δ, the phase of V_{ub}, in the first (second) quadrant.

Even a first signal in the B system is unlikely by this time so we would still have only the one (laboratory) manifestation of this important phenomenon. However, even if there is an established non-zero result, it will be important to pin down the result with higher precision. In the Standard Model, as the value of the top quark mass increases, the expected value[11] of ε'/ε decreases as is shown in Fig. 1.1.

---

[11] G. Buchalla, A.J. Buras, M. Harlander, MPI-PAE-Pth-30/90, July 1990.

When the value of the top mass is known, the range of possible values for ε'/ε will decrease motivating a more definitive test. Such an experiment

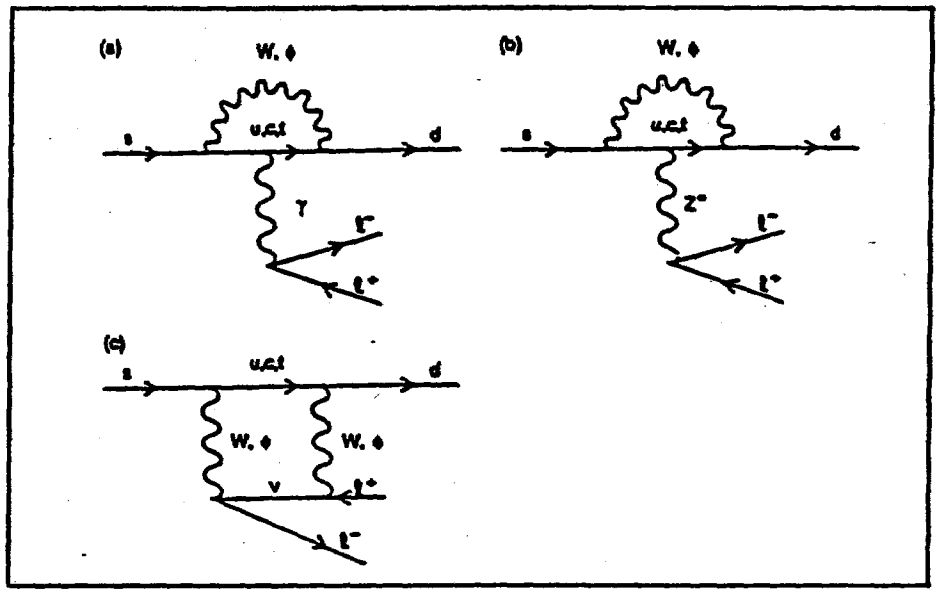

Fig. 1.2: Three diagrams giving a short distance contribution to the process $K_L \to \pi l^+ l^-$: (a) the "electromagnetic penguin", (b) the "Z penguin", (c) the "W box". (From C.O.Dib, I. Dunietz, and F. Gilman)

in the 2π system will likely require over 10^8 $K_L \to 2\pi^0$ decays with very little background; this would permit a measurement of ε'/ε with a precision of a few 10^{-5}, at a level where it would be extremely hard for the Standard Model to accommodate a null result.

Closely coupled with the issue of a non-zero ε'/ε is the branching ratio for the $K_L \to \pi^0 e^+ e^-$ mode which is expected to be of the order of 10^{-11}. A substantial fraction of this decay should be direct CP violation, arising from contributions with virtual top quarks as shown in the diagrams in Fig. 1.2. The direct branching ratio has been calculated[12] to be

$$BR\left(K_2 \to \pi^0 e^+ e^-\right) = 1.0 \times 10^{-5} \left(s_2 s_3 s_\delta\right)^2 G(M_t),$$

where G is a function of the top quark mass of order unity and the original CKM matrix element notation is used. It is easy to show that one can use

---

[12] C.O. Dib, I. Dunietz, F.J. Gilman, *Phys. Rev.* **D39**, 2639 (1989).

the constraint on the CKM mixing angles provided by the observed size of the mixing in the neutral B system to express this branching ratio in terms of β, one of the angles of the so-called unitarity triangle, B_B, the bag factor for the B_u meson system, and f_B, the B meson decay constant as well as another function of M_t of order unity:

$$BR\left(K_2 \to \pi^0 e^+ e^-\right) = \frac{5 \times 10^{-13} \sin^2 \beta}{\left(B_B f_B{}^2 F(M_t)\right)}.$$

Given what we know about the unknowns in the above expression, the value for the direct branching ratio could range from about 10^{-12} to 10^{-11} with a central value of about 3×10^{-12}.

With an extracted beam from the Main Injector, the flux necessary to permit sensitivities to this and other modes in the range of 10^{-10} per hour of running are obtainable. Further, we point out that this will be the best place to perform such experiments of any presently existing or planned facility. The acceptance of the detector to be described for the $\pi^0 e^+ e^-$ mode is about 20% with the requirement that both photons exceed 1 GeV. The decay rate for kaons greater than 10 GeV is about 33×10^6 per spill. However simply accumulating events unfortunately is not enough since there are, in addition to the direct CP violating term, three other contributions which need to be untangled. These are an indirect term, coming from the $K_1 \to \pi^0 e^+ e^-$ transition; a CP conserving term, coming from the $K_2 \to \pi^0 \gamma\gamma$ intermediate state; and a background coming from the $K_L \to e^+ e^- \gamma\gamma$ radiative decay. These have been discussed extensively in the literature.

There is a prediction[13] for the size of the indirect term. Using Chiral Perturbation Theory (and the assumption of octet dominance), the prediction for the branching ratio can be reduced to a two-fold ambiguity: the value should be either 1.5×10^{-12} or 2.4×10^{-11}. This should be directly determined. For the time being, the ambiguity can be broken by a study of

---

[13] G. Ecker, A. Pich and E. de Raphael, *Nuc. Phys.* B291, 692 (1987).

the similar $K^+ \to \pi^+ee$ rate. An experiment[14] at Brookhaven has about 700 of these events with relatively high ee invariant mass. Their spectrum favors[15] a rather stiff distribution for the e^+e^- which suggests the lower value for the corresponding K_1 transition. However, because of the assumptions involved, it will be necessary to determine the K_S rate directly. This could be done at the Tevatron, where the Lorentz factor is favorable, if the rate is high enough. Otherwise, one will need the very high rates at the Main Injector where the K_S amplitude would be determined in an interference experiment as discussed below.

For the CP conserving transition, there are competing theories[16] which give values between 10^{-14} and 10^{-11} for the two photon (CP conserving) K_2 transition to π^0ee. There are now two observations[17] of the decay $K_L \to \pi^0\gamma\gamma$ with high values for the $\gamma\gamma$ invariant mass strongly favored in both. This again favors the Chiral Perturbation Theory prediction of the lower branching ratio, although, since the observed rate is in excess of that predicted in lowest order, the conclusion is not yet definite. Further experimental data on $K_L \to \pi^0\gamma\gamma$ will be provided by Fermilab E799.

An important related decay[18] is $K_L \to \pi^0\nu\bar{\nu}$. In the Standard Model this decay is essentially pure <u>direct</u> CP violating: in principle, the clean observation of just a single unambiguous event would establish the long-sought for effect! Also, the expected branching ratio[19] is about six times greater than for the $\pi^0e^+e^-$ case: a factor of 2 comes because one has both vector and axial vector couplings and a factor of 3 is for three types of neutrinos. Thus the central value is expected to be about 2×10^{-11}. While the background and instrumental problems are challenging, it is worth pointing out that the flux to do the measurement is clearly there at the

---

14 BNL E777.

15 M. Zeller and P. Cooper, private communications.

16 See reference 13 and references therein.

17 G. Barr, *et al.*, *Phys. Lett.* **242B**, 523 (1990); A. Barker, *et al.*, EFI 91-01.

18 L. Littenberg, *Phys. Rev.* **D39**, 3322 (1989).

19 C.O. Dib, I. Dunietz, F.J. Gilman, *Phys. Lett.* **218B**, 487 (1989).

Main Injector and the relatively higher photon energies are much easier to detect, and to veto.

Another way to see direct CP violation in $\pi^0 e^+ e^-$ decays is to observe the interference between K_S and K_L near the target. The CP conserving term does not contribute to the interference, and because the K_S branching ratio is about a factor of 300 larger than that of the K_L, the $e^+e^-\gamma\gamma$ background (discussed later) is less of a problem. Thus the result would be much easier to interpret. One way to quote the sensitivity of such an interference experiment is to say that if the branching ratio for the direct CP violating term in the K_L decay were 10^{-12}, we would measure it to 30% precision. The same detector would be used for the interference measurement but with a modified beam as will be discussed later in this report.

The ability to study decays close to the production target will also allow measurements of the CP violating parameters η_{+-0} and η_{000}. These, especially the latter, are poorly determined and although the LEAR facility at CERN[20] will make improvements, it is unlikely that they will see a positive signal let alone be able to be sensitive to departures from the Standard Model predictions. At the Main Injector, one should be able to determine these parameters with much more precision than is presently known, based upon scaling from the experience of E621 and E731. In a similar vein, very precise tests of CPT conservation can be made.

We finally mention the search for lepton flavor violation. Although there are no compelling arguments for the level where such violations should become observable, many classes of theories[21] for extensions of the Standard Model include such new interactions. The higher the sensitivity, the greater the mass reach; while there is dependence upon coupling constants, an experiment with a sensitivity of 10^{-13} will probe mass scales up to about 150 TeV! We should mention that while it is important to also

---

[20] CPLEAR experiment.

[21] R.N. Cahn and H. Harrari, *Nucl. Phys.* **B176**, 135 (1980).

look for the corresponding decays in the B meson system, the sensitivity to a broad class of new phenomena there is significantly less.

We are thus considering essentially four classes of experiments for the kaon facility at the Main Injector. Each would run separately and would utilize and emphasize different elements of the detector; in addition, the configuration of the beam would be optimized for each effort.

The four different classes we denote by "High Precision" (ε'/ε); "High Sensitivity" ($K_L \rightarrow \mu e$, $\pi^0\mu e$, $\pi^0 ee$, $\pi^0\mu\mu$, etc; "K-short" (K_S decays, including η_{+-0} and η_{000}); and "Hermetic" ($K_L \rightarrow \pi^0\nu\bar{\nu}$).

The successful execution of each of the classes makes demands on the facility and on the detector and these will be treated subsequently. All of them have certain common requirements which can be listed here. The beam on the target should be "de-bunched" with only a minimal residual structure permitted This is because of the very high rates of kaon decays: at a decay rate of 100 MHz, at the usual 53 MHz of RF structure this would imply near certainty of an overlap of more than one event and, for the high sensitivity experiments where pile-up in the detector is especially troublesome, this is unacceptable. The thermal properties of the target are important at the very high intensities and particular care must be taken in the choice of target composition, dimensions, mounting and cooling. The incident proton beam should be as free of muon halo as possible and the configuration of the beam definition and beam dump are most important to avoid unacceptable halo (both muon and hadron) around the neutral beam. The kaon decay region contains an anti-coincidence system throughout and must have excellent vacuum. Large aperture high field analysis magnets of suitable uniformity are required for enough precision of the momentum of the kaon decay products and for adequate acceptance. These items together with the elements of the detector will be treated in subsequent sections of this report.

Before we treat each of the classes of experiment, we will list some of the advantages of a higher energy machine for such experiments. These

have primarily to do with those factors in the experiments which do not scale with energy.

1. With careful attention to reducing the constant term, the resolution of electromagnetic calorimeters will be dominated by the $1/\sqrt{E}$ term so that the higher the energy the better the resolution and resolution is at a premium in such experiments.

2. Background of minimum ionizing particles does not scale with energy: a muon will simulate about 600 MeV energy deposit in an electromagnetic calorimeter so that it is difficult to maintain the same relative threshold level as one decreases the energy. This point is illustrated by the fact that the minimum detectable photon cluster energy was about 1 GeV for both BNL and FNAL Tevatron experiments on ε'/ε and $\pi^0 e^+ e^-$ although the mean kaon energy was more than 10 times greater at FNAL. As a result, the acceptance for the FNAL experiments was significantly greater.

3. Since the growth of hadronic showers is governed by ln(E) rather than E, one needs a fractionally shorter beam dump region at a higher energy facility. As an important consequence, one can be situated relatively closer to the target and thus be more sensitive to K_S decays.

4. The ability to reject events with soft photons outside of the aperture of one's electromagnetic detector is important in reducing background. Again, the dominant problem with a low threshold will be the (non-scaling) minimum ionizing background. This is important for ε'/ε, for $\pi^0 e^+ e^-$ and *especially* for $\pi^0 \nu \bar{\nu}$ where the primary background comes from the $\pi^0 \pi^0$ mode.

We now consider the physics reach of each of the classes of experiments in a one year running period. At this stage, many (but

obviously not all) backgrounds[22] have been dealt with and the attainment of the listed sensitivities looks promising.

The "year" that we consider assumes the following. The machine runs with a 1 sec slow spill and a repetition rate of 2.9 sec. The running efficiency is taken to be 35% which translates into 4×10^6 pulses in a year period. Note that this is very close to the definition of a "Snowmass year", namely 10^7 seconds of operation. Of course one can run for this "year" every year. The beam energy is assumed to be 120 GeV.

The kaon production spectrum[23] at a targeting angle of 20 mr is shown in Fig. 1.3. This angle is sufficient to reduce the intense neutron flux by a factor of about 50. The spectrum shown assumes that there is additionally a (lead) gamma filter and a Beryllium moderator; the resulting factor of four loss in kaon flux could perhaps be recovered for some experiments. We list in Table 1.1 the rates and sensitivities for each of the measurements and then follow with a discussion of the major features of each. The detector for which the rates and acceptance figures are given will be discussed in detail in Section 5.

---

22 See T. Yamanaka, KAMI-60, internal note, and the proceedings of the Breckenridge conference and of Snowmass 1990, cited in Ref. 1, for a discussion of simulations of many of the backgrounds.

23 This spectrum uses the phenomenological fit to a variety of data by A. Malensek; it works very well at the Tevatron and is expected to be a good estimate at the Main Injector.

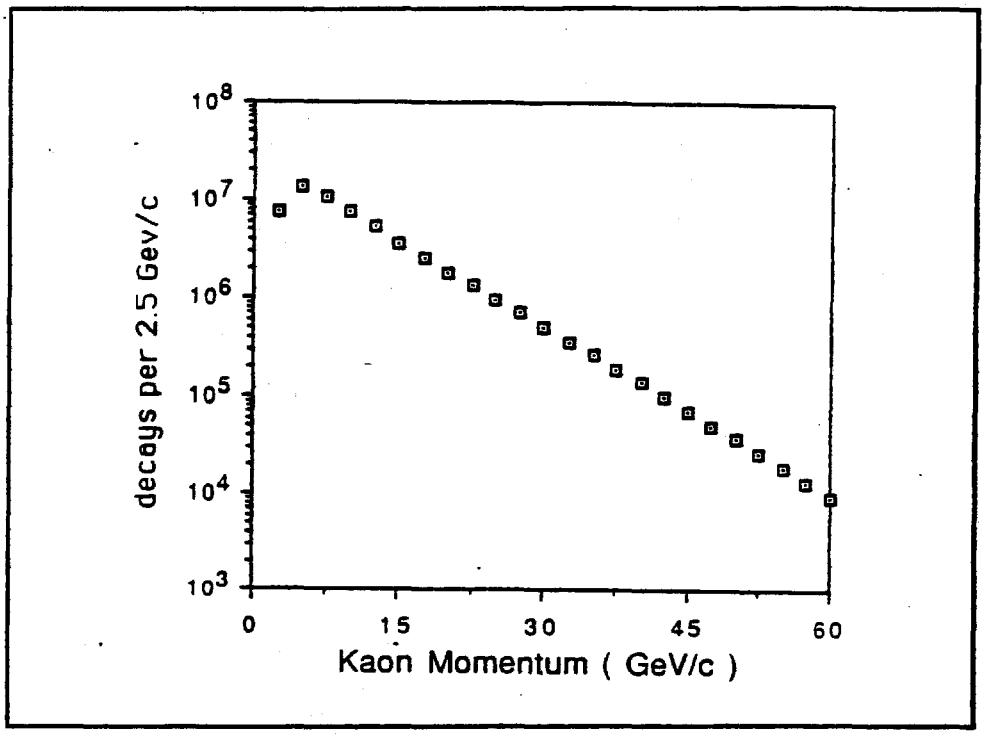

Fig. 1.3: The energy spectrum of kaons decaying in a 20 m long decay region for 3×10^{13} 120 GeV/c protons incident on a 50 cm Be target. The beam solid angle is 12 μstr.

ε'/ε (High precision)

For the accurate determination of ε'/ε, one must obtain very high statistics as well as reduced systematic uncertainty. At the Main Injector, the flux is great enough that one can still accumulate the required level of statistics while employing a small target and very small solid angle beams to reduce the level of systematic uncertainty. Very likely a variation of the double beam method of E731 will be employed. To aid in understanding the relative beam acceptances, the proton beam needs to be as stable as possible and we should be able to monitor its position on the target at the 10 μm level. The singles rate in the detectors is modest and is dominated by the interaction rate in the regenerator which is placed in one of the beams. For this to be so, it is necessary that the muon flux at the detector be $\leq 10^{-7}$ per incident proton.

The decay rate shown in Table 1.1 is only for K_L decays within the fiducial decay volume of about 18 m. The acceptance shown is for the four body $\pi^0\pi^0$ mode and it is large for the higher momentum range indicated; this range is also favorable since the gamma energy resolution improves with energy and, to accurately compare bin-by-bin the decay rates into $2\pi^0$ and $\pi^+\pi^-$, the best possible energy resolution is needed. In the analysis, only 2π decays in a 2 m region downstream of the regenerator for both beams are used; in this fashion systematic uncertainty from any acceptance difference between the two beams becomes small.

The final source of systematic error will be the uncertainty in the residual background. There are effects arising from scattering in the regenerator where a K_S decay can wind up in the vacuum beam (in the neutral mode). With the small beams used and with a fully active regenerator[24] in vacuum (*i.e.* one made entirely of scintillator), this effect is less than 1% and more importantly is identical for charged and neutral decays so that it largely cancels and in any case, it can be very well determined. The background from $3\pi^0$ decays which fake $2\pi^0$ decays is at the 0.4% level in E731; this background is not as easy to simulate and thus it should be lowered significantly. This will be accomplished with a fine grained, high precision electromagnetic calorimeter and in addition an extensive anti-counter system surrounding the decay region to catch missing gammas from this mode. Thus is appears that a determination with nearly 10^{-5} precision could be performed.

$K_L \rightarrow \pi^0 e^+ e^-$ (High rate)

To reach the level of direct CP violation in this mode, it is necessary to run the detector in a much higher rate environment. Many backgrounds are understood[25] for this mode, including a whole variety of accidental

---

24 Such a regenerator, made of plastic scintillator, has been built by S. Somalwar for E773 and tests already show a substantial suppression of inelastic regeneration.

25 See Fermilab E799 proposal and addenda, also T. Yamanaka, KAMI-60, internal note.

effects. The most severe background[26] appears to arise from the $K_L \rightarrow e^+e^-\gamma\gamma$ decay; its branching ratio has recently been determined to be at the level of 5×10^{-7} (depending upon cutoff). These decays tend to have one very low energy gamma and a very low mass ee pair. However, after reasonable cuts on these quantities, still a sizable background remains and one has only the π^0 mass as a final constraint. With the high precision calorimeter, this background is about 10^{-11} and one will probably have to live with it at this level. For the indicated configuration, one would have about 3800 background events leading to a three sigma sensitivity for a residual (presumably direct CP violating) branching ratio of about 5×10^{-13} where, according to the Standard Model, a signal should be seen. For this and the other high-rate running conditions, the singles rates are about 100 MHz in the largest chamber but the maximum rate on a single wire (3 mm pitch) is about 600 kHz.

$K_L \rightarrow \mu e$ (High rate)

The backgrounds to this mode arise from $K_L \rightarrow \pi e \nu$ where either the π is mis-identified as a muon, or as an electron with the e mis-identified as a muon. For these backgrounds, it is important to have an extra kinematic handle and this comes from a measurement of the muon range. Hence, the experiment is optimally run in the lower momentum range indicated in Table 1.1 although the same spectrometer as for the four body decays can be employed. Hence the rates are the same as those discussed above for $K_L \rightarrow \pi^0 e^+e^-$. Two analyzing magnets (or one with a high enough transverse momentum kick with a chamber in its center) permitting redundant momentum determinations are required for background suppression. At this time, the backgrounds for this mode are only really understood to be less than about 10^{-13} but it is clear that a highly sensitive experiment can be performed.

---

26 H. Greenlee, *Phys. Rev.* **D42**, 3724 (1990).

Mode	Class	Sensitivity		Beam flux	Target length [cm]	Solid Angle [μstr]	P range	Decay rate [MHz]	accep. [%]	singles rate [MHz]	sensitivity (per year)
		Today	in 5 yrs.								
ε'/ε	High precision	10^{-3}	10^{-4}	3×10^{13}	8	1	10-50	0.6	35	7.5	2.0×10^{-5}
$K_L\to\pi^0e^+e^-$	High rate	10^{-9}	10^{-11}	3×10^{13}	50	12	10-50	33	20	100	3.8×10^{-14}
$K_L\to\mu e$	High rate	10^{-11}	10^{-12}	3×10^{13}	50	12	1-15	33	34	100	2.2×10^{-14}
$K_L\to\pi^0\mu e$	High rate	-	10^{-10}	3×10^{13}	50	12	10-50	33	20	100	3.8×10^{-14}
$K_L\to\pi^0\nu\bar{\nu}$	Hermetic	10^{-3}	10^{-7}	3×10^{13}	20	4	2-50	10	20	10	3.0×10^{-12}
$K_S\to\pi^0e^+e^-$	K-short	10^{-5}	10^{-8}	1×10^{12}	50	36	10-50	15	30	75	1.0×10^{-12}

Table 1.1: Rates and sensitivities for several K_L decay modes.

$K_L \rightarrow \pi^0\mu e$ (High rate)

This mode could also be sought simultaneously with the $K_L \rightarrow \pi^0 e^+e^-$ and $K_L \rightarrow \mu e$ searches. The backgrounds are probably less than for the $K_L \rightarrow \mu e$ case because the corresponding background process, $K_L \rightarrow \pi^0\pi^\pm e\nu$, has a much smaller branching ratio. Both should be sought in that one does not know *a priori* whether the flavor violating interaction is vector or axial vector, or both.

$K_L \rightarrow \pi^0\nu\bar{\nu}$ (Hermetic)

For this search, only the instrumented decay volume and the electromagnetic calorimeter are needed. The signature is not terribly stringent: only two electromagnetic clusters in the event, consistent with coming from a single π^0. The dominant, and perhaps only, background comes from the $\pi^0\pi^0$ decay at a branching ratio of 10^{-3}. It is possible to effectively exclude this background by making a P_T cut above the end-point for the $\pi^0\pi^0$ decay. However, because of the finite beam size and the lack of precise information on the transverse vertex position, a Dalitz decay is required to make this cut cleanly. In the end, one would loose about a factor of 1000 in sensitivity which is probably too great a price to pay. Hence the emphasis is on effectively vetoing the extra gammas.

The decay volume needs a system of anti-counters within the vacuum and the vacuum itself needs to be 10^{-6} Torr in order to eliminate the background[27] from the hadron beam interacting in the residual gas. The problem is difficult because there are many mechanisms by which a photon can be missed and these largely nuclear effects are not well enough known to be certain of the residual inefficiency. This problem has been faced already by the E787 collaboration at Brookhaven, but in a lower and more difficult energy region and we have benefitted from their experience[28].

---

[27] W. Slater, KAMI internal notes.

[28] D. Marlow, BNL E787 TN #31 .

Nevertheless, a detailed simulation[29] shows that the single event background level with a veto system of the type discussed in Section 5.4 would be better than 10^{-11}. Of course, to be certain, dedicated tests will be in order.

For the exposure indicated in the Table, one would have about 80 of these background events and, with the plausible assumption that we would be able to determine this background level independently, after subtraction we would have a three standard deviation sensitivity at about 3×10^{-12}. The rates are modest and the beam is well defined to help exclude background. By using the large P_T Dalitz decays, however, the sensitivity would be about 10^{-10} and could probably be improved by running at higher rates. Considering that at present, the deduced branching ratio is little less than 10^{-3} and that at the Tevatron, one will improve this to perhaps the 10^{-7} level, this represents a major advance. We also should point out that with such a hermetic detector there is the potential for the discovery of other unexpected decay modes.

The subsequent sections of this report, then, discuss the facility and detector requirements for attaining the goals outlined above. The group responsible for the preparation of this report met almost weekly for the last eight months of 1990 and then at least every other week up to the present (6/91). A variety of topics have been written up along the way, and these documents (KAMI internal notes) are useful for a fuller understanding of the many issues addressed herein.

---

[29] S. Somalwar, KAMI internal notes.

2. SITING AND STAGING

To address siting of the Main Injector Kaon physics program, several requirements must be considered, these include:

i) Beam transport from the Main Injector.
ii) Very high intensity capability, both for beam transport and targeting.
iii) The large detector and beam dump hall.
iv) Efficient utilization of existing and projected resources.
v) Compatibility with the fixed target program.

Additionally, kaon physics using Main Injector beams will be a continuation of the current and projected Tevatron program in kaon physics. This leads naturally to a goal of sharing to the greatest degree possible common detector elements, as well as experimental hall and technical facilities; allowing the most cost efficient use of resources, both facility based and human. Programmatic and available funding inputs which are beyond the scope of this effort will be necessary for final siting decisions; however, a model of viable locations for siting of the Main Injector Kaon physics program can be developed here.

Beam transport capability from the Main Injector to each of the existing fixed target experimental areas is currently projected as a source of test beams and calibration for use during collider operation. Thus, an extraction system from the Main Injector and transport link to the existing Switchyard for low intensity 120 GeV beam is already a fundamental part of the Main Injector CDR. However, high intensity 120 GeV beam transport through the existing Switchyard elements would not be compatible with simultaneous Tevatron beam transport because of the larger emittance of the high intensity 120 GeV beam relative to the narrow electrostatic septum apertures required for Tevatron beam splitting. The alternative of time

sharing between 120 GeV and 800 GeV beam transport is unproductive for physics potential, and is operationally difficult.

A viable, cost efficient solution is to utilize existing Switchyard tunnels where possible for a new dedicated high intensity 120 GeV beam transport system. Details of how this is accomplished are addressed in Section 4.1 on Primary Beam options. Design solutions have been developed for high luminosity 120 GeV beam transport to the Neutrino, Proton and Muon experimental areas. The Meson area is the one existing area to which separate 120 GeV beam transport can not be readily added using existing beam enclosures.

Beam intensity requirements for the 120 GeV Kaon physics program have a considerable impact on options for experimental siting. Beam transport through much of the existing external primary beam transport system is expected to be viable with relatively minimal upgrade, as these beam lines will already be shielded for high intensity Tevatron beams. Current primary beam shielding design is most conservative for the Proton area and to the current Muon primary target. The Meson and Neutrino areas could require significant shielding upgrades for transport of primary beams with significantly increased luminosity. The 120 GeV beam shielding requirement is typically less severe for single pulse accident conditions due to the lower beam energy, but significantly more severe for other beam loss and targeting modes due to the very large increase in instantaneous and integrated beam intensity.

The most severe problems associated with the beam intensities from the Main Injector for the Kaon program are related to targeting and dumping of the beam. Technical solutions for target and beam dump thermal requirements, and muon and neutral beam halo rejection at the detector are presented in Section 4.2. These are site independent, but define requirements for sizing the beam dump hall. Another very significant issue with dumping of the high intensity beam is accomplishing this in a manner which is environmentally safe.

Environmental requirements for the kaon program beam dump dictate that solutions be found to several potentially significant radiation hazards:

a) Muon shielding - This is best accomplished by locating the beam dump below grade, and using horizontal sweeping for the active beam dump. Location in an above ground facility seems not viable for the intense beams targeted.

b) Ground water protection - Solution to this concern is accomplished by maintaining a minimum of six feet of steel around the primary target and beam dump. This protection will be an integral part of the beam dump system design.

c) Residual radioactivity - Extreme caution will be required in handling the target and beam dump core after beam exposure. Residual activity levels will be an order of magnitude greater than previously experienced at Fermilab. The target and beam dump system design will allow modular disassembly of components by remote crane manipulation. This will be followed by crane operated encasement in lead shields before removal. A crucial requirement is adequate sizing of the beam dump hall crane, and space for efficient component staging.

A survey of existing detector halls has been made to determine potential options for siting the Main Injector Kaon physics program. Desired specifications for the beam dump/experimental hall are as follows:

SIZE: (Dimensions in feet) 230 L. × 40 W. × 30H.

BELOW GRADE LOCATION

CRANE: At least 20 Ton capability

Additionally, upstream beam enclosures must be adequately shielded to permit transport of the intense Main Injector beam.

These requirements seem to preclude an existing location in either the Meson or Neutrino experimental areas. Currently, muon problems associated with existing Meson area beam dumps are formidable at rates of under 10^{11} protons per second. These would be unmanageable at Main Injector rates of 10^{13} protons per second, unless an extensive downstream muon shield were constructed. In the Neutrino area, shielding is adequate in the primary target hall (Neuhall), but hall size is inadequate and without crane coverage. Additionally, experimental use of this hall would be at the expense of all other usage of the Neutrino area.

The existing Proton area has two viable candidates for location of a Main Injector kaon program. Both the High Intensity Lab in PWEST and the Wide Band Lab in PBEAST are large, below grade facilities. Primary 120 GeV high intensity beam transmission is also feasible with minimal upgrade. Another experimental area which rates consideration for the kaon program is the NMUON lab. The large experimental hall is below grade, with viable crane coverage. Primary beam transmission beyond the current target hall in NM2 requires the addition of significant earth shielding along the current muon beam enclosures. However, the enclosures were designed to structurally accept the additional earth overburden required for beam transport. The much greater potential problem of muon shielding is solved by the below grade hall.

Table 2.1 lists characteristics of the three existing experimental halls which can be considered as candidates for the Main Injector Kaon program:

LOCATION	SIZE [L × W × H ft.]	BEAM HEIGHT below grade	CRANE
PWEST	230 × 30 × 20	14 ft.	20 TON
PBEAST	227 × 52 × 38	7 ft.	TWO 15 TON
NMUON	240 × 60 × 30	11 ft.	TWO 25 TON

Table 2.1: Existing options for Kaon Experimental Hall.

Shown in Fig. 2.1 are the locations of these three experimental halls within the Fermilab experimental areas.

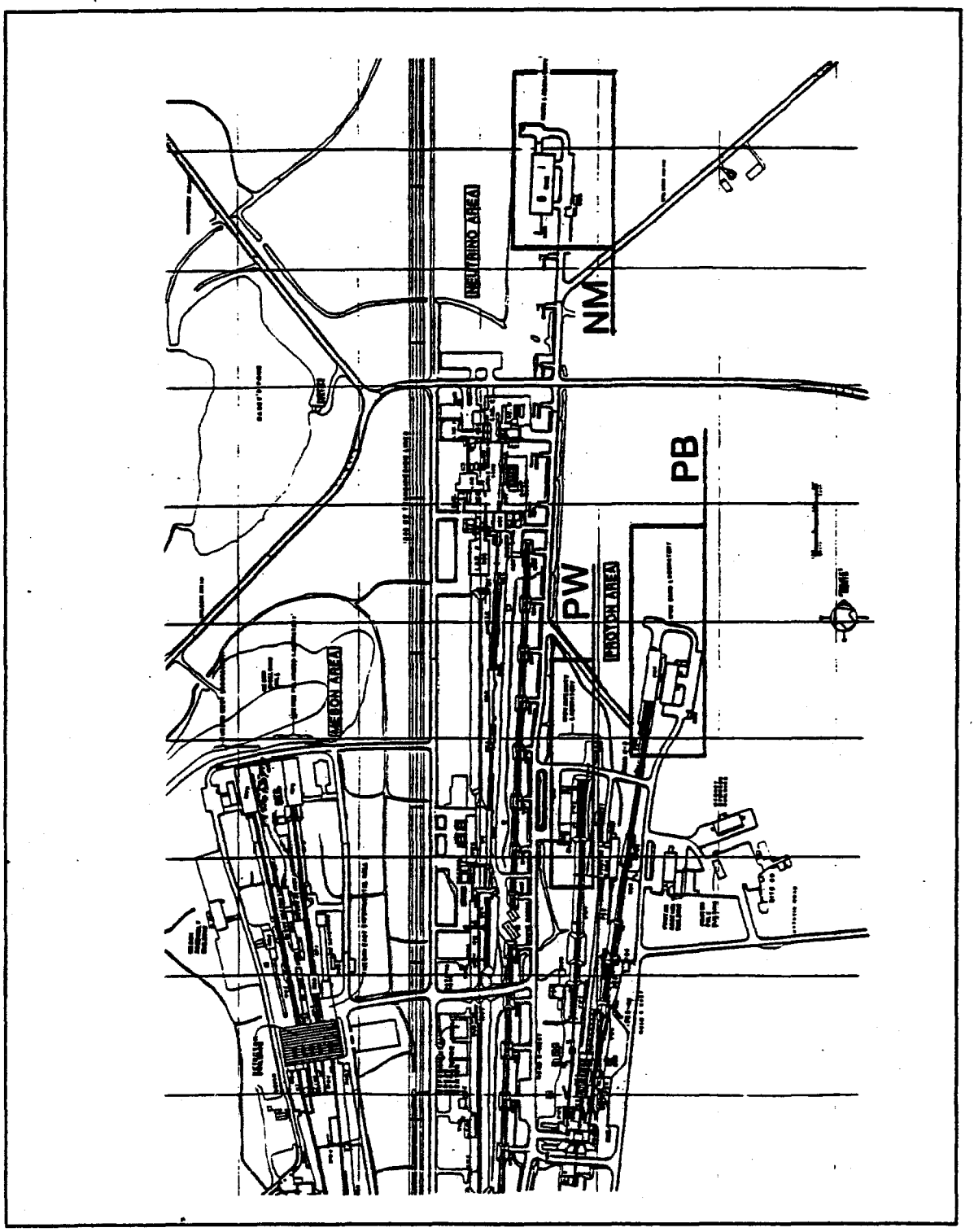

Fig. 2.1: Possible candidates for Kaon Experimental Hall.

Utilization of one of these facilities is preferred to the construction of a new experimental area for this program. However, if use of an existing experimental facility were precluded due to programmatic considerations, several possible options for a new area seem feasible. One possibility is to share the extraction channel to the East of the Main Injector at location MI-50, designated for the machine abort line. The Neutrino physics CDR actively considers this location, and a more complete 120 GeV experimental facility could be developed here. Another potential location could be to the West of the existing Neutrino area, as detailed in TM-1599. This site would require significant rework of existing utilities, and has logistical conflicts with the Tevatron Neutrino area program.

Another constraint is compatibility with the evolving Tevatron Kaon physics program. As intensity needs increase for this effort, either a complete rebuilding of the existing beam dump and experimental area in MCENTER, or a move to a new area will be required. The most cost efficient use of resources is to simultaneously consider siting requirements for the complete Kaon physics program, utilizing both Tevatron and Main Injector beams. Such a solution could be developed based on technical needs using any of the three experimental halls PWEST, PBEAST, or NMUON. Potential long term cost savings for this approach are seen as very significant.

Besides the significant cost benefits derived from use of an existing experimental facility for the Kaon program, the considerable expense projected for construction of the large gap analysis magnet system in Section 4.3 indicates that potential use of existing analysis magnets should also be considered. A promising analysis magnet candidate, is the venerable Chicago Cyclotron Magnet now located in the NMUON experimental hall, and around which the building was constructed. It will need to be regapped for larger acceptance.

As a model for developing a quantitative assessment of the total costs required to stage the Main Injector Kaon experimental program, we have looked in detail at all known costs for one siting option. While specific costing details would differ dependent on final siting selection, this should

be representative of the required resources to stage this experimental effort with optimal utilization of existing facilities. The beam line and experimental hall chosen for the Kaon program in this model is the NMUON.

3. LAYOUT

The KAMI facility will be used to perform a variety of high precision, high sensitivity experiments with neutral kaon beams. In this Section, we give the general layout of the elements that reside in the detector hall for a selection of configurations. The detector hall contains three systems: secondary beam production, decay space, and detection. The secondary beam region consists of the production target, sweeping magnets, collimation, and the beam dump. The neutral beam emerges into a large evacuated decay volume which is surrounded by a veto system. The decay products exit through a thin window to a detection apparatus consisting of calorimetry, magnetic tracking, and particle identification.

Figures 3.1 and 3.2 show the plan and elevation views of the facility as it will be configured for many K_L experiments. A notable feature of the apparatus is the two large dipole analysis magnets. Since one site under consideration for the KAMI facility is the NMUON lab, which already houses the Chicago Cyclotron Magnet (CCM), we have considered the CCM as an option to replace the pair of dipoles. The pros and cons of using the CCM or building new dipoles are discussed in detail in Section 4.3 Analysis Magnets. Figure 3.3 shows the layout of the KAMI facility designed around the CCM.

Other options that have been discussed are $K_L \rightarrow \pi^0\nu\bar{\nu}$, an experiment which requires a rearrangement of the detector elements, and $K_S \rightarrow \pi^0 e^+e^-$, which requires rearrangement of the secondary beam production elements. Figure 3.4 shows the $K_L \rightarrow \pi^0\nu\bar{\nu}$ layout. Since the large photon veto system and the calorimeter must form a totally hermetic detector, the calorimeter is re-stacked at the end of the decay space for this experiment. The layout for $K_S \rightarrow \pi^0 e^+e^-$ is shown in Fig. 3.5. Here a reduced intensity primary beam passes through the normal targeting area, and hits a target much closer to the detector. The small distance to the detector is essential for sensitivity to K_S decays.

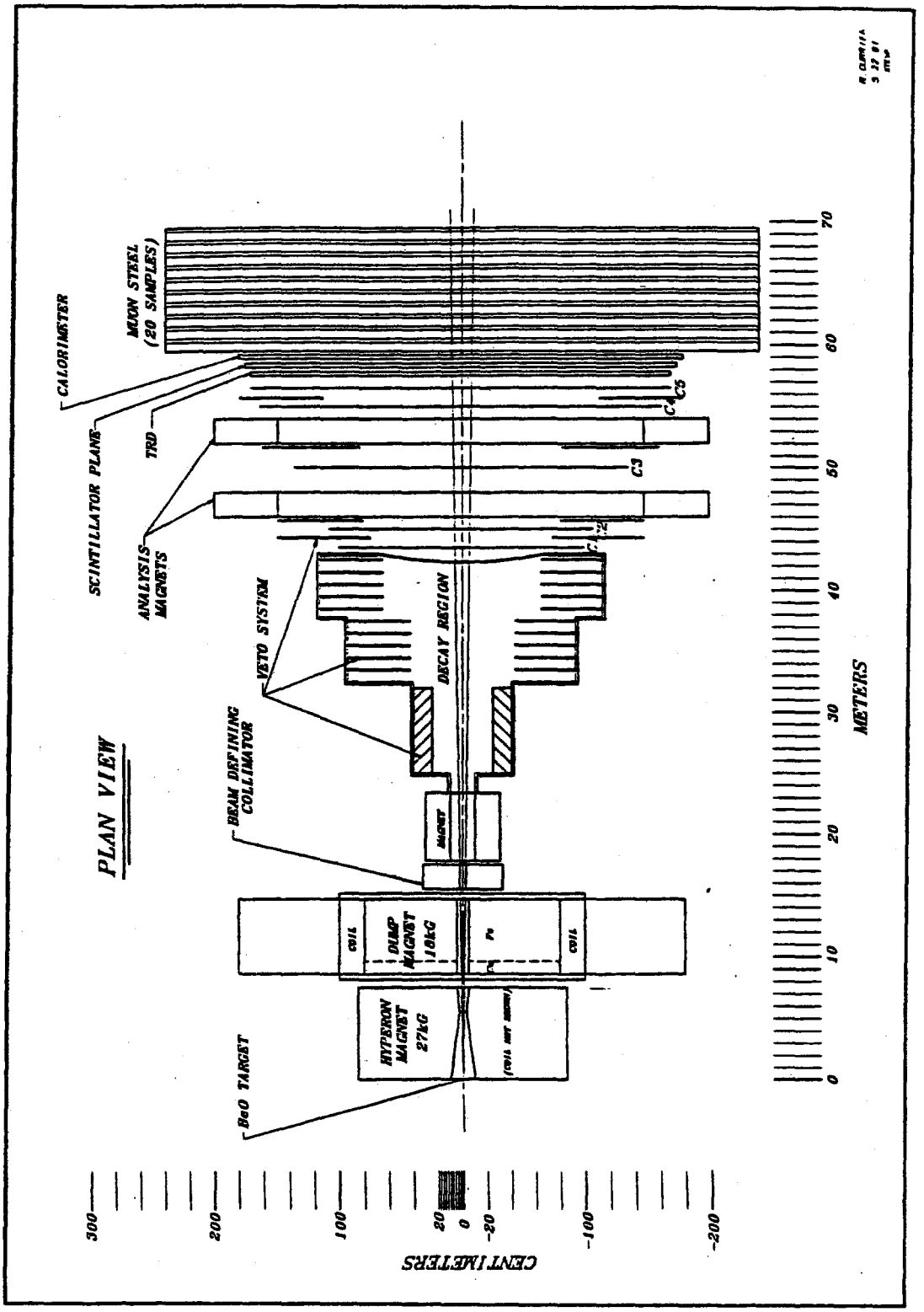

Fig. 3.1: Plan view of KAMI Facility showing secondary beam formation, decay space, and apparatus. This figure illustrates the "standard" K_L configuration.

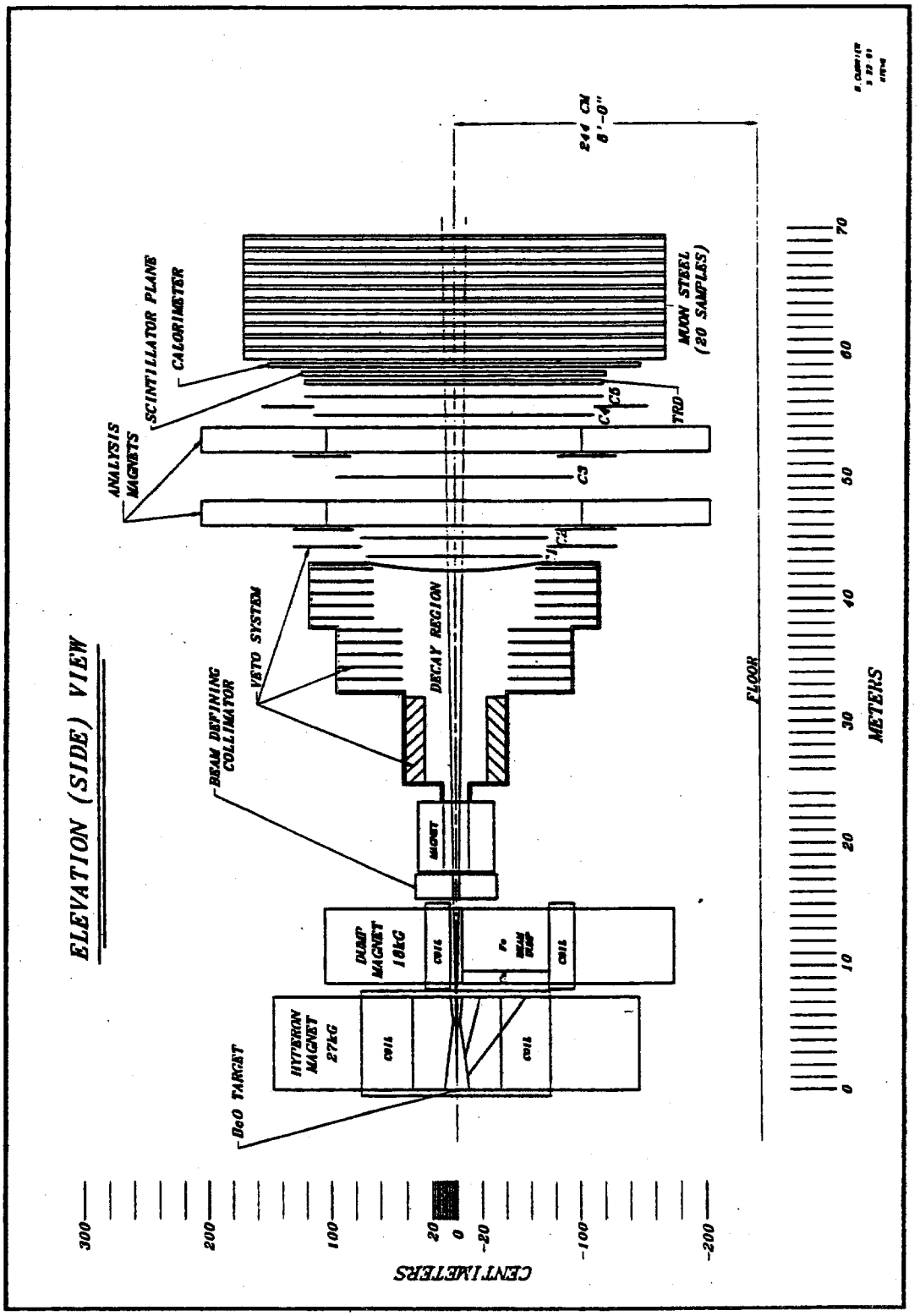

Fig. 3.2: Elevation view of KAMI Facility showing secondary beam formation, decay space, and apparatus. This figure illustrates the "standard" K_L configuration.

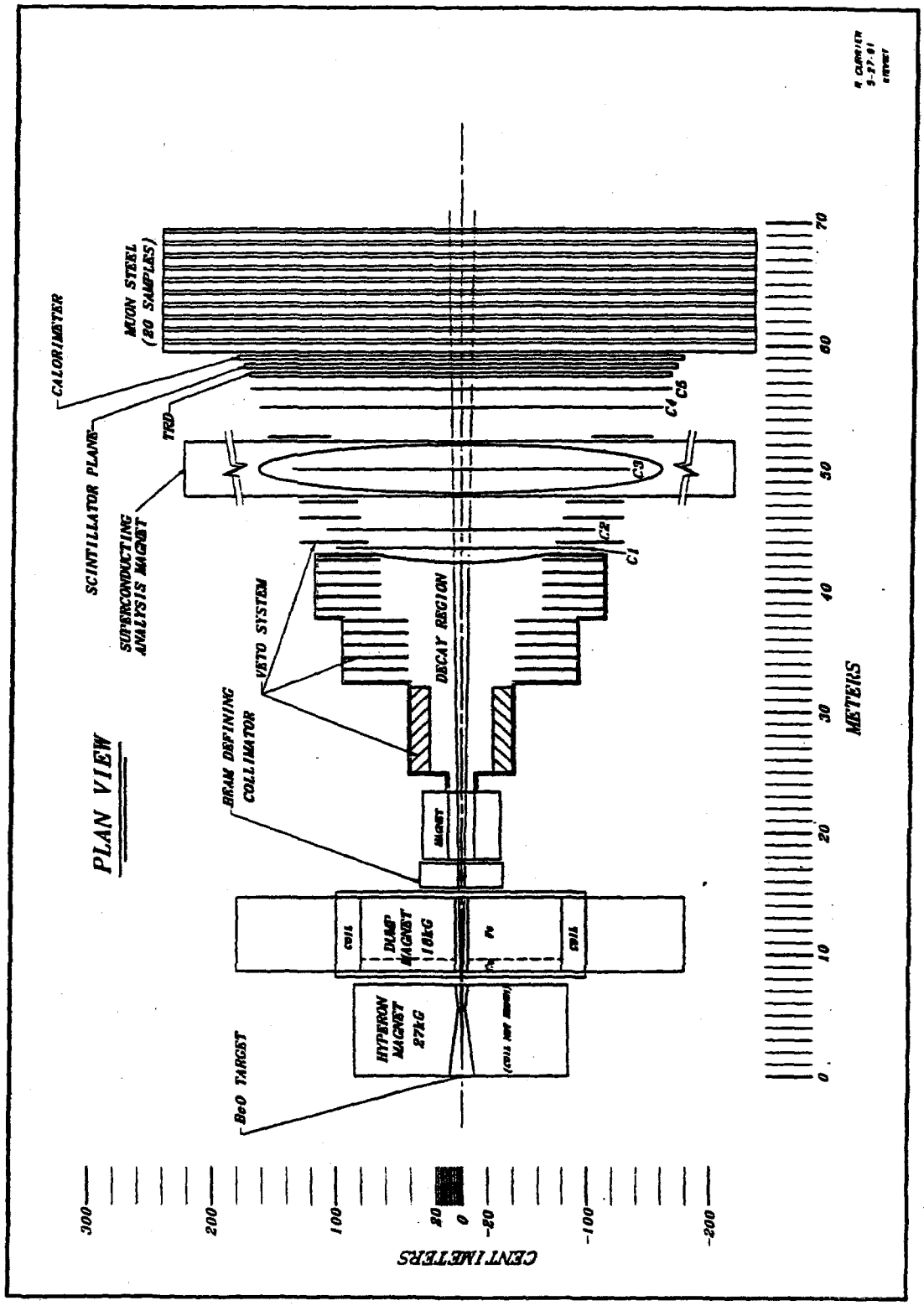

Fig. 3.3: Plan view of KAMI apparatus using Chicago Cyclotron Magnet.

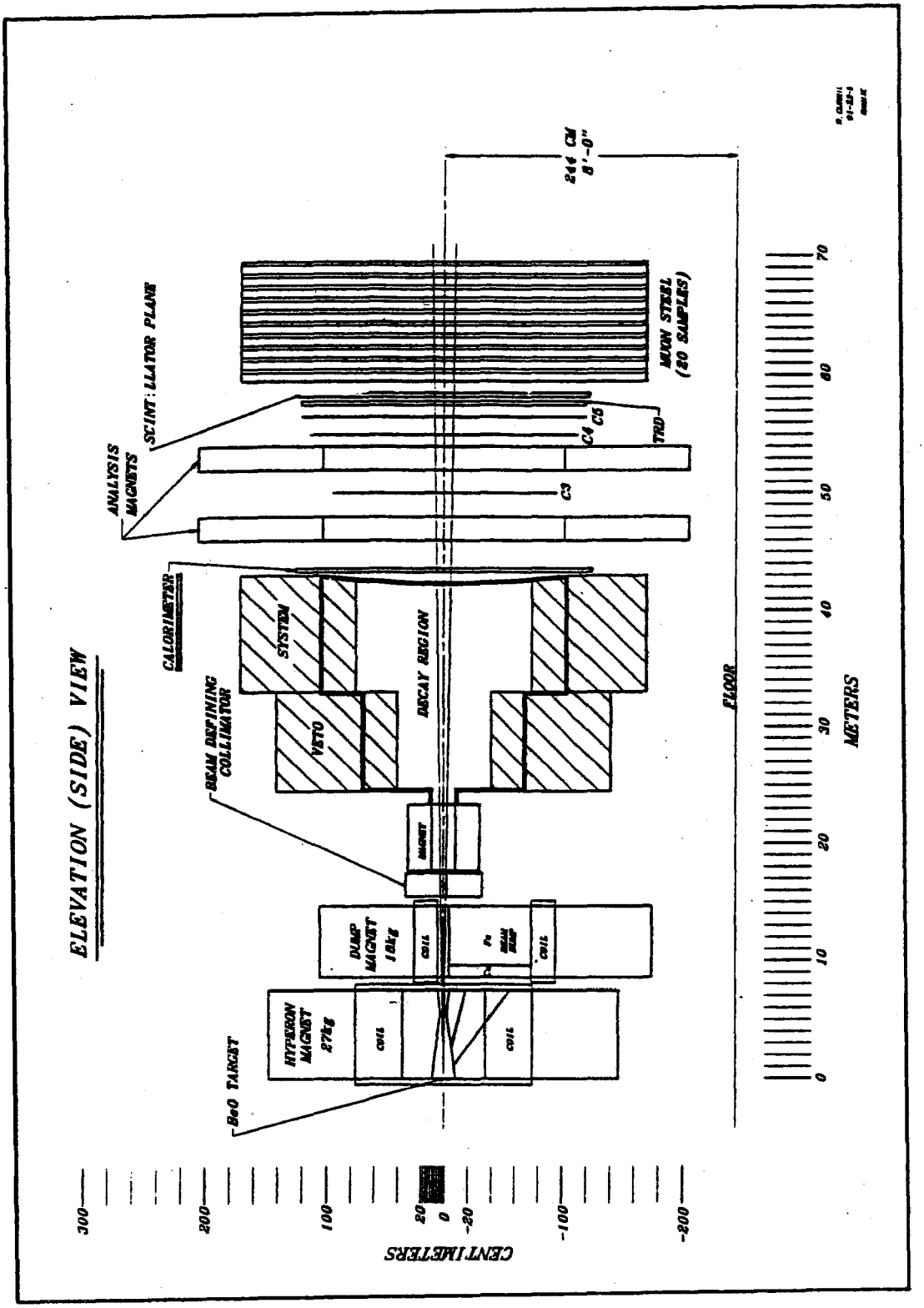

Fig. 3.4: Plan view of KAMI apparatus in $K_L \rightarrow \pi^0 \nu\bar{\nu}$ mode.

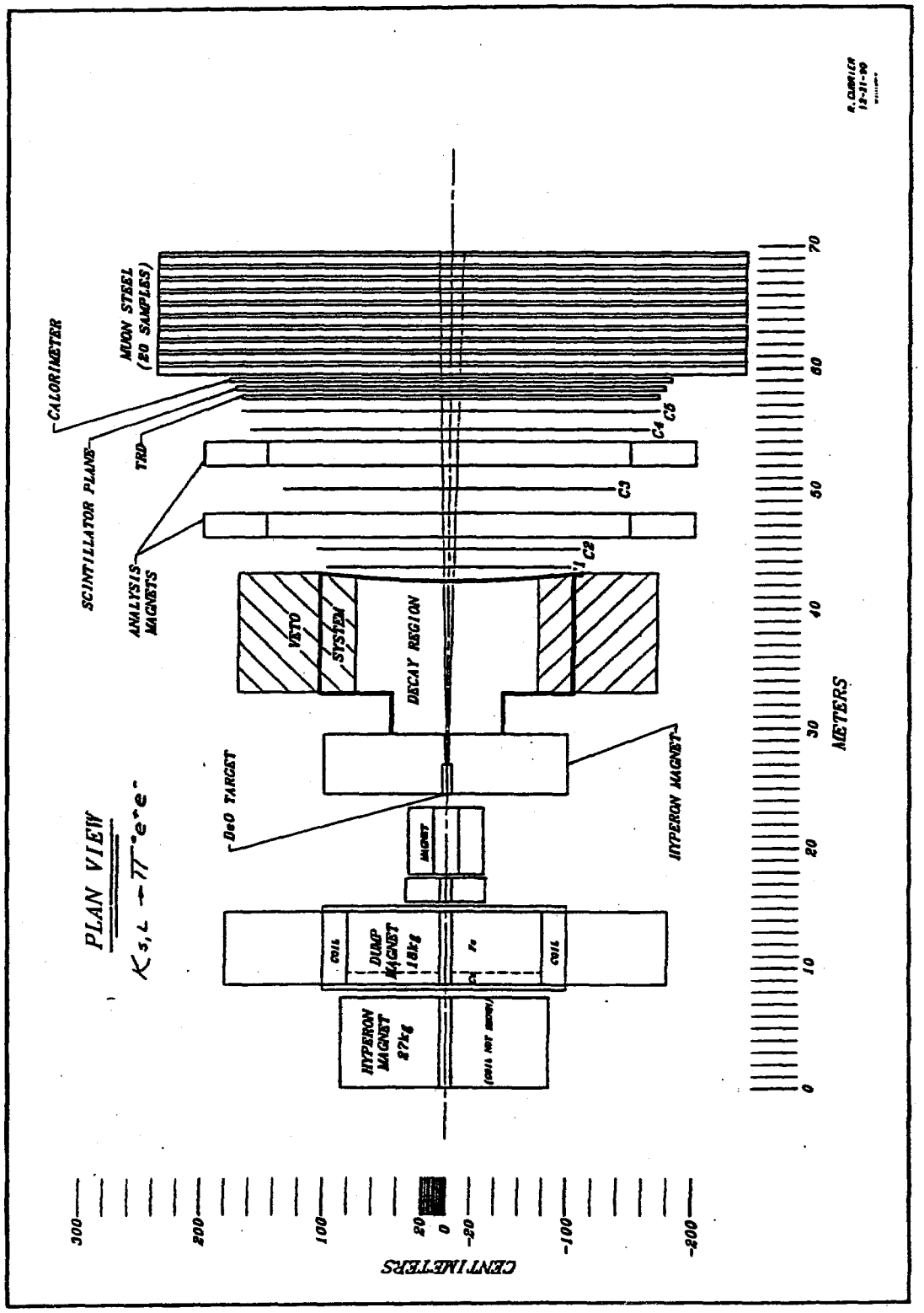

Fig. 3.5: Plan view of KAMI apparatus in $K_S \rightarrow \pi^0 e^+ e^-$ mode.

4.0 TECHNICAL DESIGN of the FACILITY

For the purpose of this report, we distinguish the KAMI *facility* from the KAMI *detector*. The facility consists of the detector hall, primary beam transport, secondary beam elements, and analysis magnets. In this Section we give the technical specifications for the facility. The detector hall itself is not treated in detail as the NMUON lab is taken as a model. Since the primary beam transport can only be discussed in the context of a specific choice of site for the KAMI program, we have included a description of primary beam transport options for each viable site. Although details of the secondary beam and analysis magnets do not depend on site selection, one candidate site, NMUON lab, contains an existing large analysis magnet, the Chicago Cyclotron Magnet (CCM). Consequently, the discussion of analysis magnets contains an evaluation of the CCM as an option for KAMI.

4.1 Primary Beam

4.1.1 Rates

The Main Injector Conceptual Design Report[1] lists several modes of operation. For 120 GeV dedicated slow spill extraction to KAMI, the cycle time would be 2.9 sec with a 1 sec flat top, yielding an average duty factor of 34%. The length of the flat top is limited by power considerations; it could be lengthened at the cost of a longer cycle time. With an intensity of 3×10^{13} protons per pulse, this implies an average delivered proton current of about 2 μA. For the neutrino program at the Main Injector (NUMI), the dedicated short spill cycle time would be 1.9 sec.

---

1 *Fermilab Upgrade: Main Injector*, Conceptual Design Report (April, 1990).

A major advantage of the Main Injector for high sensitivity Kaon physics is that it can provide high intensity 120 GeV fixed target beams during both collider and Tevatron fixed target operation. For example, one might load the Main Injector with six Booster batches containing a total of 3×10^{13} protons, accelerate to 120 GeV, fast extract one batch (5×10^{12}) to the antiproton production target, and slow extract the rest of the beam over a one second period. This would give slightly more than half the standard antiproton flux into the source and provide 83% of the dedicated beam intensity for KAMI. Table 4.1.1 gives the fraction of the Main Injector dedicated beam intensity available to KAMI and NUMI for a variety of different operating configurations.

Note that, in general, Table 4.1.1 assumes pulse sharing between users, not intensity sharing within a pulse. The primary exception is collider operation as discussed above and in Ref. 2 of the table. Intensity sharing between KAMI and Main Injector test beam activity is also a possibility if an appropriate splitting station is provided for the test beams. Equal-time sharing between KAMI and NUMI has been assumed for the sake of simplicity. Depending on the operational status of the programs, unequal sharing is also possible. Intensity sharing (within a spill) between NUMI and KAMI is not presently envisioned in the Main Injector design.

There are also plans to use 120 GeV protons from the Main Injector to provide test beams in some fixed target areas. Compatibility considerations for this activity are also included in Table 4.1.1. Simultaneous fixed target Tevatron operation and Main Injector test beam operation are not presently envisioned because of beam transport constraints. Of course, the Tevatron itself can provide primary protons for test beam activities during fixed target running periods, so this does not appear to be a very troublesome limitation.

Main Injector Modes	TEVATRON MODES								
	Fixed Target			Collider			Off		
	Beam Fractions		Ref.	Beam Fractions		Ref.	Beam Fractions		Ref.
	KAMI	NUMI		KAMI	NUMI		KAMI	NUMI	
KAMI Alone (3 sec cycle)	0.90	0	1	0.83	0	2	1	0	3
NUMI Alone (2 sec cycle)	0	0.90	1	0	0.83	2	0	1	4
KAMI + NUMI	0.45	0.45	1,5	0.41	0.41	2,5	0.50	0.50	5
KAMI + Test	X	X	6	0.75	0	2,7,8	0.90	0	7,8
NUMI + Test	X	X	6	0	0.75	2,7	0	0.90	7
KAMI + NUMI + Test	X	X	6	0.37	0.37	2,5,7,8	0.45	0.45	5,7,8

Table 4.1.1: Fraction of dedicated beam intensity available to KAMI and NUMI for various operating configurations.

---

1 Assumes 2 MI pulses per minute (6 seconds out of 60 seconds) devoted to Tevatron fixed target operation.

2 Assumes 5×10^{12} (out of 3×10^{13}) for collider $\bar{p}$ production in every MI cycle.

3 This is the definition of 100% beam delivery for KAMI assuming 3 sec cycle time and 3×10^{13} protons per pulse.

4 This is the definition of 100% beam delivery for NUMI assuming 2 sec cycle time and 3×10^{13} protons per pulse.

5 Assumes that KAMI and NUMI share pulses on an *equal time* basis; *e.g.*, 30 sec. (10 pulses) to KAMI and 30 sec (15 pulses) to NUMI in a minute when they have full access to the MI. Of course, unequal distribution would also be possible.

6 As currently envisioned, MI test beam operation and Tevatron fixed target operation are *not* compatible because of primary beam transport constraints. During fixed target operation, the Tevatron can provide primary protons for test beams.

7 Assumes 2 MI pulses per minute (6 sec out of 60 sec) for MI test beam operation.

8 Intensity sharing (during each spill) between KAMI and MI test beams is also a possibility if a splitting station is located between the MI and A0.

The primary conclusion of this discussion is that a wide variety of shared-activity operating modes are available. Of course, for flat-out data taking, the most cost effective mode for KAMI and NUMI is alternate running for "macroscopic" periods of time (*e.g.*, weeks to months).

4.1.2 Debunched Beam in the Main Injector

The KAMI program is being designed to utilize the full slow spill Main Injector intensity, with the beam being debunched in the Main Injector before extraction. Debunching of the RF structure provides a significant increase in effective duty cycle, enabling essentially uniform spill structure over the 1 second flat top. A small bunch structure modulation of perhaps 10% will be maintained in the spill so bunch-sensitive beam instrumentation can be used.

Debunching of the beam in the Main Injector does not appear to present great technical difficulty. The RF cavities used will be the present Main Ring cavities; hence, existing experience with beam loading of the RF cavities will be immediately transferable. Additionally, the Main Injector interior walls will be much smoother than the Main Ring, without sharp interface boundaries; thus, overall longitudinal impedance will be much smaller in the Main Injector, enabling better control of bunch structure.

Two general methods of producing debunched beam differ in how quickly the RF is turned off. The first method is to quickly reduce the RF voltage, letting the bunches shear at a large dp/p. This method has a quick debunching time in terms of a uniform distribution of charge. A disadvantage is that beam loading on the cavities would tend to rebunch the beam immediately after the RF is switched off. However, beam loading compensation is feasible and could be made to track the intensity remaining in the ring. The second debunching method is to adiabatically reduce the RF voltage by first paraphasing stations, then turning stations off, inserting cavity shorts, and finally paraphasing to zero voltage with two RF stations. Using this method the beam loading effects are greatly reduced at the expense of a longer charge debunching time. A second

advantage of adiabatic debunching is that momentum spread effects in the slow extracted beam are also reduced.

4.1.3 Primary Beam Transport

The existing FNAL switchyard was examined to determine the feasibility of transporting a new dedicated high intensity 120 GeV beam to the Neutrino, Muon, Proton, or Meson areas. Here, feasibility options are explored for each of the experimental areas. The final choice of the area chosen for the Kaon Main Injector program will be determined using the criteria detailed in Section 2.

The Neutrino area option has been previously worked out in some detail.[2] Study of other primary beam areas has been done in somewhat less detail; and as yet without detailed study of the beam optics. However, beam transport optics to each experimental area is expected to be similar to the Neutrino area option. This is due to the common source, as well as comparable beam transport enclosure geometries. A comparison of civil construction and elements required for 120 GeV beam to the areas considered is given at the end of this section.

Neutrino Area

Design criteria for the new Switchyard high intensity primary beam line from the Main Injector to the Neutrino area were that the following conditions be satisfied, to minimize costs:

The new line should stay within existing Switchyard tunnels, with a minimum of civil construction.

---

2 *Fermilab Fixed Target Beams from the Main Injector*, S. Childress, *et al.*, Fermilab TM-1599 (1989).

Trajectory through the Switchyard beam dump should remain within the existing beam transmission pipe, thus avoiding major civil construction involving the beam dump.

A design has been found which satisfies both of these criteria, with no major compromise required. (TM-1599). Figures 4.1.1a and 4.1.1b illustrate the manner in which the 120 GeV beam transport line and the existing Switchyard Tevatron lines are fit within common beam enclosures.

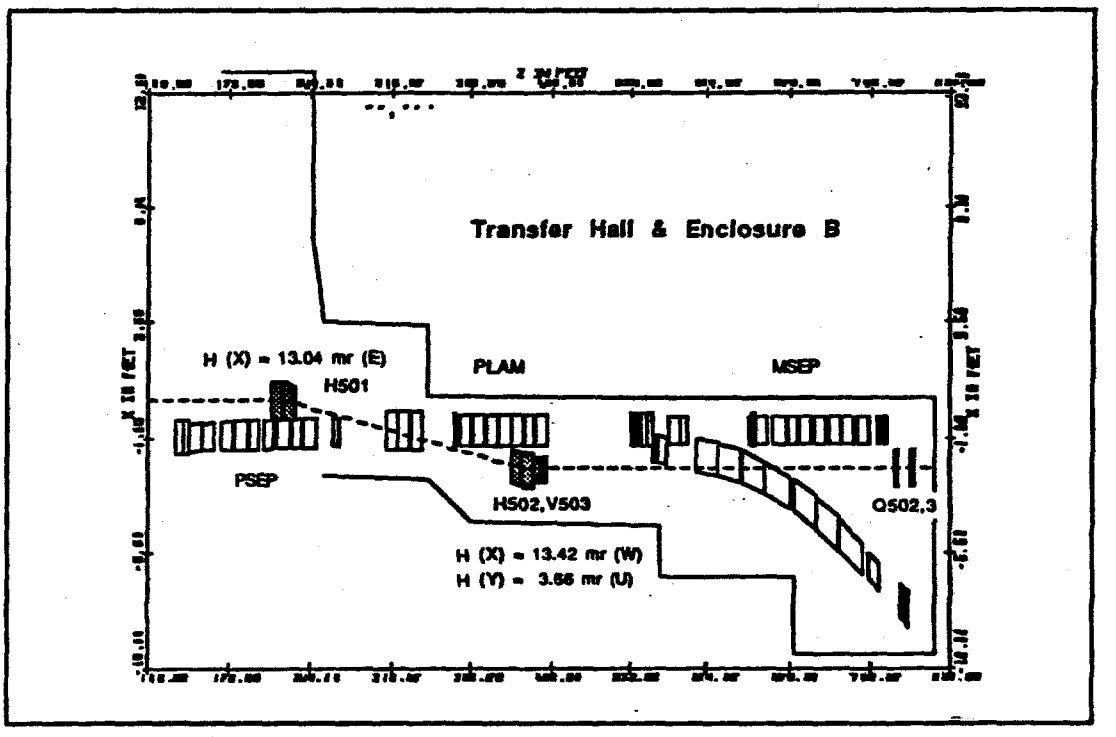

Figure 4.1.1a: Plan View of 120 GeV primary beam line (dashed line) in existing Switchyard Encl. B.

Civil construction is required in general for new berm pipe between each enclosure, as the existing eight inch diameter pipes are completely shadowed by present Switchyard magnets, with no room for a new beam. This is typically less expensive by an order of magnitude than adding new tunnel sections, however. Additionally, much berm pipe replacement may be necessary on this time scale in any regard, due to the aging of existing buried carbon steel pipes.

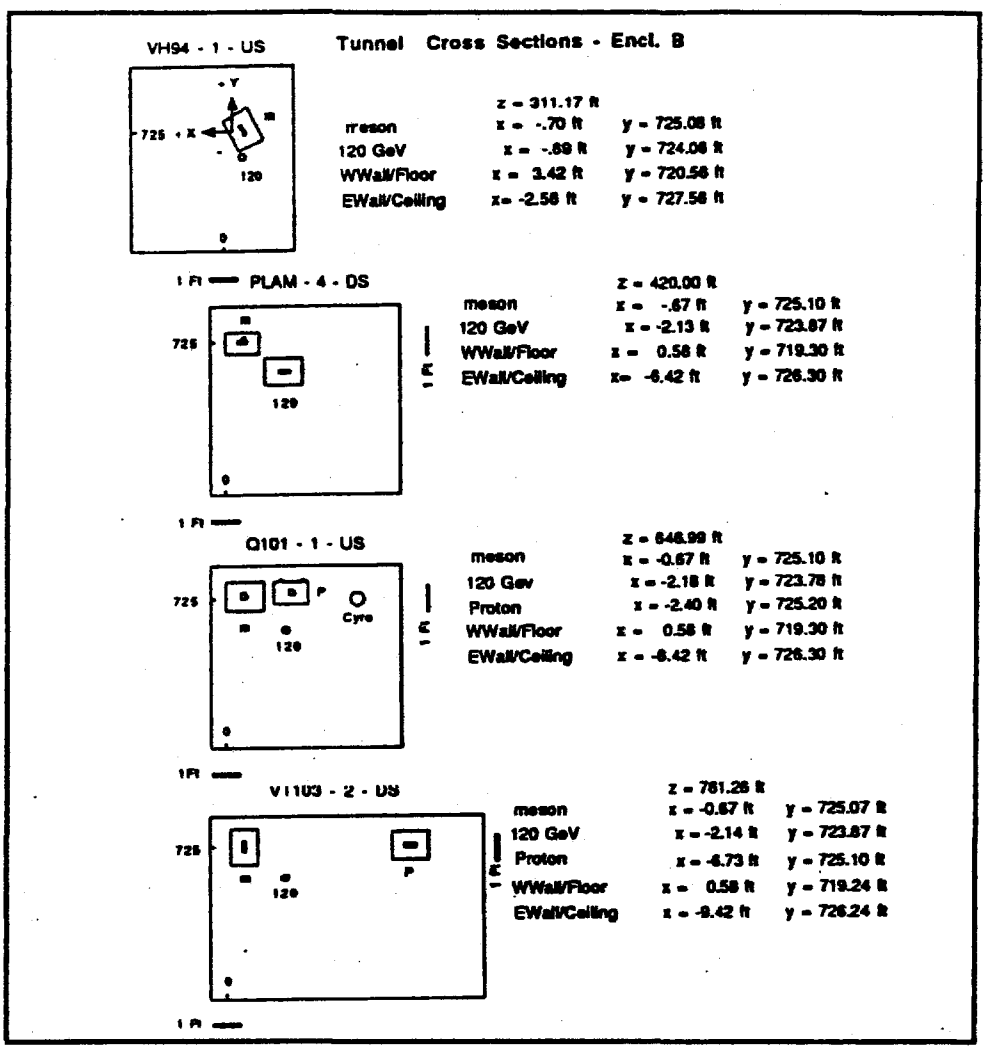

Figure 4.1.1b: Cross section view of 120 GeV beam primary transport in Switchyard Encl. B. Beam direction is into the page.

A major design hurdle for a 120 GeV beam transport line is compatibility with the existing Switchyard beam dump, located between Switchyard Enclosures C and G1. The dump has an eight inch diameter transmission pipe through a 26 ft. long core box. Entrance hole to the dump itself is near the dump box center, while the transmission hole is toward the top. The new beam trajectory is designed to cross the existing Tevatron beam at a point near the beam dump, thus sharing the same transmission beam pipe. New berm pipe is required both upstream and downstream of this region, but civil construction at the beam dump is not required.

Spatial constraints may require a short tunnel extension of 35 ft. for SY Encl. G1, the only location where new tunnel length is being considered. Additionally, a total of about 690 ft. of new berm pipe would be required between existing Switchyard tunnels to transport 120 GeV beam to the Neutrino area.

Beam optics for a dedicated High Intensity line through the Switchyard is discussed in Section 4.1.4. As narrow aperture electrostatic septa are not utilized in this beam line, the beam optics envelope is very well constrained.

Muon Area

The Muon line 120 GeV transport is identical to the Neutrino solution to Encl. G1. At this point a shift into the existing Tevatron Muon line in Encl. G2 is required. This can be accomplished by adding a vertical EPB dipole in G1 to give the correct position in G2. One more EPB dipole (rotated) is needed to match the Muon beam angle in the upstream end of G2. From this point on the existing Tevatron Muon line transport can be used.

Proton Area

The Proton line transport is identical to the Neutrino solution to SY Encl. B. At this point the 120 GeV line transport is given a set of horizontal bends, producing a similar trajectory to the existing Tevatron Proton beam transport. Civil construction is again required for new berm pipe between existing enclosures.

The major constraint in the Proton area option is the Switchyard service building located over the berm pipe between Encl. D and Encl. E. Here the 120 GeV line must match into the existing 8" diameter berm pipe under the service building, to avoid major civil construction. This matching in Encl. D can be accomplished with an EPB dipole dogleg in both planes, along with 2-way Switchyard style Lambertsons for the final

linkage. Another set of Lambertsons downstream of the pipe initiates separation of the 120 GeV and Tevatron beam trajectories again. Positioning of the 120 GeV beam in Enclosure P01 would be dependent on the Proton area experimental hall to be used. The large P01 enclosure allows considerable flexibility for the 120 GeV beam transport.

Meson

The Meson area is the most difficult line to transport a dedicated 120 GeV beam because of the left bends in SY Encl. C. These cryogenic magnets and their associated plumbing fill the narrow 5' × 7' tunnel, such that without major civil construction the passage of a dedicated 120 GeV beam is extremely awkward if not impossible. The Meson area is also the most weakly radiation shielded area, and considered the poorest choice for locating a very high intensity experimental facility. Hence, a dedicated high intensity 120 GeV line to this area is not considered further.

Comparisons

Table 4.1.2 illustrates the requirements for magnets to provide a new 120 GeV beam transport to the Neutrino, Muon and Proton Areas. Since the Muon line has only one experimental area, an efficient tie in can be made to the existing Tevatron Switchyard beam line. The Proton transport could require additional elements depending on the choice of experimental hall. All magnets considered are standard external primary beam elements. Also listed in the table are civil construction requirements for transport to each area.

Location	# Dipoles	# 3Q Quads		Lambertsons	New Berm Pipe	Comments
	10' EPB	10'	5'	SY 2-way	length (ft.)	
Neutrino	22	4	5	0	690*	Transport to exp't.
Muon	8	0	4	0	690*	Transport to Encl G2
Proton	21	6	5	6	934	Transport to P01

* 35' extension of Encl. G1 is also needed

Table 4.1.2: Magnet requirements for 120 GeV beam transport.

4.1.4 Target Focus

Primary beam optics design should match beam size at the final focus to the specified target sizes of as small as 1 mm diameter. The Neutrino Area design detailed in TM1599 meets this requirement using a symmetric triplet for the final target focus. A similar target focus can be obtained in other beam lines with a matched phase-space and sufficient space for placement of elements. Large aperture 4Q120 quadrupoles are projected for the optical elements near the target. The increased aperture of these magnets can be used to improve spot size at the target, as well as beam halo.

Figure 4.1.2 shows the 120 GeV beam sizes given by the program TRANSPORT starting at a distance of 1250 ft. upstream of the primary target. The calculation is for beam transport to the Neutrino area, but would be similar for any other experimental area for beam from the Main Injector. Location of beam elements is expressed as a distance upstream of the target. Beam sizes shown are half-width at the base with the top (positive scale) showing the horizontal beam, while the bottom (negative scale) shows the vertical beam size.

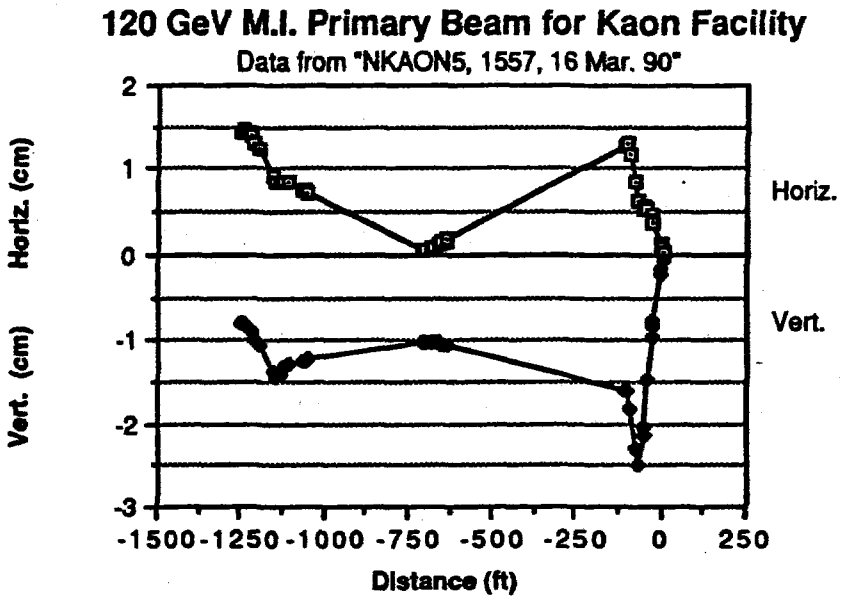

Figure 4.1.2: 120 GeV primary beam optics prior to targeting.

Figure 4.1.3 shows the beam sizes as given by TRANSPORT with expanded resolution in the region adjacent to the KAMI target. The calculated values for the vertical and horizontal half-widths at the base at the target position are 0.59 mm and 0.46 mm respectively.

Required 120 GeV quadrupole specifications in the region upstream of the primary target are given in Table 4.1.3. Final focus quads are assumed to be 4Q120's, the rest 3Q120's. Negative values for the quadrupole gradients are used to indicate defocussing quadrupoles, i.e., defocus in the

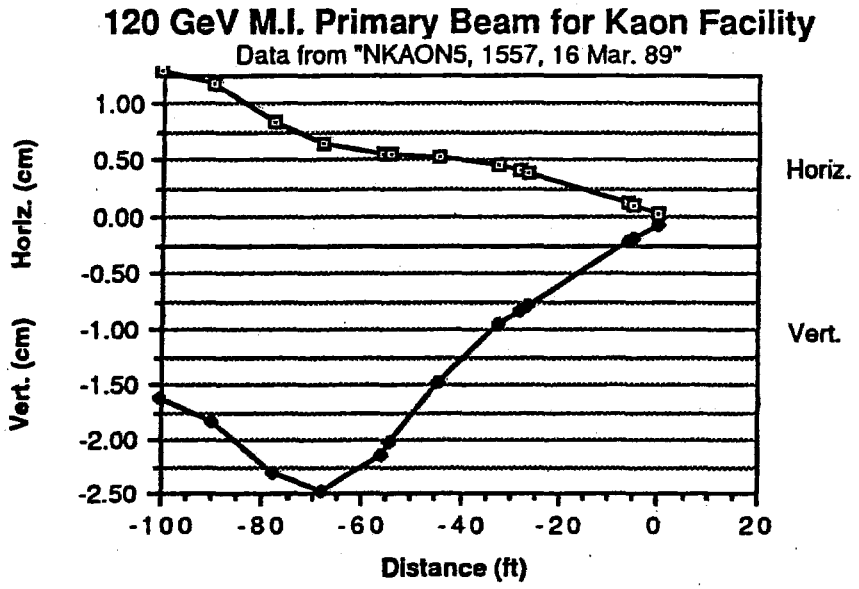

Figure 4.1.3: Calculated TRANSPORT primary beam sizes before final target focus.

horizontal plane. Required field gradients for the 4Q120's are well within specifications of these magnets. For the beam transport quadrupoles (3Q120's), the issue is one of power supply regulation at the low currents projected, compared to Tevatron 800 GeV beam operation. This will be simplified by the dedicated nature of the 120 GeV beam transport, enabling the use of power supplies matched to these low current conditions.

Magnet Type	Location before tgt.(ft)	Field (KG/in)	Current (amps)
3Q120	1232.4	0.38	7.32
"	1144.4	-0.72	13.81
"	1122.3	0.32	6.91
4Q120	95.3	3.21	685.90
"	67.4	-4.73	1010.47
"	37.4	3.21	685.90

Table 4.1.3: Quadrupole specifications for 120 GeV target focus.

4.1.5 Beam Stability

For high precision measurements of the KAMI program, a crucial factor in understanding and maintaining accurate knowledge of secondary beam acceptance is the position stability of the primary beam. For the previous Tevatron kaon experiment E731, changes in beam position were closely monitored. A 200 micron change in centroid beam position at the primary target, typical of the variation observed, was found to change acceptance by 0.5%.[3] For the Main Injector program, the need for acceptance stability is projected to be 0.01%; an accuracy which will require beam monitoring and position control at the target to less than 10 microns.

Although this is a major improvement beyond current capabilities, to achieve < 10 μm beam position control should require only incremental improvements beyond what has already been achieved in parts of the present primary beam system. The most crucial change needed will be extending an active beam control system to the complete primary beam line from extraction to target. Some of the upgrades needed are:

1) Develop beam position servo systems which take out the large beam motions due to changes in momentum phase space during the resonant extraction process. Such systems are made simpler by the pulse to pulse repetition of this beam instability, with only slow time variations.

2) Extend current beam position control capabilities to improved resolutions [present operational limits = 200 μm]. This is discussed in detail in the beam instrumentation Section 4.1.7.

3) Considerable attention to improving power supply regulation capabilities throughout the primary beam transport. This is predominantly a more extensive use of existing technology.

---

[3] Fermilab E731.

4) Utilize final focus targeting beam optics de-magnification to gain a significant factor in position stability.

Damping Beam Instabilities with a Symmetric Triplet

To illustrate the damping nature of a final focus symmetric triplet optics design, several beam position offsets were simulated using the ray tracing program TURTLE[4]. In each case, the triplet used in the final focus was able to significantly reduce the magnitude of position offset at the target.

Figure 4.1.4.a shows a series of TURTLE profiles for the 120 GeV primary beam. Profiles illustrated are in the upstream beam transport, at the entrance to the final focusing quads, and at the target. It should be noted that the scale at the target has been expanded by a factor of ten, with one bin = 100 μm. For upstream profiles, one bin = 1 mm. In Fig. 4.1.4.b, a vertically off-axis slit was inserted into the beam at an upstream location. The centroid of the collimated beam is shifted off-axis by 10 mm; flux is normalized such that the number of particles reaching the target is unchanged. It can be seen that even though the beam is offset by almost one centimeter entering the front face of the final focus quads, the beam centroid shift is less than 100 μm at the target.

Next, an angular offset was placed in the TURTLE deck at the last major bend string to represent a possible instability caused by a poorly regulated power supply (0.1% current fluctuation). As shown in Fig. 4.1.4.c, the triplet does not respond to the angular offset as well as the previous spatial offset; it does however produce a reverse magnification or damping factor of .04 in the horizontal and .06 in the vertical plane. Thus, an angular instability causing 1 cm centroid motion entering the quads produces a shift of about 400 μm motion on the target.

---

[4] TURTLE, Trace Unlimited Rays Through Lumped Elements, D. Carey, *et al.* (1982).

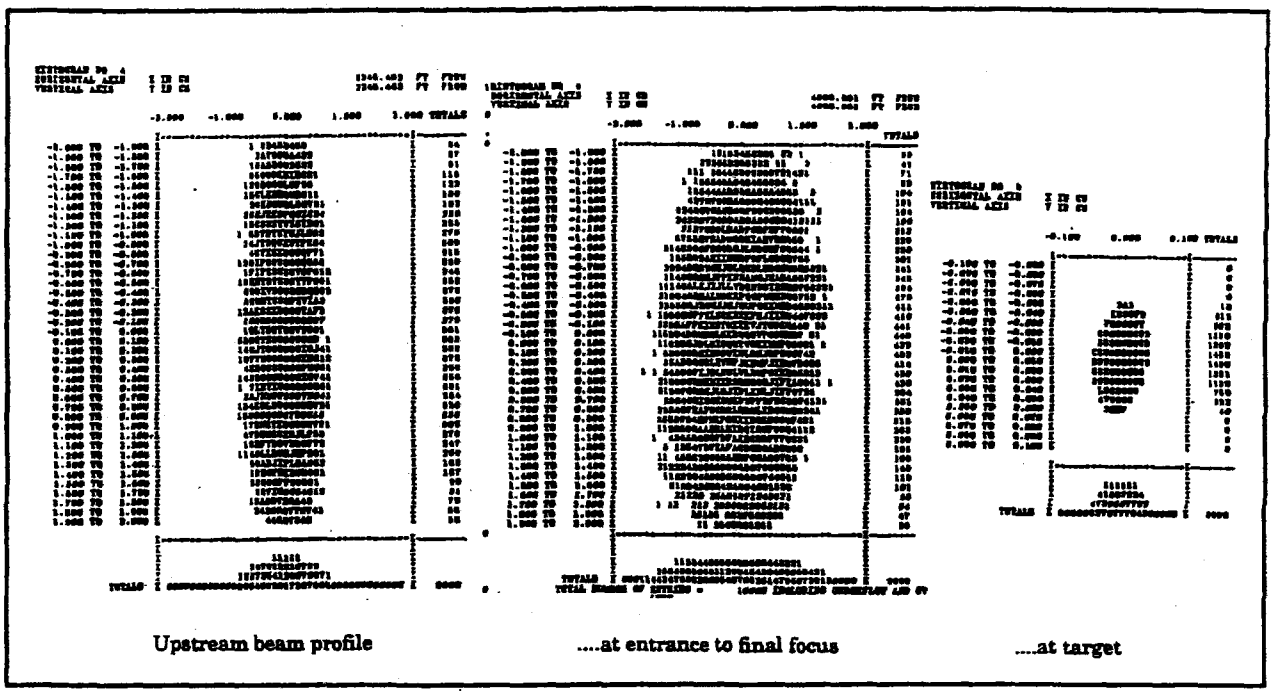

Fig. 4.1.4a: Kaon Beam with no instabilities.

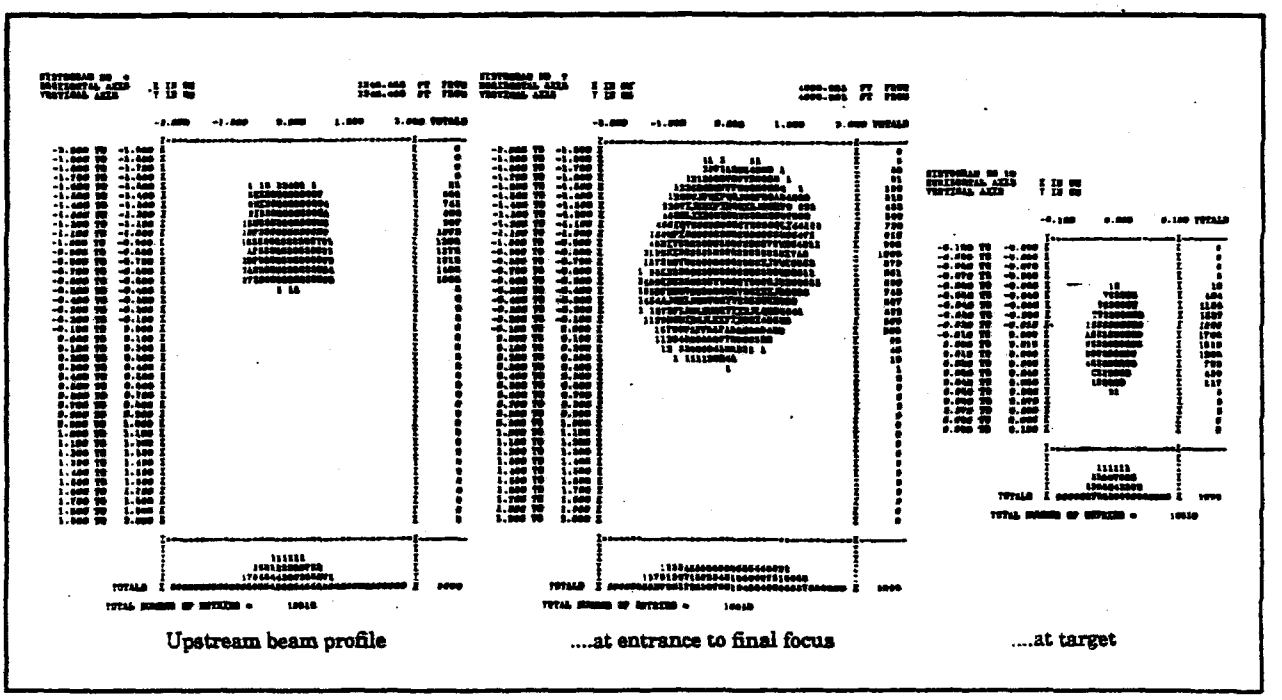

Fig. 4.1.4b: Kaon Beam with off axis slit.

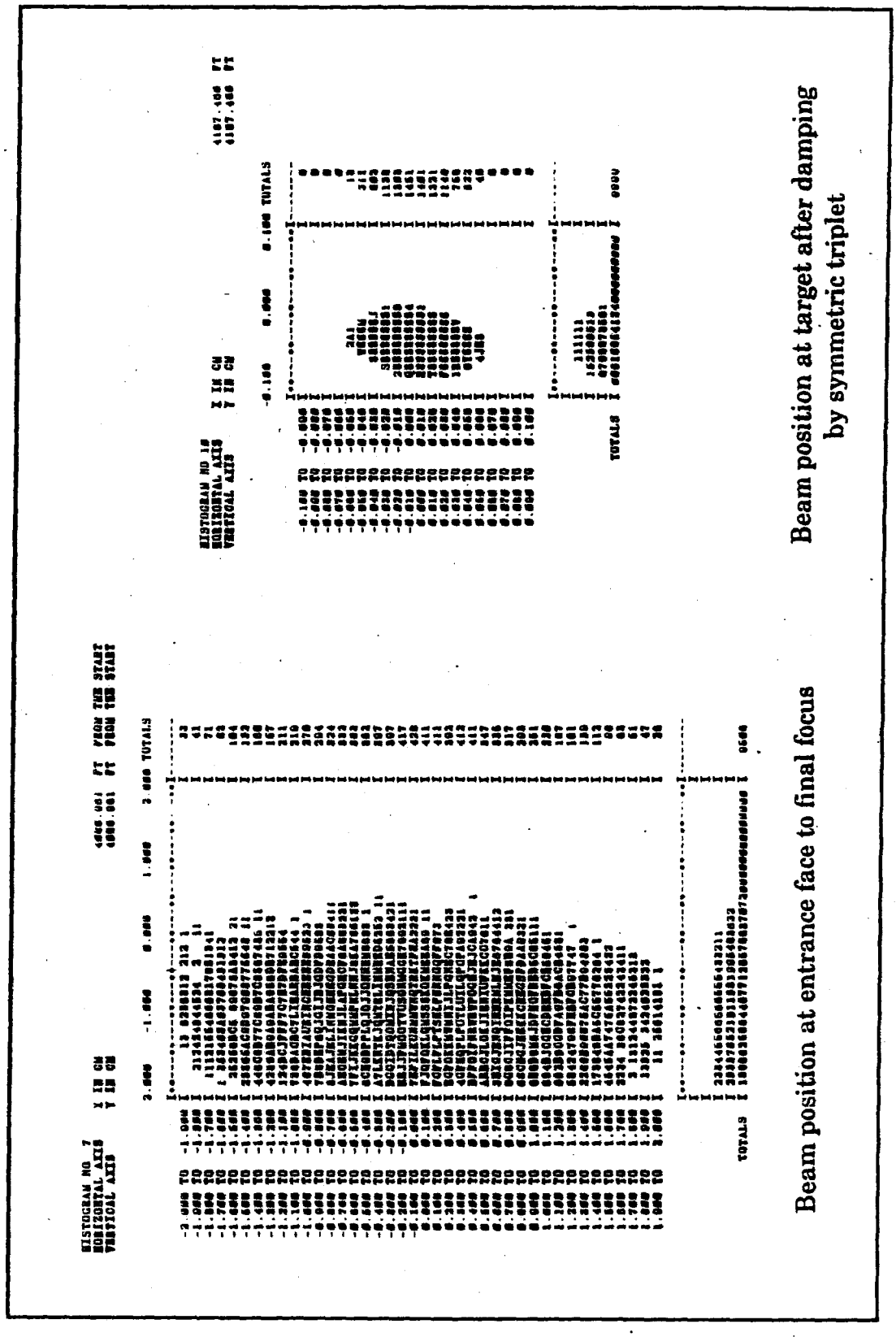

Fig 4.1.4c: Instability from .1% PS fluctuation on bend string 650 feet from target.

The strategy for controlling the 120 GeV beam will be to maintain position control upstream of the final focus to an accuracy of about 50 μm. This then should provide position stability within a few microns at the target. Careful control of power supply regulation and instrumentation calibration will be required. Precision control of the beam centroid at the primary target should be feasible.

4.1.6 Beam Halo

Muons from upstream sources can create a significant background for the KAMI detector if not carefully controlled. CASIM studies, as detailed in Section 4.2.8, have modeled the effects of primary beam halo, with results indicating the need to maintain an incident halo rate of less than 10^{-6} muons per primary proton.

The target sweeping magnet and beam dump are quite efficient for removing muons incident in the central region of the magnets. Rejection is considerably reduced for incident particles in the outer steel return legs, where the magnetic sweeping is reversed. Additionally, little effect will be seen for muons which largely miss the dump sweeping system.

The best approach for controlling muon halo is careful control of the primary beam, preventing interactions along the beam transport. Previous efforts of producing low halo primary beams at Fermilab have successfully reached integrated halo levels of about 10^{-6} μ/p.[5] Designs have been projected using detailed modeling studies for levels of less than 10^{-7} μ/p.[6] Other considerations are maintaining a good beam transport vacuum to reduce residual gas interactions, large magnet apertures, sweeping with large bend strings, and non interactive beam position monitors.

Detailed design to minimize muon halo in the KAMI primary beam transport will be be initiated after final selection of beam line for siting the

---

5 Fermilab E613.

6 *An Econodump Design for the Fermilab Direct Neutral Lepton Facility*, Fermilab TM-1415 (1986).

kaon program. However, some general considerations can be qualitatively projected, using a KAMI location in the NMUON area as a model. The most fundamental source of beam halo is the extraction septa, required for the resonant extraction process. Projections are that extraction losses at the percent level will be experienced.[7] A major advantage for KAMI is that the extraction loss occurs far upstream, with the opportunity for significant cleanup along the beam transport.

Relatively large aperture elements of the existing Main Ring will be used to transport the primary extracted beam to A0, where link up is made with the new dedicated 120 GeV beam line. A significant advantage of this line compared to the existing Switchyard is that electrostatic septa are not required.

Projections for beam vacuum requirements in the external transport line are for 10^{-4} Torr, compared to present levels of a few times 10^{-3} Torr. The largest background source is expected to be the carbon steel berm pipes, enabling beam transport between primary beam enclosures. Additional studies need to be carried out to determine whether some of the most downstream existing pipes must be replaced with stainless steel. At present, this is not projected.

Beam instrumentation throughout the 120 GeV primary line will need to be non-interacting, unlike the SWICs currently in use throughout the external beam areas. [More than 10^{-3} of the beam interacts in a typical SWIC]. Beam position monitors used in the Switchyard beam lines should be viable for KAMI use.

A major advantage of the NMUON line for a clean KAMI primary beam is the series of quad enclosures upstream of the experimental hall. These have very large aperture 4Q120 quads, along with a total of hundreds of meters of berm pipe surrounded by dirt between the enclosures. Hence, there should be significant ranging of halo muons which are outside the narrow cone of the pipes, especially for the reduced momentum 120 GeV

---

[7] C. Moore & S. Childress, *Physics at Fermilab in the 1990's*, Breckenridge, CO., (1989).

primary beam. More central muons, which transmit through the pipes, can be effectively rejected by the dump sweeping system.

4.1.7 Instrumentation

Primary beam instrumentation requirements for the Kaon program are set by the stringent needs of minimal beam halo and precision beam stability. These needs seem best met using the beam position monitors developed for the Switchyard external beam system. The detectors are non interacting parallel plate pickups tuned to the machine RF frequency. It should be recalled that approximately 10% of the RF modulation will be maintained in the debunched beam.

For 3×10^{13} protons/pulse the inherent resolution of the primary beam centroid measurement should be about 10 microns, using beam detectors of existing design with a 10 Hz sample rate. Prototype detectors have been tested with an improved gain and 5 times better signal to noise ratio.[8] A significant effort will be required to understand and maintain electronic stability at this level. Previous measurements in high intensity Switchyard beams have achieved monitoring precision at a level of 50 microns.

SWIC profile monitors of existing design will be useful for beam studies, but must be retracted from the beam during data collection. Additionally, beam loss monitors of existing design can be used to monitor beam loss to a level of 10^{-6} of the $\bar{p}$ primary intensity. Scintillator telescopes along the beam transport can extend this monitoring precision to a level of 10^{-8}.

R&D efforts need to be carried out for development of precision monitors which can provide independent confirmation of targeted beam position to an accuracy of a few microns. These need not be non-interacting, but can provide precision calibration on non data pulses. Possibilities include fibre probes and flying wire monitors.

---

[8] Q. Kerns, private communication.

4.2 Secondary Beam

In this Section we describe the design of a secondary neutral kaon beam for the KAMI facility. The formation of the secondary beam involves four elements; a production target, sweeping magnets to remove charged secondaries, collimators to define the neutral beam, and a beam dump for the uninteracted primary protons. The design goal is to make the facility flexible for the full range of high precision and high sensitivity experiments, and to utilize the full intensity available at the Main Injector. Specifically, the following issues were considered:

1) *Muon Flux* - At high beam intensities, detector singles rates are important, especially for the large photon veto system. Muons from the decay of pions produced in the beam dump or near the target could be the dominant contribution. The magnets used to separate the charged secondaries from the neutral beam must simultaneously sweep most of the muons away from the detector.

2) *Target Heating* - A beam intensity of 3×10^{13} protons per spill will test the limits of target technology. While a point-like target is ideal for most experiments, a larger target is preferable for reasons of thermal and mechanical stability. The design must strike a balance between these conflicting considerations.

3) *Beam Dump Design* - A conventional beam dump for 3×10^{13} protons per spill would use a low Z core to spread the heat load. Spreading the shower however means that pions have a longer distance in which to decay, resulting in increased muon production. In addition, increased lateral shower size means that more soft shower debris gets back into the neutral beam. The KAMI beam dump design must use absorber of the highest possible Z to minimize muon flux and maximize shower containment. Also, since the thermal load on the beam dump will cause it to expand and contract, the dump must be thermally and mechanically isolated from the

precisely aligned components that will define the neutral beam apertures.

4) *Variable Beam Solid Angle* - High sensitivity experiments will require large beam apertures for rate, while high precision experiments like ε'/ε will require sharply defined beams. The design must provide a mechanism for changing the beam defining apertures and must accommodate beams up to at least 12 μstr.

5) *Variable Targeting Angle* - The targeting angle affects the kaon flux and the neutron to kaon ratio. The optimum targeting angle may be different for each experiment. The design should allow variation of target angle from 10 to 30 mrad.

6) *K_S Option* - The KAMI facility can also be used to study the decays of K_S. The secondary beam design should allow for conversion into this mode.

7) *Charged Beam Option* - Although the primary focus of this report is the physics of K^0 decays, a charged kaon beam is also an option. The design should not preclude conversion to a charged beam. (See Appendix A.)

4.2.1 Layout

The elements of the neutral beam are illustrated schematically in Fig. 4.2.1. The primary beam is initially pitched down. It strikes the production target located at the upstream end of a sweeping magnet which bends positives down. The targeting angle and the magnetic deflection combine to help separate the primary beam from the neutral beam. The uninteracted primary beam passes out through a slot to the beam dump. The beam dump is located in a second sweeping magnet which bends horizontally. The neutral beam is initially defined by a tapered collimator that fills the gap of the target sweeping magnet. The neutral beam then passes through the beam dump magnet above the beam dump to the

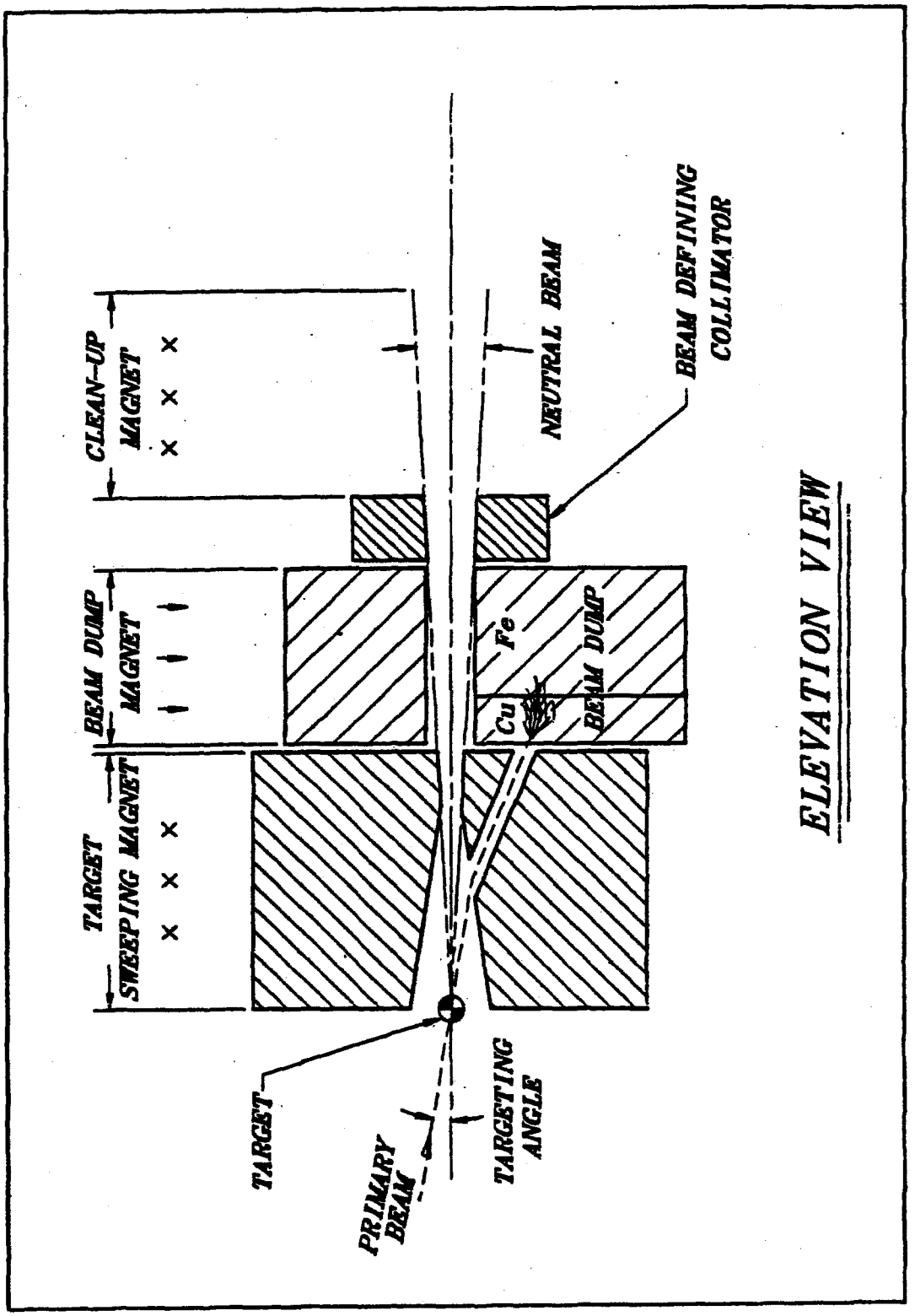

Fig. 4.2.1: Schematic illustration of KAMI secondary beam.

defining collimator. Additional cleanup magnets follow the defining collimator. Both collimators are removable to facilitate reconfiguration of the neutral beam(s).

A notable feature of this design is the use of separate magnets for the target and beam dump. This is crucial for muon sweeping. Figure 4.2.2 illustrates the problem. In order to dump the beam cleanly, it is desirable to separate the protons from the neutral beam as much as possible. This is accomplished by moving the dump downstream. Muons of both signs however are produced in the beam dump, initially following the direction of the proton beam away from the detector. Positive muons continue to be bent further away from the apparatus, but negative muons are initially bent back toward it. Rotating the B field orientation by 90° at the beam dump causes muons of both signs to continue to be bent away from the apparatus. An additional virtue of the two magnet design is that the beam dump is naturally isolated from both beam defining collimators. A plan view of the physical elements of the neutral beam is presented as Fig. 4.2.3.

4.2.2 Secondary Particle Yields

The optimization of the neutral kaon beam involves the choice of target size and material, targeting angle, and the selection and placement of filters. Each of these affects the kaon rate and backgrounds. The yield of secondary kaons, as well as background photons and neutrons, was calculated as a function of targeting angle and for a selection target materials and filter configurations. The results are summarized in this Section. The closely related issue of thermal and mechanical constraints on the choice of target material is dealt with in the following section.

The empirical formulation given by Malensek[1] of data of Atherton, *et al.*[2], is a standard reference for secondary particle production from thick

---

1 A.J. Malensek, Fermilab FN-341, (1981).

2 H.W. Atherton, *et al.*, CERN 80:07, (1980).

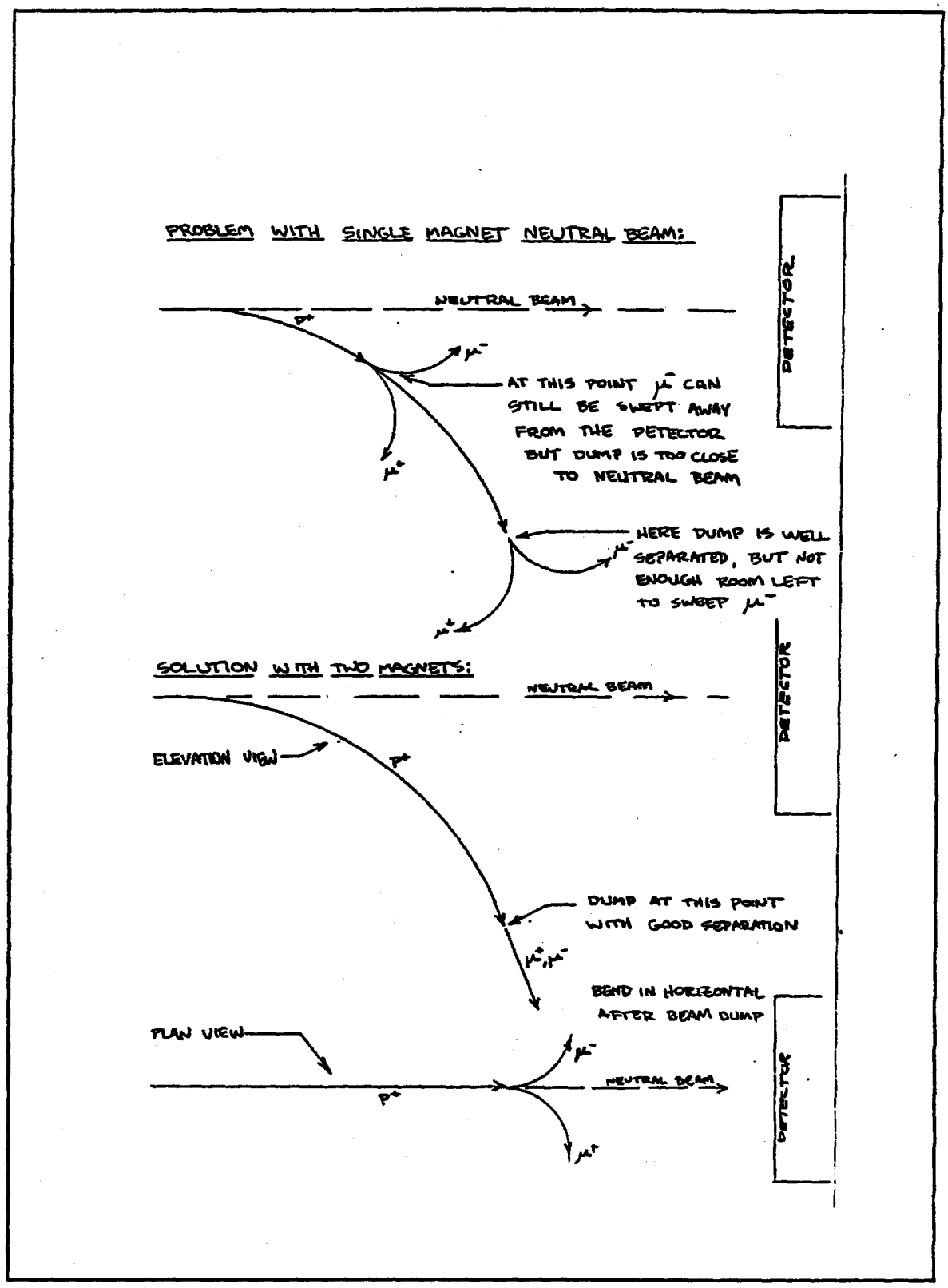

Fig. 4.2.2: Justification for separate beam dump and target magnets.

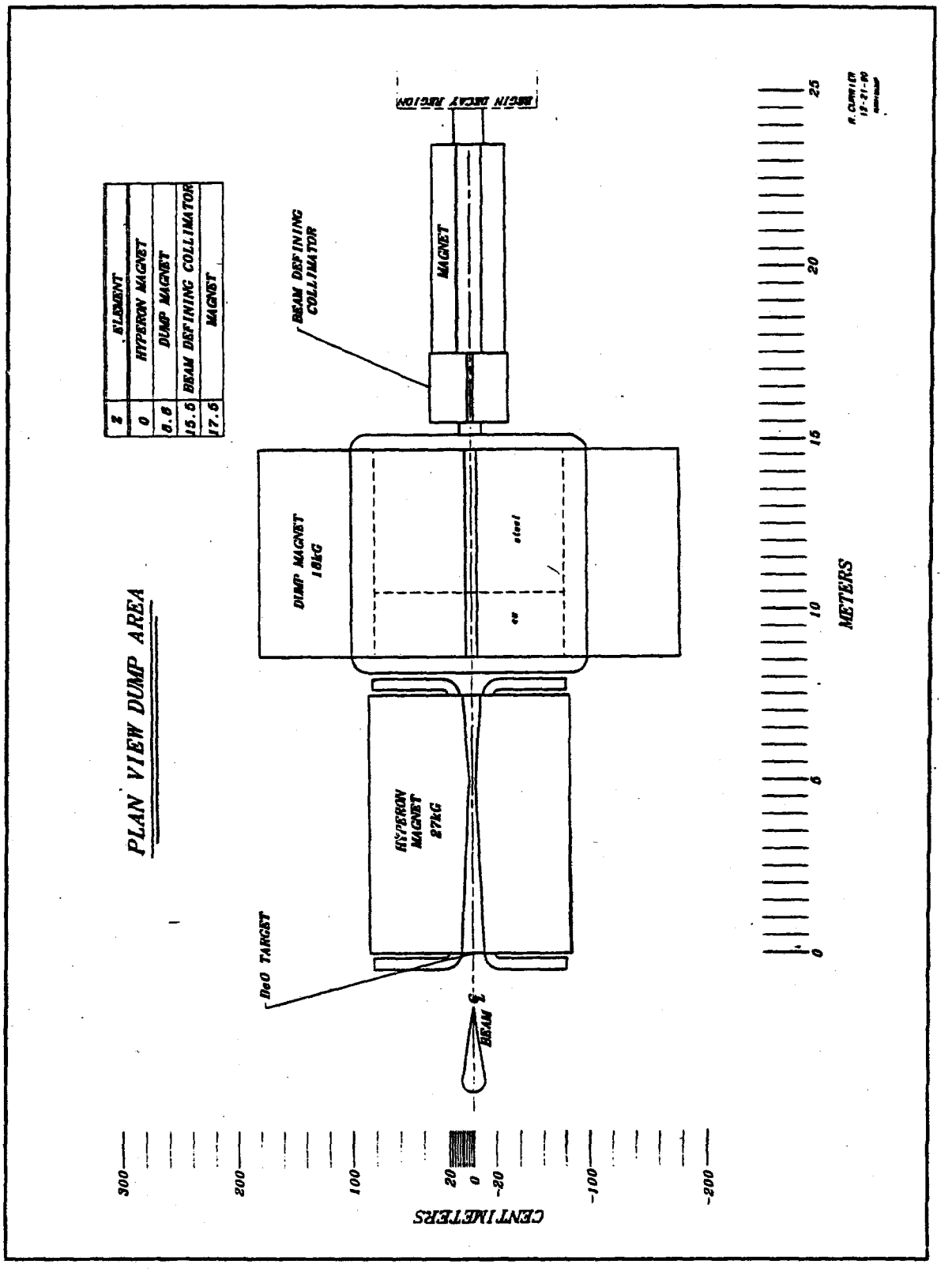

Fig. 4.2.3: Plan view of target / beam-dump area.

targets. We have used the Malensek formula to determine the kaon production rate for a Be target. The neutron flux was obtained from Edwards, *et al.*[3] . In order to consider more complicated issues such as target A-dependence (the Malensek formulae are given for Beryllium only) and photon production (for which showering in the target is important at high Z) the yields were also calculated using GEANT[4].

To check the equivalence of the two approaches, GEANT yields were compared to the Malensek and Edwards results for a 50 cm Be target at a production angle of 22 mrad. The comparison is shown in Fig. 4.2.4. There is relatively good agreement for π^+, π^-, K^+, and K^-, but there is a significant disagreement for protons and neutrons. Since the Malensek and Edwards results agree with kaon and neutron rates from previous Fermilab experiments[5] , we have not used GEANT results for absolute neutron flux estimates. GEANT neutron results have been used only to study relative effectiveness of filtering schemes.

Comparison of Targeting Angles

Using the Malensek parameterization for K_L and the Edwards parameterization for neutrons, we have studied the relative yields of K_L versus neutrons as a function of target angle. The calculation assumes a 50 cm Be target, a 45 cm thick Be filter to enhance the n/K ratio, and a 8 cm thick Pb filter to reduce the photon component of the beam. The result is shown in Table 4.2.1. The conclusion is that by using a targeting angle of 24 mrad, a factor of 22 improvement is attained in the ratio of K_L to neutrons. The cost of this improvement is a factor of 2.6 in K_L flux per proton. Figure 4.2.5 shows the Kaon momentum spectrum for a 24 mrad targeting angle.

---

3 Edwards, *et al.*, *Phys. Rev.* D18, 76 (1978).

4 *GEANT3 User's Guide*, CERN DD/EE/84.

5 E731, E621.

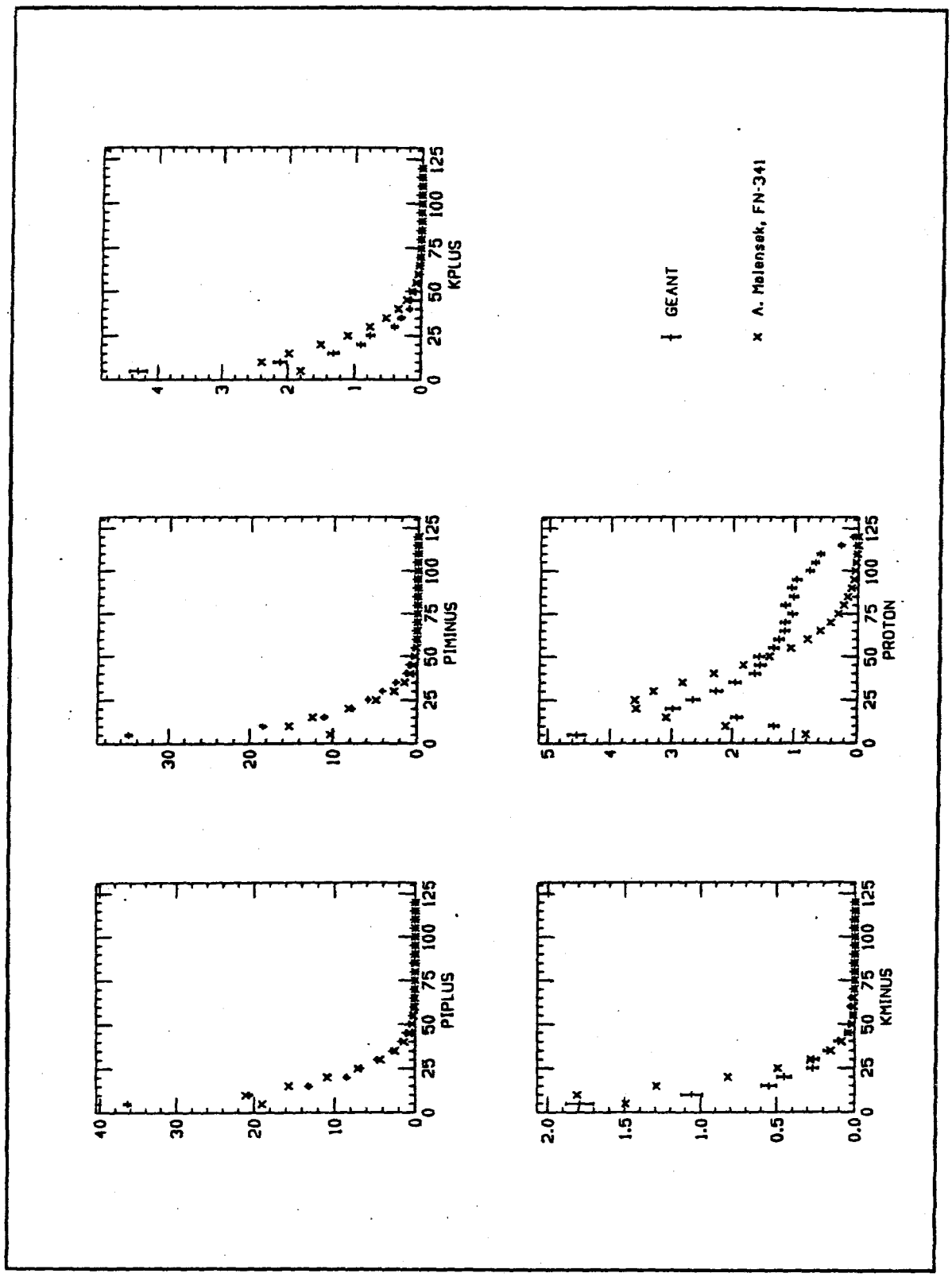

Fig. 4.2.4: Comparison of Malensek secondary particle yields to GEANT results.

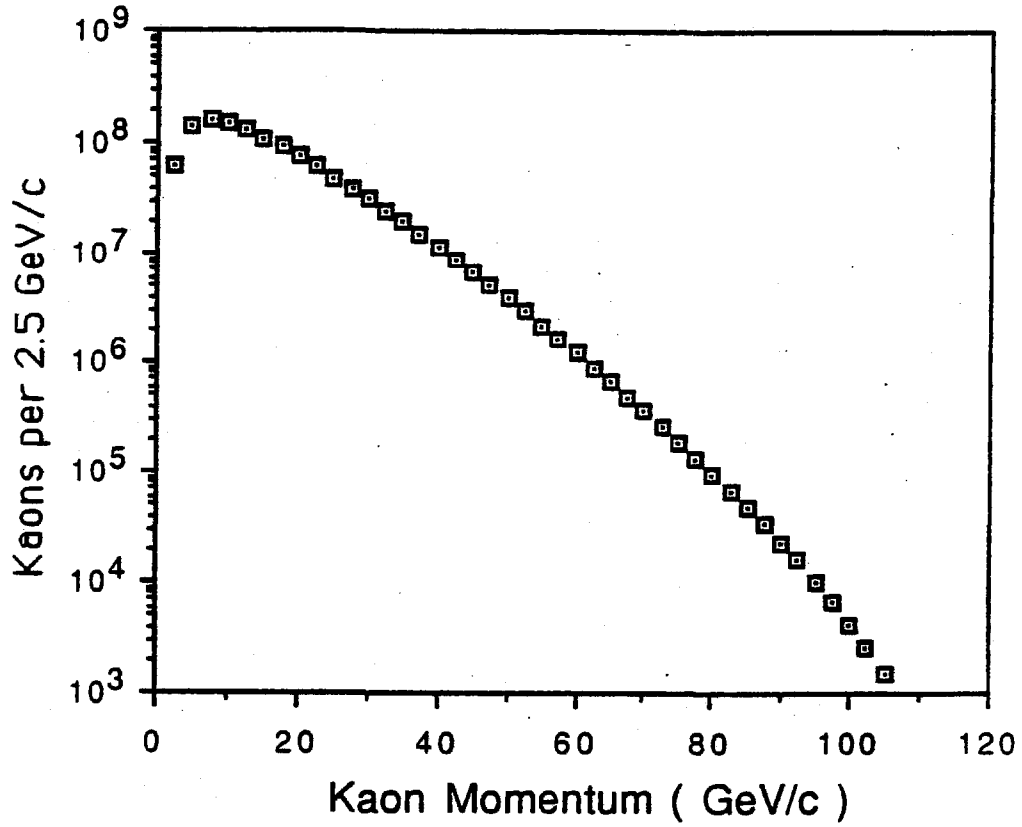

Fig. 4.2.5: Kaon flux per 2.5 GeV assuming 3×10^{13} protons on a 50 cm target, 12 μstr beam, at 24 mrad targeting angle, including absorbers and filters.

θ target	0 mrad	8 mrad	16 mrad	24 mrad	32 mrad
K_L	1024	816	557	401	306
n	15170	2938	655	275	151
n/K_L	14.8	3.6	1.2	0.68	0.49

Table 4.2.1: K_L and neutron yields as a function of targeting angle for 12 μstr beam normalized to 10^{13} protons on a 50 cm Be target. All entries × 10^6

Comparison of Target Materials

For the production angle interval 20 mrad < θ < 24 mrad, Table 4.2.2 shows the K_L, γ and neutron fluxes predicted by GEANT for a selection of targets. Yields are normalized to 10^{13} protons on a 5 cm target and a 3 μstr channel. No filters are included. The most striking feature is the very large photon flux produced with the high Z targets. Clearly, a low Z target is favored, either Be of BeO. The table shows that BeO yields 35% more neutral kaons per proton on target with about the same background fraction.

	Be	BeO	Cu	W	U
γ	93	133	2268	3800	5000
K_L	4.1	5.6	10.6	13.2	11.8
n	15	21	44	135	135
n/K_L	3.69	3.75	4.2	5.98	11.4
γ/K_L	22.6	23.6	215	288	424

Table 4.2.2: GEANT Particle Yields Normalized to 10^{13} Protons on a 5 cm target and 3 microsteradians neutral beam. All entries × 10^7

Filters

The photon contamination in the beam will increase drift chamber current due to conversions. To reduce this effect, it will be necessary to introduce a lead filter of the order of 15 radiation lengths in the neutral beam. Since the filter will be a source of hadronic interactions, careful choice of its location may be critical. If the filter is located close to the

target, it will be exposed to a substantial flux of charged particles from the target. Figure 4.2.6 shows a z-distribution of particles leaving the upstream section of the neutral channel to illustrate this. Locating the filter closer to the channel neck will reduce this source of hadronic background.

Another issue is alignment. The filter should be just large enough to cover the neutral beam. Any additional area outside the neutral beam will be a source of hadronic interactions but will have no effect on photon flux. If the filter is very close to the target, it is small and must be very precisely aligned. If it is located closer to the channel neck, it will be larger and the alignment relatively simpler.

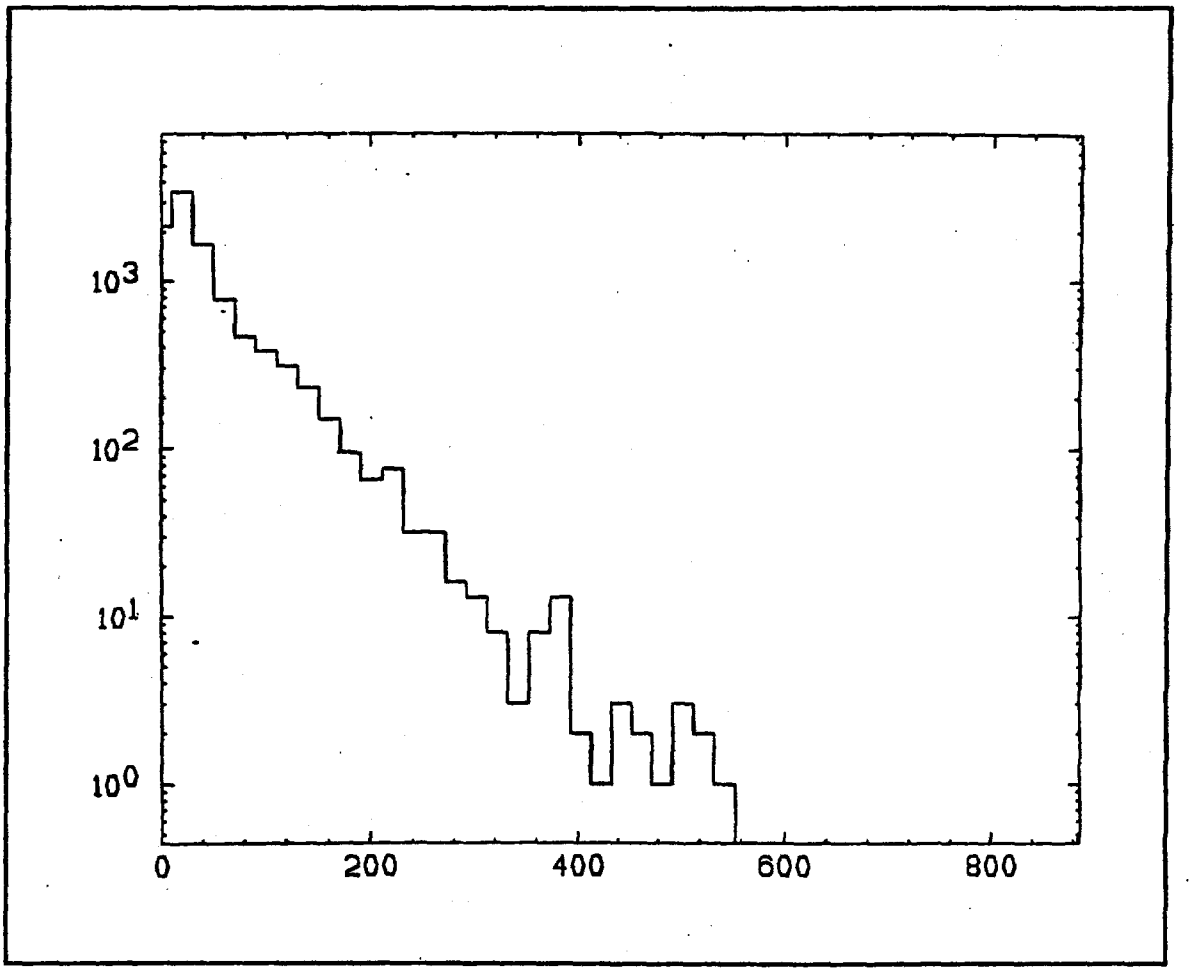

Fig. 4.2.6: Z distribution of particles leaving neutral channel.

4.2.3 The KAON Target

At Main Injector beam intensities, target heating will be a serious issue. In the previous section it was shown that a low Z target is important to minimize photon backgrounds in the neutral beam. Be and BeO emerge as candidate materials with comparable background rates. BeO is favored because because the kaon yield is 35% higher. In this Section, we consider the thermal and mechanical issues, and show that BeO is also favored because of superior thermal properties.

Figure 4.2.7 shows the target support which is modeled after an existing CERN design[6]. A 1 mm diameter, 8 cm long BeO rod is suspended between thin aluminum squares. A second target, 3 mm in diameter by 50 cm long is also shown. The targets will be cooled via forced convection and radiation. Helium gas at a flow rate of 4 m/sec perpendicular to the target is used for the convection mechanism. For the 1 mm target and 4 m/sec, helium has a convection coefficient of 0.008 cal/cm^2 sec ^{o}C. For radiation an emissivity of 0.25 is used. The energy deposition in the target was calculated using CASIM[7]. Because the diffusion time for heat in a 1 mm BeO rod is small compared to the spill time (6 msec / 1 sec), the target will heat uniformly. Both the so called "dynamic" stresses (shock) and the "quasi-static" stresses (due to a non-uniform temperature within) are negligible. Thus melting and not fracturing is the main issue and it is only necessary to consider the average energy deposition.

Assuming a one second spill every three seconds, and using an average energy deposition of 0.4 GeV/cm^3 obtained from CASIM for 3×10^{13} protons at 120 GeV, the temperature of the target as a function of time was calculated. A steady state is attained after about ten pulses. Figure 4.2.8 shows temperature versus time after the steady state has been achieved. A

---

6 R. Bellone, A. Ijspeert, P. Sievers, *Targets for High Intensity Beams at CERN: Design, Operational Experience and Developments*, CERN 86/ST/TE/A/113, June 1986.

7 CASIM, A. Van Ginneken & M. Awschalom, *High Energy Particle Interactions in Large Targets*, (1975); A. Van Ginneken, Fermilab Report FN-272 (1975).

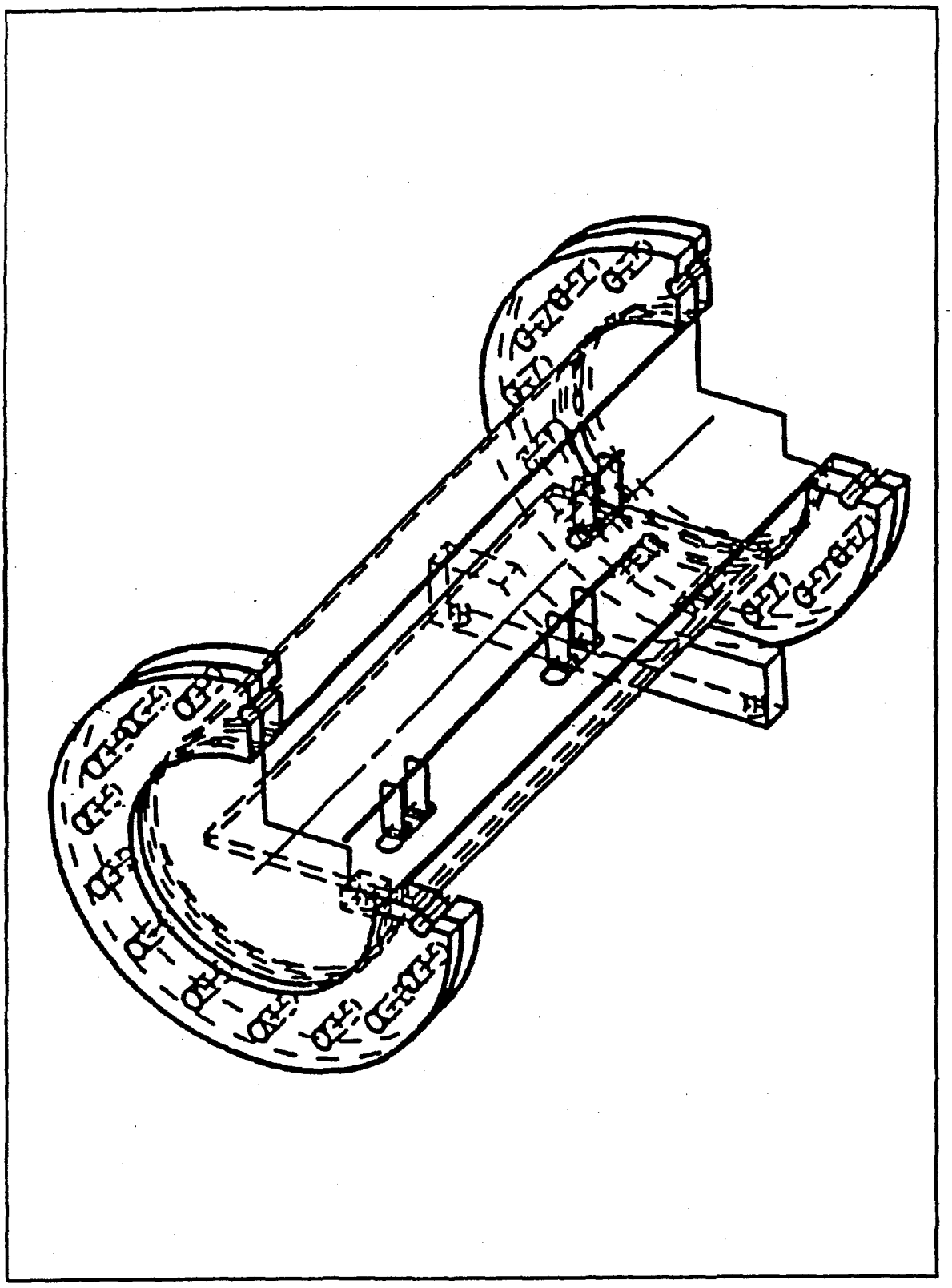

Fig. 4.2.7: Kaon target support.

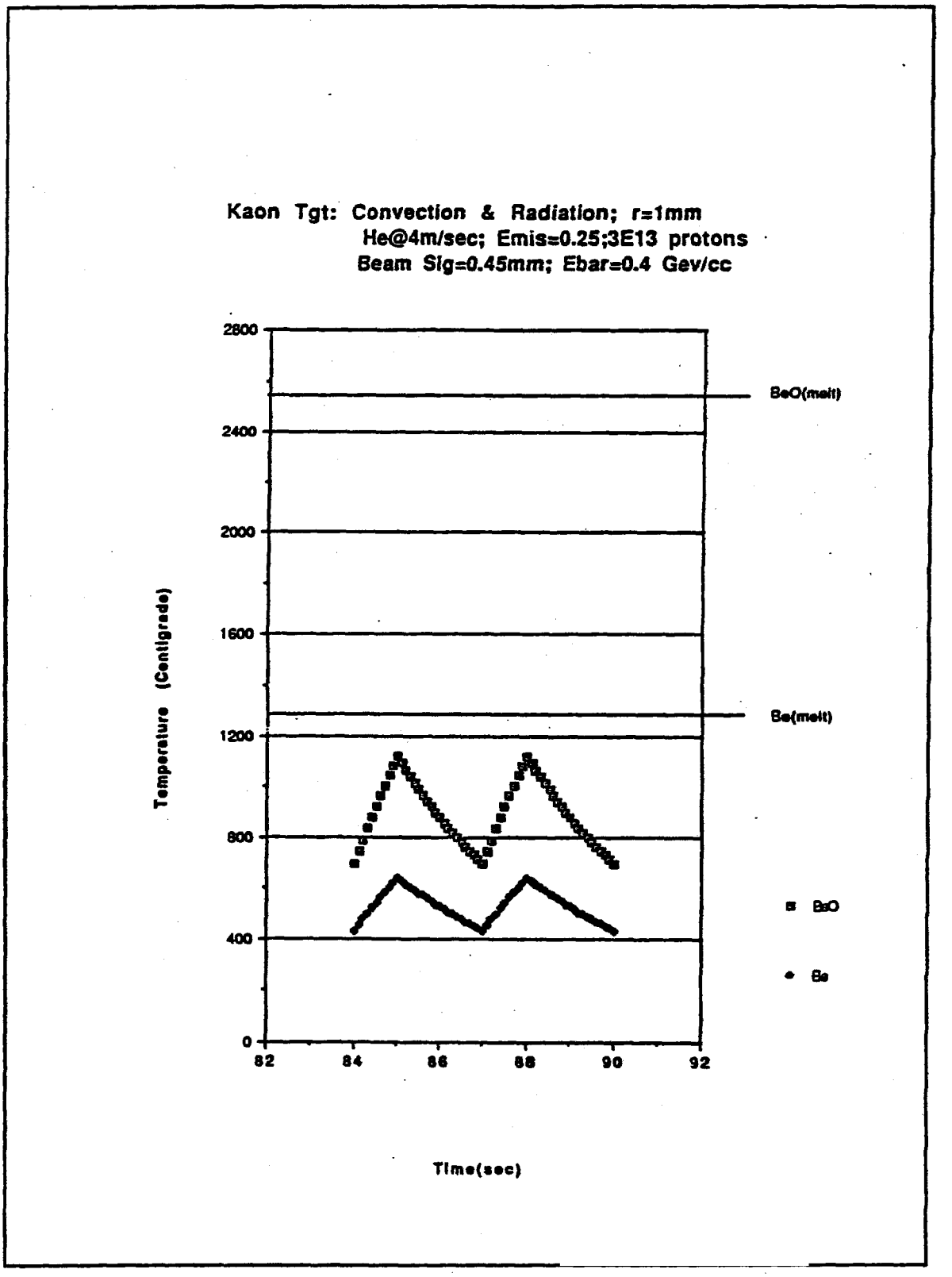

Fig. 4.2.8: Steady state target temperature as a function of time. Shown for both Be and BeO targets.

comparison between the peak temperature and the melting point for Be and BeO shows there is a comfortable safety margin and that BeO is the best choice.

4.2.4 Magnet Design

The Target Sweeping Magnet

The target sweeping magnet requires the largest practical field along its center axis. Its design, which allows for variation in the targeting angle, is based on the hyperon magnet used by experiment E497 which employs tapered pole tips to concentrate flux into a small gap region. Figure 4.2.9 shows the construction of the magnet. The field was calculated using POISSON[8]; Fig. 4.2.10 shows the resulting plot of field lines. Assuming a 10 cm gap and the same coil specifications as the E497 hyperon magnet, a 27 kGauss field can be attained.

The Dump Magnet

The beam dump magnet is a conventional "H" dipole, shown in Fig. 4.2.11. The beam dump is located in the gap of this magnet filling most of the volume with iron. This reduces the effective gap to 10 cm. An 18 kGauss field is easily obtained with relatively low power. The POISSON field simulation is shown in Fig. 4.2.12.

Defining Collimator Clean-up Magnets

There are no specific constraints on the design of these magnets. They are intended to provide a clean-up field to sweep soft particles produced in the defining collimator. Conventional magnets could be used. The available space will accommodate 2 standard BM-109's.

---

8 The CERN-POISSON Program Package (POISCR).

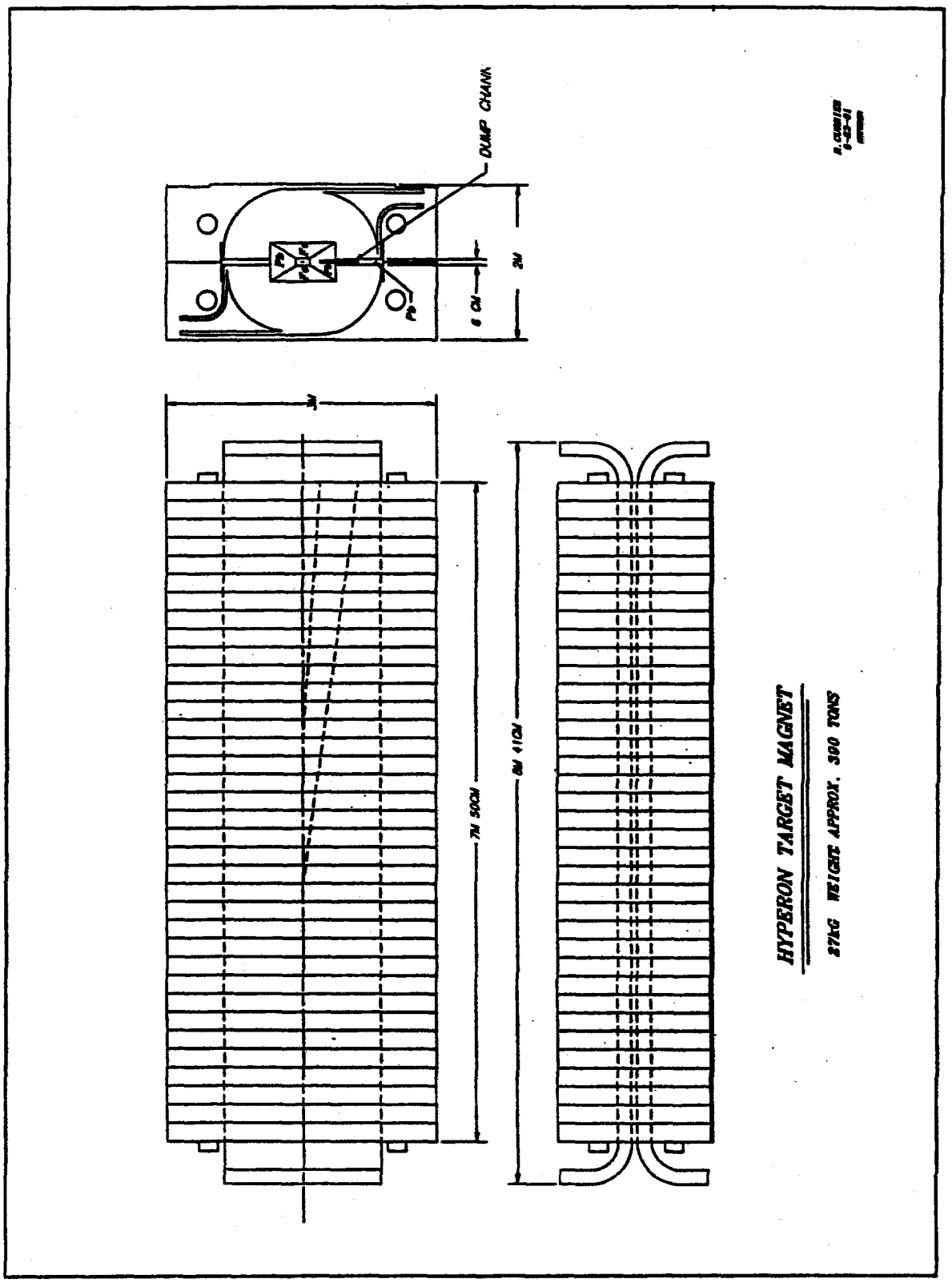

Fig. 4.2.9: Cross section of target sweeping magnet.

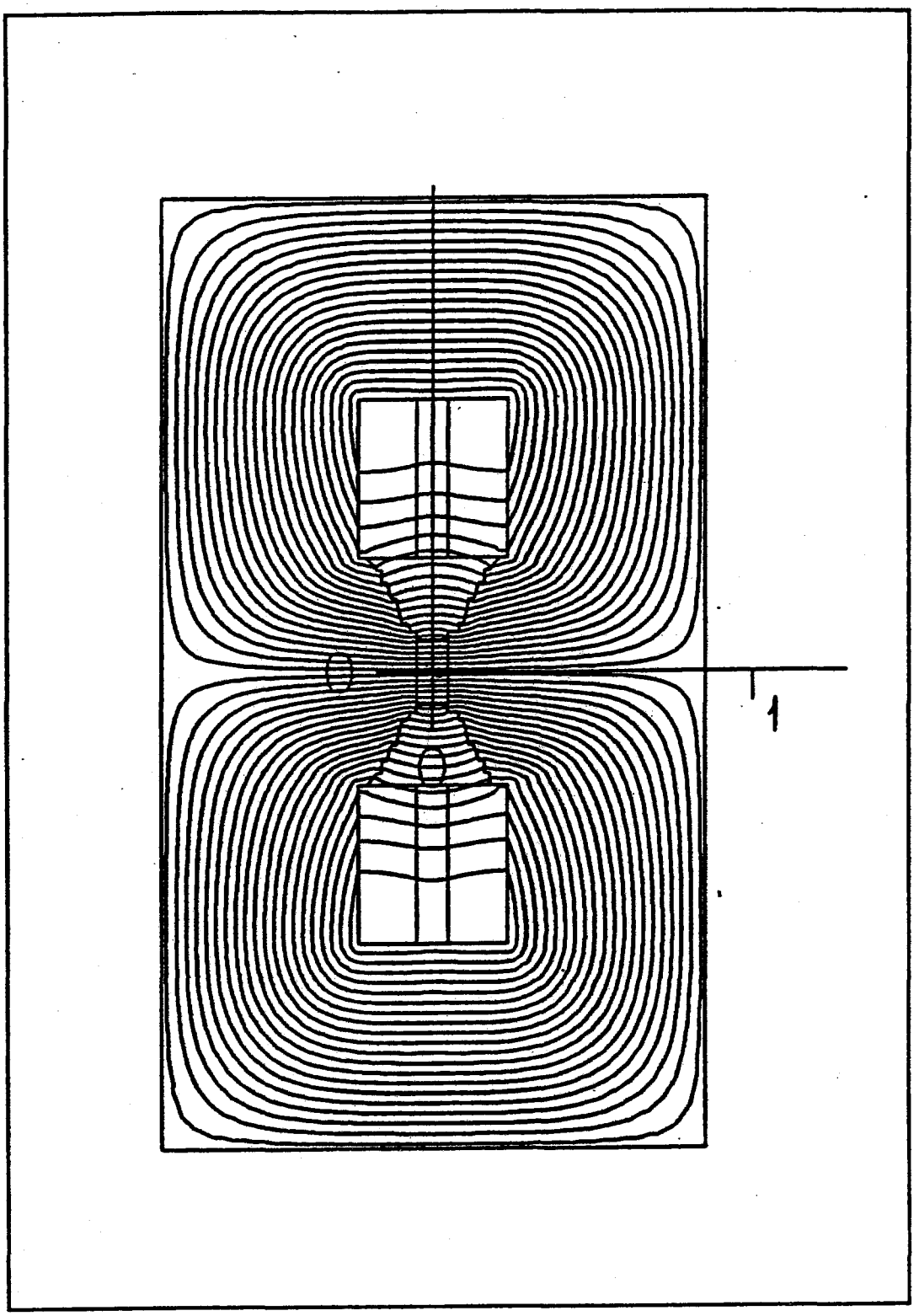

Fig. 4.2.10: Poisson generated plot of field lines for target magnet.

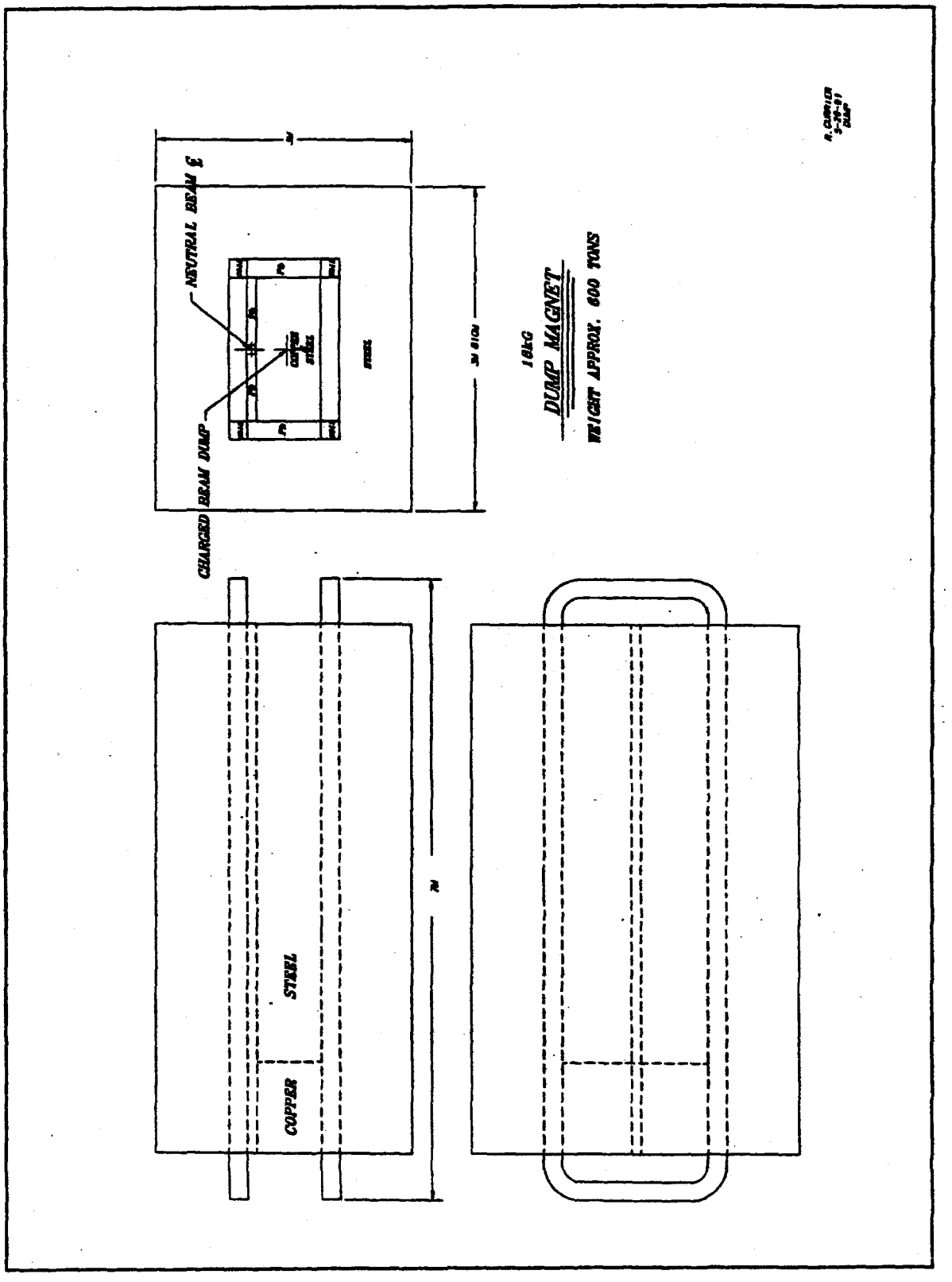

Fig. 4.2.11: Beam Dump magnet cross-section.

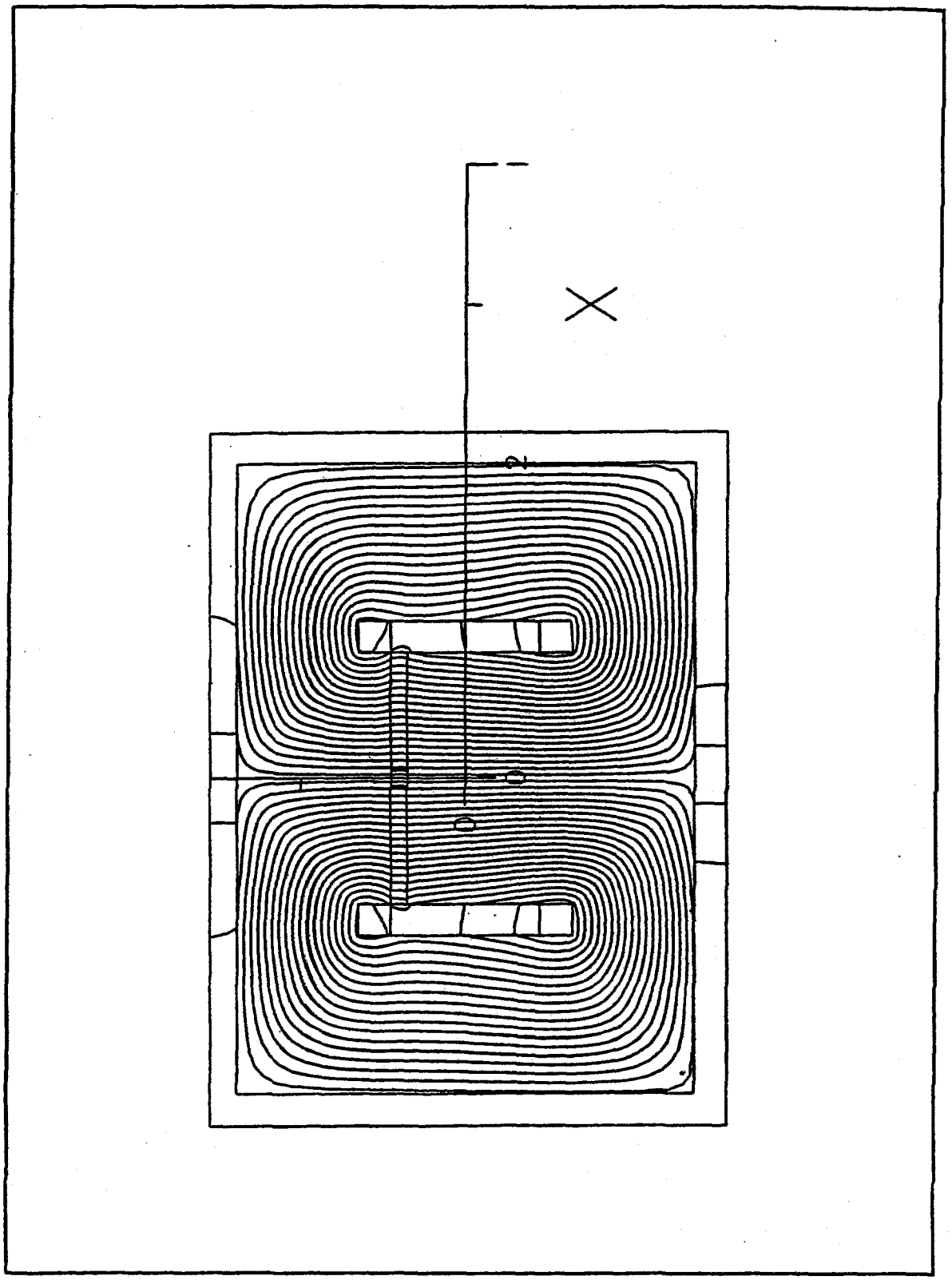

Fig. 4.2.12: Beam Dump magnet field lines generated by POISSON.

Radiation Hardness

Radiation hardness of the magnet coils for the target and dump sweeping magnets is a serious issue. The radiation doses for both magnets have been calculated using CASIM, and 5 year accumulated doses in the range 10^9 to 10^{10} rads are expected. Since most organic materials will break down in that range[9] the coils must be radiation hard, possibly employing ceramic insulators. The properties of the three magnets are summarized in Table 4.2.3 below.

	target sweeping magnet	beam dump sweeping magnet	defining collimator clean-up magnet
type	tapered-pole "hyperon magnet"	conventional "H" dipole	standard dipole (2) BM 109's
gap	10 cm	10 cm	20 cm
length	7.5 m	6 m	3.8 m
width	15 cm	10 cm	20 cm
field	27 kG	18 kG	18 kG
amp-turns	346,000	180,000	350,000
power	310 kW	140 kW	500 kW

Table 4.2.3. Magnet specifications for KAMI secondary beam.

9 Finley Markley, private communication.

4.2.5 The K_L Neutral Channel

The geometry of the neutral beam is fixed by the target and by a system of three collimators as shown in Fig. 4.2.13. Each collimator is a water-cooled, Hevimet block with a tapered rectangular hole. The first and second collimator blocks fill the aperture of the target sweeping magnet. The walls of the first collimator absorb the charged secondaries produced in the target. The second collimator provides the initial definition of the neutral beam. The final or defining collimator is located 15.5 m downstream from the target and is the limiting aperture of the beam.

To provide a simple description of the operation of the collimator system, we assume that the target is point-like, and that the second and third collimator apertures subtend exactly the same solid angle. The walls of the neutral beam defining collimators are tapered to point back to the target. If we denote the angle of the taper in x and y by β_x and β_y, respectively, then the beam solid angle is given by

$$\Delta\Omega = 4\beta_x\beta_y \qquad 4.1$$

To complete the description of the system requires specification of the z positions, z_1 and z_2, of the upstream ends of the two beam defining collimators, and the angles, α_x and α_y, of the tapered walls of the first collimator. Figure 4.2.14 illustrates our parameterization of the collimator system.

The choice of the parameters which describe these collimators is determined by three considerations. First, the neutral particles produced in the walls of the first collimator must have no direct line of sight through the defining collimator. Second, the first two collimator assemblies must fit between the pole tips of the target sweeping magnet. Third, charged secondaries produced in the target must be absorbed in the first collimator

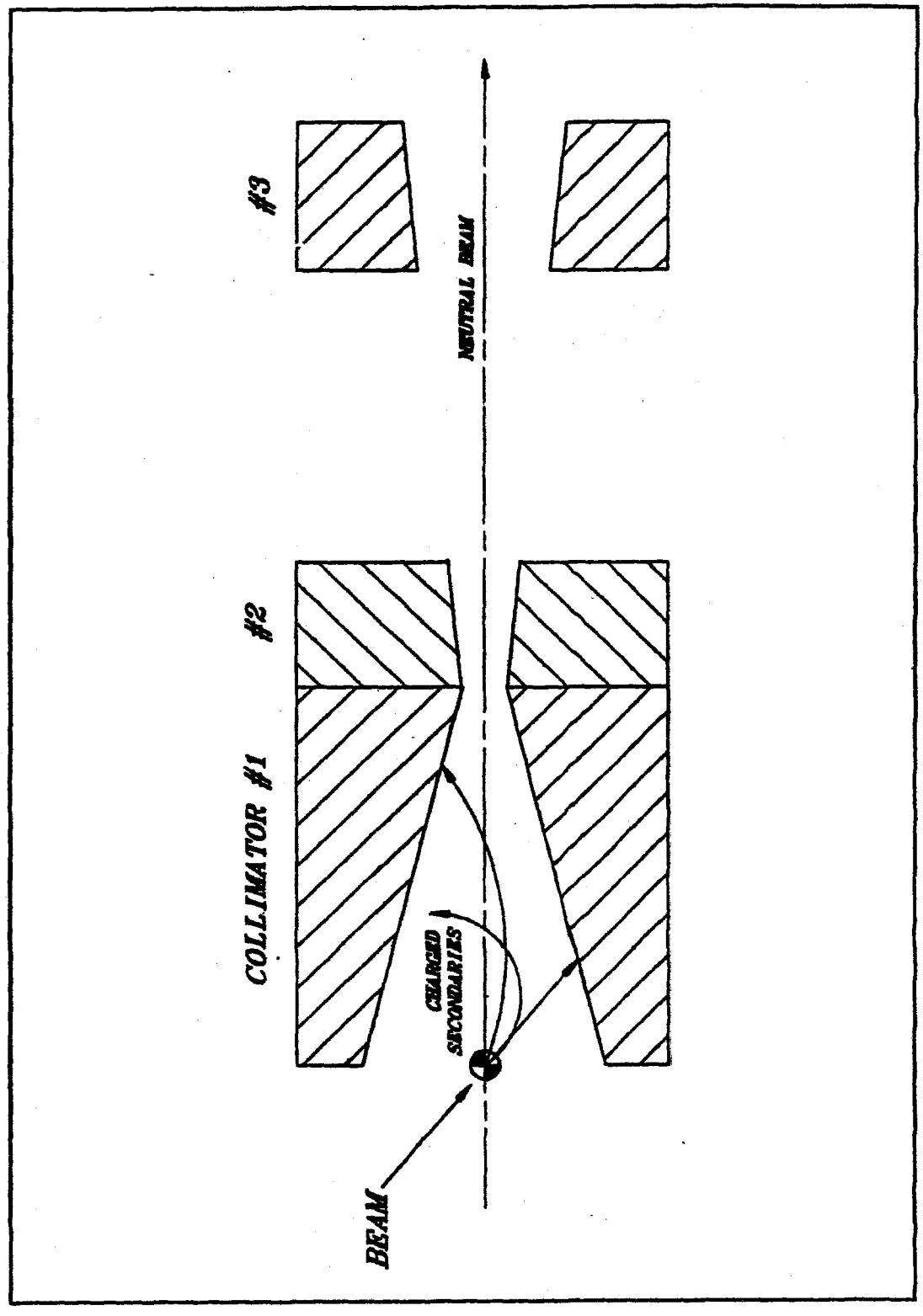

Fig. 4.2.13: Schematic representation of the neutral beam collimation scheme.

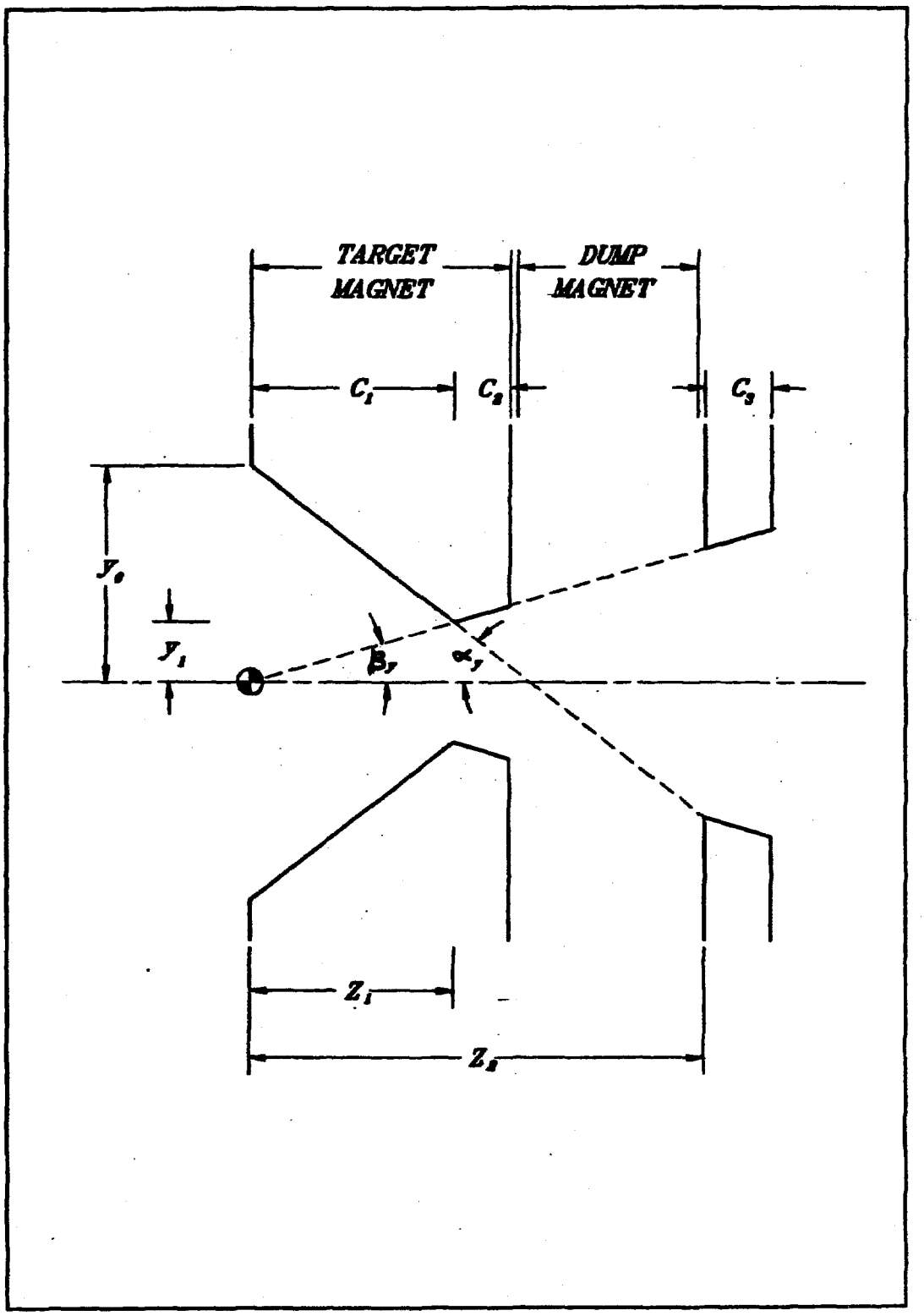

Fig. 4.2.14: Variables used to describe the collimators.

for all momenta and production angles. The first consideration fixes the values of α_x and α_y. If we take z_1 and z_2 to be fixed, it is straightforward to show that

$$\alpha_x = \frac{z_1 + z_2}{z_1 - z_2}\beta_x \equiv \rho\beta_x, \quad \alpha_y = \rho\beta_y \qquad 4.2$$

The second consideration fixes the largest allowed value of β_x. The half width, y_0 of the opening at the upstream end of the first collimator is given by

$$y_0 = z_1(\alpha_x + \beta_x) = z_1(1+\rho) \qquad 4.3$$

Since y_0 must be less than the magnet gap, g, we have that

$$\beta_x < g / 2z_1(1+\rho) \qquad 4.4$$

The third consideration determines the maximum value allowed for β_y. The situation is illustrated in Fig. 4.2.15. For negative secondary tracks with sufficiently large momenta, there is a pass band, or range of production angle, θ, such that the track is deflected enough to miss the lower wall of the first collimator enter the opening of the second collimator. These tracks will shower in the walls of the second collimator, which has a clear line of sight through the defining collimator to the experiment. For a given momentum, the boundaries of the pass band in θ are given by

$$\frac{z_1}{2R} - \beta_y < \theta < \left(\frac{2(\alpha_y + \beta_y)z_1}{R}\right)^{1/2} - \rho\beta_y \qquad 4.5$$

where R is the track radius of curvature, R = 33 p/B. There is a minimum momentum, P_{min}, for which the inequality is satisfied by only one critical production angle θ_c. For momenta less than P_{min} no transmission into

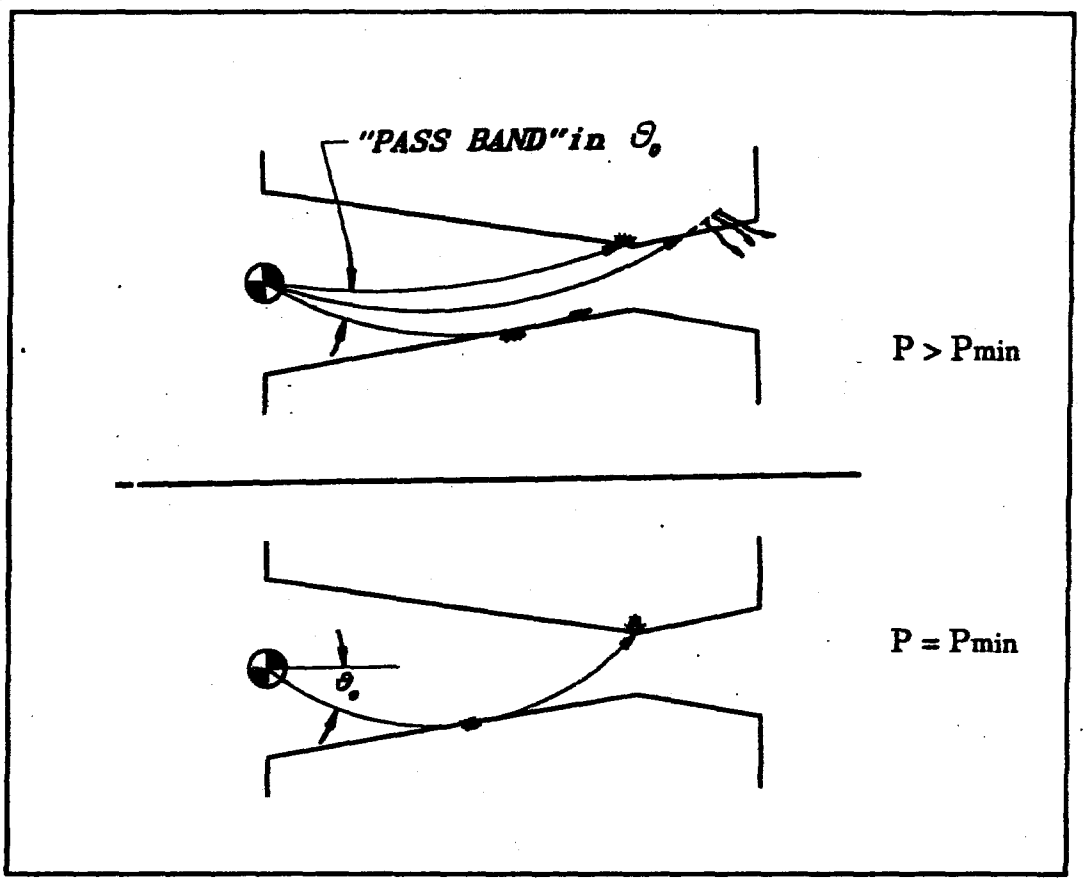

Fig. 4.2.15: Illustration showing high momentum negative tracks produced with very little $p_\perp$ deflected into the neutral beam collimator.

the neutral channel is possible. The pass band, P_{min}, and θ_c are illustrated schematically is Fig. 4.2.16. Using the previous approximation, P_{min} is given by

$$P_{MIN} = \frac{B z_1/66\beta_y}{\left[2^{1/2} + (1+\rho)^{1/2}\right]^2} \qquad 4.6$$

By setting P_{min} equal to the beam energy, it is possible to design a collimator that is completely closed to charged secondary tracks. The collimator is closed if β_y satisfies

$$\beta_y < \frac{z_1/2R_{120}}{\left[2^{1/2} + (1+\rho)^{1/2}\right]^2} \qquad 4.7$$

Where $R_{120} = 33\ P_{beam} / B$ is the radius of curvature of a beam energy track in the field of the target sweeping magnet. Taking $z_1 = 5.5$ m, $z_2 = 15.5$ m, B = 27 kGauss, and g = 10 cm, we find that $\beta_x = 2.93$ mrad and $\beta_y = 1.86$ mrad are the limits. This gives a maximum beam solid angle $\Delta\Omega = 21.8\ \mu$str.

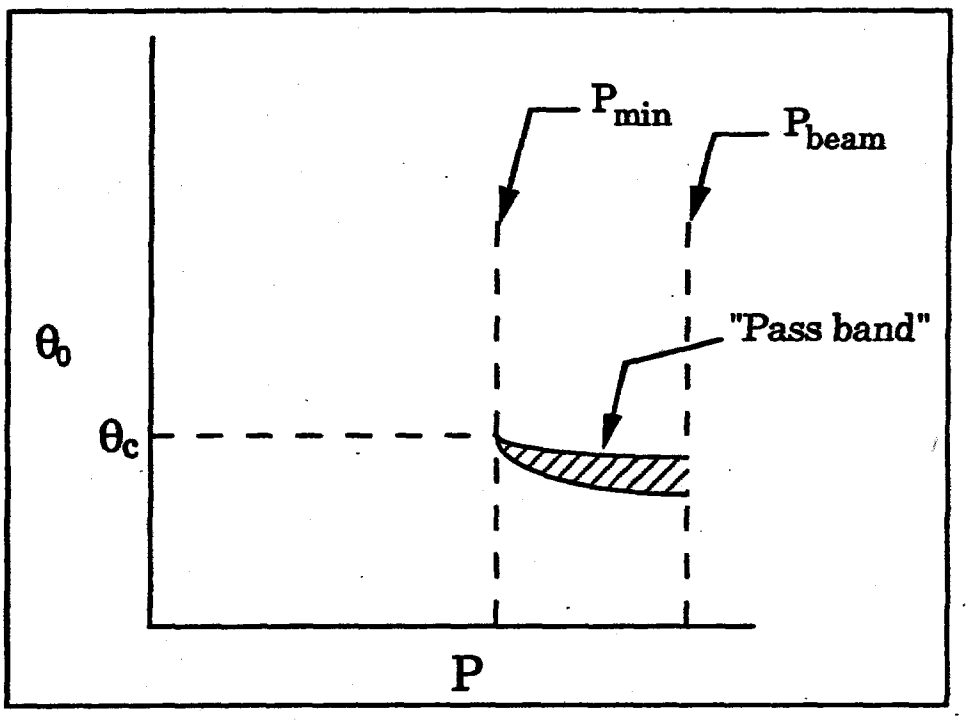

Fig. 4.2.16: Representation of pass band in the p - θ plane.

4.2.6 The KAON Beam Dump

There are three factors that govern the design of the primary proton dump. (1) Locate the dump inside a large magnet so that the muons created can be swept outside the detector. (2) Use high Z material so the hadron shower can be well contained. (3) Cool the section that receives the most power and make the rest simple and reliable.

Figure 4.2.17 shows the physical elements of the beam dump. The first section that intercepts the beam is a water-cooled copper block 20 cm horizontally by 75 cm vertically by 1 m long. This active section is of such a

weight and dimension that it can be removed for repair if necessary. On either side of the water-cooled piece are stationary copper blocks extending laterally out to the steel yoke. The vertical dimension is necessary to cover the two extreme possibilities of (a) the "hyperon magnet" off, and (b) the "hyperon magnet" on plus the initial angle onto the target of 30 mradians. A RAW (radioactive water) system with four parallel paths of 1/2 inch tubing will supply a total of 15 gallons/minute to remove the heat. The steel section in the core will be built as part of the magnet, will have the same cross-sectional dimensions as the copper, and will be 2 meters long. Making the copper section as short as possible and the iron as long as possible, insures that the largest B dl is available to bend muons produced in the dump away from the detector.

From the viewpoint of personnel radiation protection, one needs about 150 cm of Fe radially and 4.5 meters longitudinally from the center of where the beam dumps. The large magnet which surrounds the dump core exceeds all these dimensions. The iron shown outside just becomes part of the large magnet used to sweep dump muons away from the detector.

CASIM was used to obtain the local energy deposition as well as the total power in each section. Figure 4.2.18 shows an X vs. Z view of the dump, indicating the thermal loads in each region. Of most concern is the central core of copper followed by steel. The beam deposits roughly 130 kwatts into the copper section and about 30 kwatts in the downstream steel core.

Figure 4.2.19 shows the beam size as a function of Z position in the beamline. At the beam dump, the spot is about 6 mm across. Even if the focus of the beam spot ($\sigma \equiv 0.45$ mm) moved downstream from the target to the beam dump, the stresses and the temperature in the water cooled section are still acceptable. As long as the fast spill will not be taken on the dump, one can say that the temperature rise during the spill is well below the melting point of the metal.

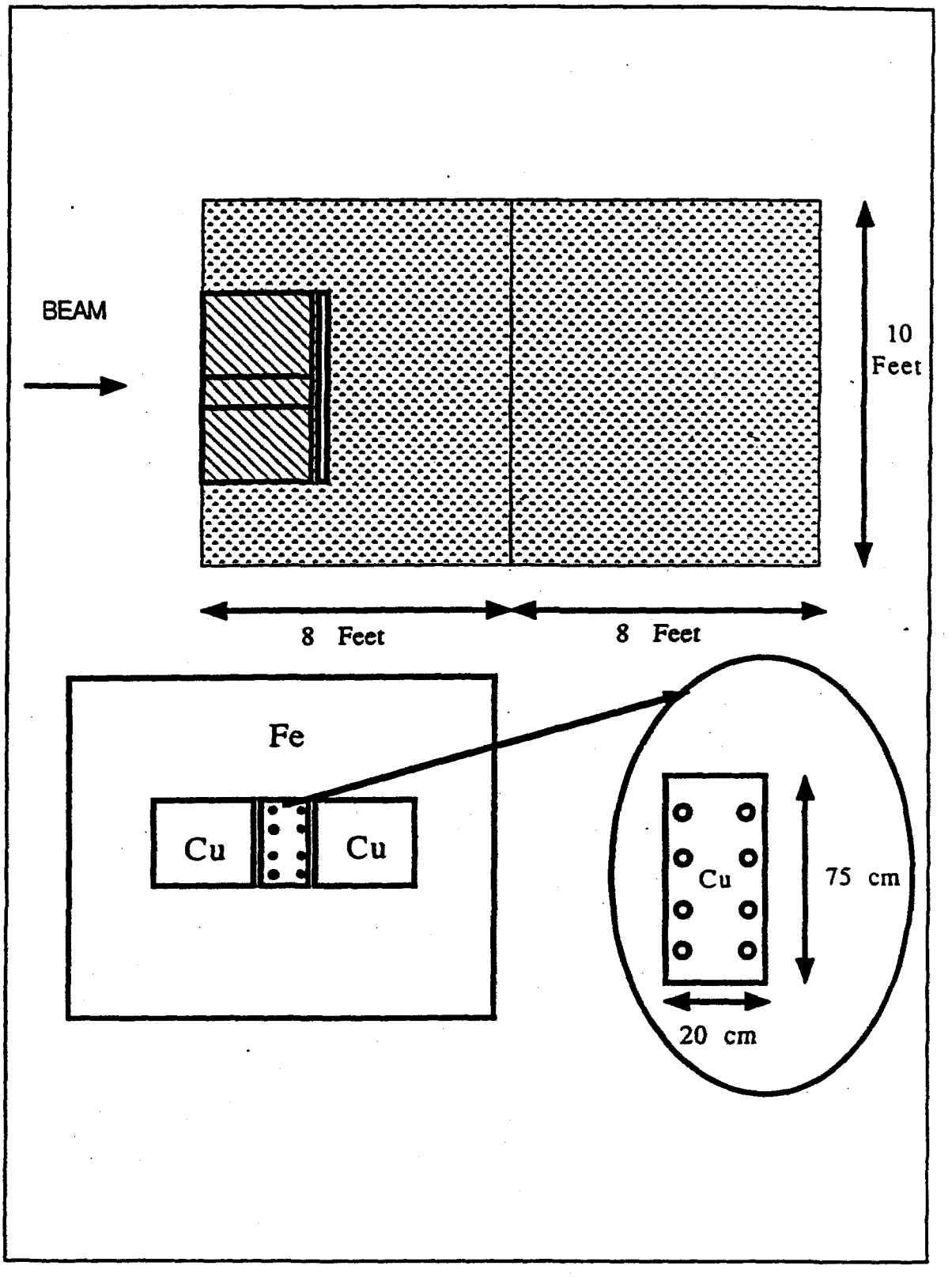

Fig. 4.2.17: The KAMI beam dump assembly.

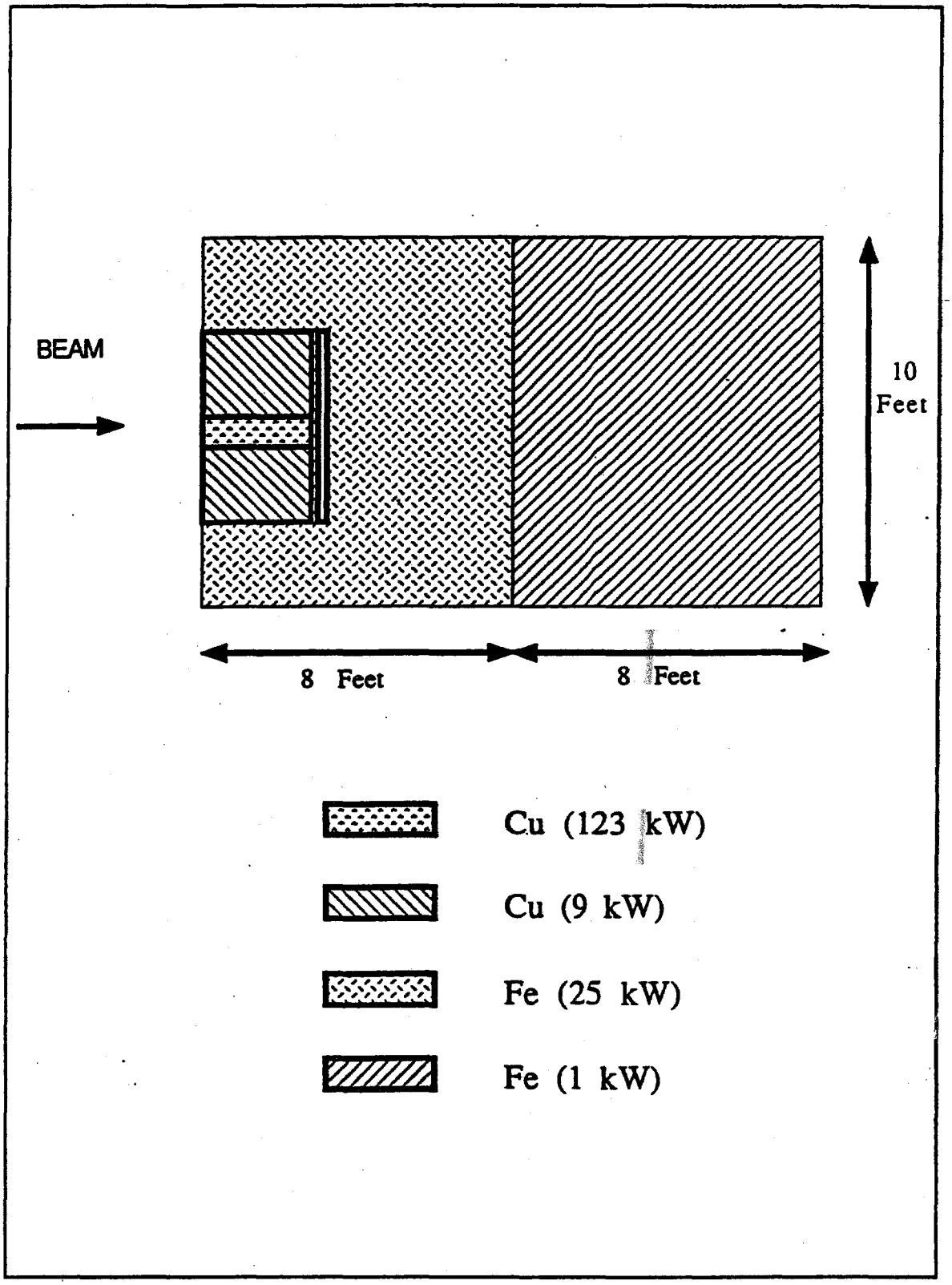

Fig. 4.2.18: Energy deposition distribution in the KAMI beam dump as calculated by CASIM.

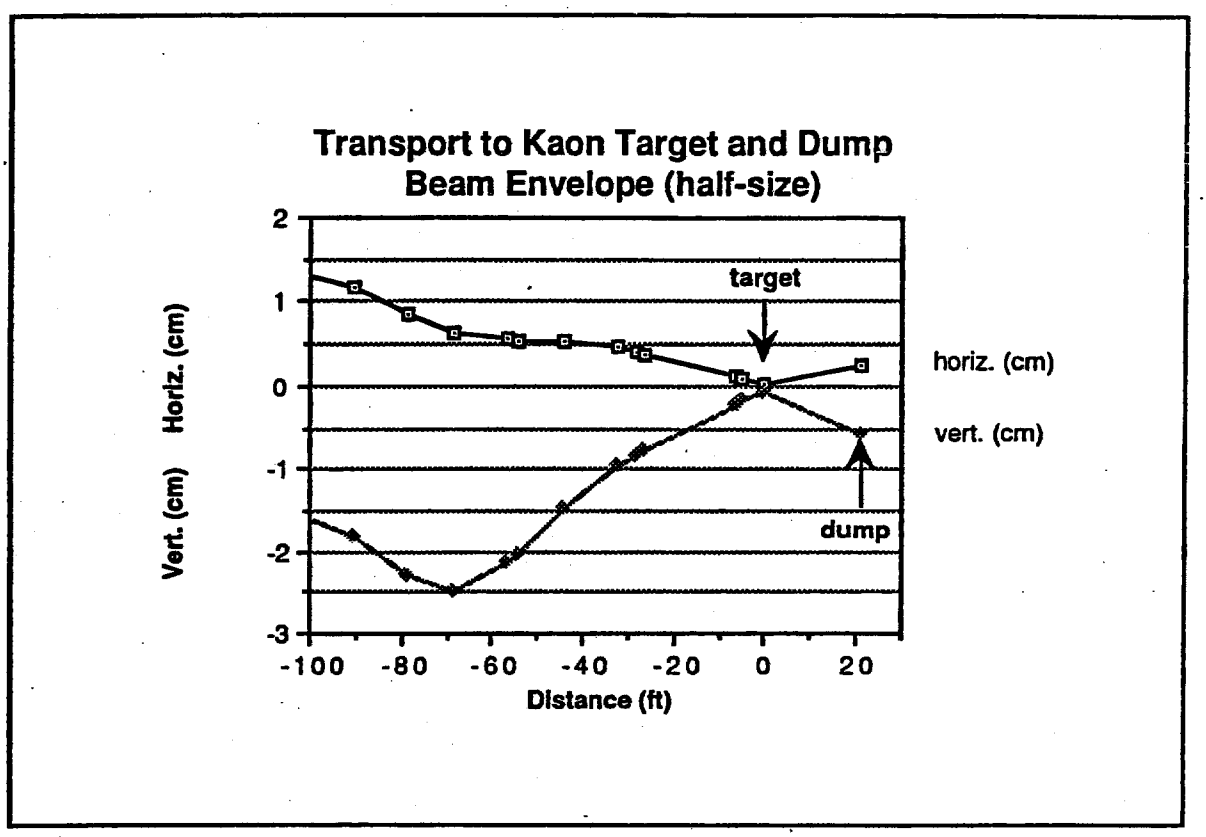

Fig. 4.2.19: Beam size as a function of position in the beam line.

4.2.7 Vacuum System

The most serious design constraint placed on the vacuum decay volume will be for the $K_L \to \pi^0 \nu\bar{\nu}$ experiment. That configuration requires a vacuum level of 10^{-6} torr. Approximately half of the gamma veto system must be housed inside the vacuum vessel. The large volume of scintillator combined with over 1600 cables and a thin, mylar vacuum window will add up to a considerable load on the system. These constraints must be met without sacrificing the hermeticity of the veto system or modularity to accommodate the other proposed experiments.

This Section will address the general requirements for all the KAMI experiments and focus specifically on the constraints for $K_L \to \pi^0 \nu\bar{\nu}$ since

they are perceived to be most stringent. All of the given requirements are considered achievable, however, some studies are not yet complete.

General Dimensions and Layout

For all experiments except the K_S configuration, the vacuum decay system will start at approximately z = 23 m and end at z = 43 m, as shown in Fig. 5.5 (Section 5). The present design comes in three sections. The upstream section will be 20 cm in diameter and will be removed to make room for a fully active regenerator during the ε'/ε experiment. The second section will be 8.5 m long and 1.5 m in diameter and house part of the gamma veto system. The third section is 10 m long, 2.1 m in diameter, and ends with a 2 m thin vacuum window. It will also hold the majority of inner gamma veto channels. Total system volume is 4.96×10^4 liters. The outer (liquid scintillator) veto system will be supported around sections 2 and 3 by a 2.8 m and 3.4 m pipe respectively. The vacuum system will be designed to have an operating pressure of 10^{-6} torr except for possibly, the ε'/ε configuration, which may run at 10^{-4} torr with the regenerator mover under vacuum.

For ε'/ε, the regenerator will be under vacuum. E731 has successfully used a moveable regenerator under vacuum, but for only two beams. If more than two beams are used at the Main Injector, an additional engineering effort will be required to design a mover to allow motion in both x and y directions. In either case, the entire unit will be designed to fit into the area downstream of the final sweeper and upstream of the veto system.

2 m vacuum window design

The present requirements for a vacuum window are that it is larger than the solid angle created by the kaon decay space and that the interaction length is minimized. Fermilab already has good experience in this design and has successfully used a 1.8 m and the existing 1.2 m window for E617 and E731 respectively.

The current 1.2 m window uses a Kevlar/Mylar sandwich. Kevlar was chosen because it provides the greatest tensile strength to density ratio while providing minimal elongation.[10] This provides an interaction length of 0.2% using Kevlar 29 Type 964 1500 Denier with a 2 × 2 basket weave and 5 mils of Mylar. A finite element method (ANSYS) analysis was done on this design and shows that the window diameter can be increased up to 3 m without changing materials and still maintaining a factor of two safety factor.[11] The only concern would be an increased creep rate which would require window replacement more often.

The KAMI window design will be 2 m in diameter and use aluminized Mylar to reduce the water vapor permeation rate. The window must also be made light tight since normal wrapping cannot be used on the scintillator. The fabric clamping method is well understood. Soft aluminum round wire is clamped into an O-ring groove to prevent slippage. The only information still needed is the radiation hardness of the Kevlar. No problems have been previously encountered, but due to the increased flux rates of the Main Injector, this needs to be understood. It is known that Kevlar is sensitive to ultraviolet radiation, but no information has yet been obtained for the high-energy range.

Calculation of system load and pumping capacity

For the $K_L \rightarrow \pi^0 \nu\bar{\nu}$ requirement of 10^{-6} torr operating pressure, a careful analysis of system load is required to determine if such a vacuum can be obtained and, if so, the pumping speed required. The total system load Q_T is expressed as the summation of the loads from outgassing, leaks, and permeation. The pumping speed, s, is then calculated from the equation,

$$s = Q_T/P_u$$

---

[10] DuPont preprint No. 375, "Characteristics and Uses of Kevlar 29 Aramid", Sept. 28, 1976.

[11] Analysis by Ang Lee, Bob Wands.

where P_u is the ultimate system pressure and is usually 1 to 2 orders of magnitude lower than the operating pressure. Since this system will probably use organic seals, we will assign P_u to be 10^{-7} torr. Note that this relation is independent of volume. To determine Q_T, an analysis of a least the major sources of load must be performed. There are three major sources of load perceived for the KAMI vacuum system: 1) water vapor permeation from the mylar window, 2) outgassing from the huge amount of scintillator and cables inside the vacuum, 3) leaks from the over 1600 vacuum feedthroughs.

Water vapor is by far the largest source of permeation through mylar. Due to the large variation in published data, it was determined that an independent measurement was necessary. An apparatus built by the Physics Department and Research Division for diffusion measurements was suitable for this purpose. It used a volume separated into two by a mylar window with one side filled with 100% humid air at 20° C, the other with vacuum. A differential pressure gauge was placed with a reference vacuum on one side and the subject vacuum on the other. A rate of 2.6×10^{-6} torr·l/sec·cm^2 for a 1 atm/mil pressure gradient was recorded[12]. This is five times higher than advertised by DuPont[13] but is lower than other published data[14].

Another measurement was made using aluminized mylar. This produced a rate of 1.4×10^{-7} torr·l/sec·cm^2 for a 1 atm/mil pressure gradient[15]; a factor of 18 lower than standard mylar. Extrapolating this number linearly to 5 mil thickness and for a 3.1×10^4 cm^2 vacuum window produced a total load from water vapor permeation of $q = 8.8 \times 10^{-4}$ torr·l/sec. The pumping speed required to offset this load is 8800 l/sec based on $P_u = 10^{-7}$ torr.

---

12 Measurements made by J. Krider and R. Tschirhart with 2 mil mylar.

13 DuPont Mylar Product Information for Mylar 98A.

14 D. Holkeboer, *et al.*, *Vacuum Engineering*, Boston Tech. Publishers, Cambridge, Mass., 216-218 (1967).

15 Measurements made by J. Krider and R. Tschirhart with alum. mylar.

It was hoped that this same device could be useful for measuring the outgassing rates of the scintillator candidates for the gamma veto system, but the mechanics of breaking the vacuum to insert the scintillator prevented distinguishing the signal from the background. However, by including both the signal and background into the calculation, an upper limit can be established until a better measurement can be made. A maximum system load of 0.37 torr·l/sec for PVT and 0.39 for polystyrene results using an area of 1.2×10^7 cm^2. This translates to about a 3.9×10^5 l/sec pumping speed requirement for $P_u = 10^{-6}$ torr and 3.9×10^6 l/sec for $P_u = 10^{-7}$ torr. The latter number would not be practical for this system, but 3.9×10^5 l/sec can be matched with $6 \times 60{,}000$ l/sec cryopumps. The load could be reduced using several methods e.g. low temperature bakeout, paint, longer pumpdown times, etc.

A published figure[16] for outgassing of HV and signal cable (PVC) is 1.4×10^{-7} torr·l/sec·cm^2. This gives $q = 3.5 \times 10^{-3}$ torr·l/sec for 1600 5 ft. long 1 cm diameter cables or 3.5×10^4 l/sec for $P_u = 10^{-7}$ torr.

The other source of system load will be leaks from the hundreds of possible sources, but diligence in leak detection can overcome this problem. Although significant engineering work will be required for this vacuum system, it is believed that all constraints can be met for this design. Further work is needed to decrease the scintillator outgassing rate by an order of magnitude.

4.2.8 Muon Flux Calculation

A fundamental design consideration for the KAMI secondary beam is to keep background muons away from the sensitive detector elements. As described in Section 4.2.1, this is accomplished by two magnets. The production target is located in the upstream end of the first magnet. Charged secondaries produced in the target are swept in the vertical plane. The beam dump sits at the upstream end of the second magnet. Charged secondaries produced in the beam dump are swept horizontally.

---

[16] J.F. O'Hanlon, *A User's Guide to Vacuum Technology*, Wiley, New York (1980).

In this design, there are two principle sources of muons associated with the interactions of the primary beam. First, pions produced in the target can decay into muons before being absorbed in the tapered walls of the target magnet. Second, pions produced in the beam dump will produce muons if they decay before interacting. Since muons produced by pion decay tend to follow the direction of the parent pion, the target and the center of the beam dump will be apparent source points for muons.

Two other important muon sources were considered; the defining collimator, and primary beam halo. The defining collimator naturally must absorb a fraction of the secondary neutral beam. Like the interactions of beam particles in the beam dump, the interactions of these neutrals will produce pions which can decay into muons. Though there are fewer of these interactions, they occur much closer to the apparatus, and so were considered as a potential source of muons hitting the detector. Beam halo muons are inevitable in any transported proton beam and were also considered as an important muon source. Because they arrive off-axis, magnets intended to sweep target produced muons away from the apparatus can pull halo muons toward it.

To estimate the muon flux from these sources, the KAMI secondary beam was simulated using CASIM Muons produced in the target, the beam dump, the defining collimator, and from primary beam halo. Each of these sources was considered separately. In order to estimate the reliability of the simulation, CASIM was also used to simulate the beam dump from Fermilab E613, a completed experiment from which muon flux measurements are available.

CASIM Benchmark calculation, FERMILAB E613

The E613 beam dump[17] consisted of 10.4 m of magnetized iron and 21 m of passive iron. The 400 GeV beam was normally pitched 4 mrad

---

[17] *Magnet Design Study from the Conceptual Design Report for the Direct Neutral Lepton Facility*, T. Murphy, ed. TM-1155R 1183.000 (1985).

upward. Coincidence rates were measured between a moveable 17.8 cm × 25.4 cm probe counter located 39 m downstream from the target and each of five 30.5 cm × 152.4 cm counters located 55 m downstream from the target. Rates were measured with the nominal beam pitch and with the beam at 0°.

This configuration was simulated in CASIM and the predicted muon fluxes compared with the E613 data. Figure 4.2.20 shows the spatial distribution of muons predicted by CASIM and the experimental data for a 4 mrad beam pitch. The simulation correctly predicts the features of the spatial distribution of muons, but predicts a rate that systematically a factor of two higher than the measurements.

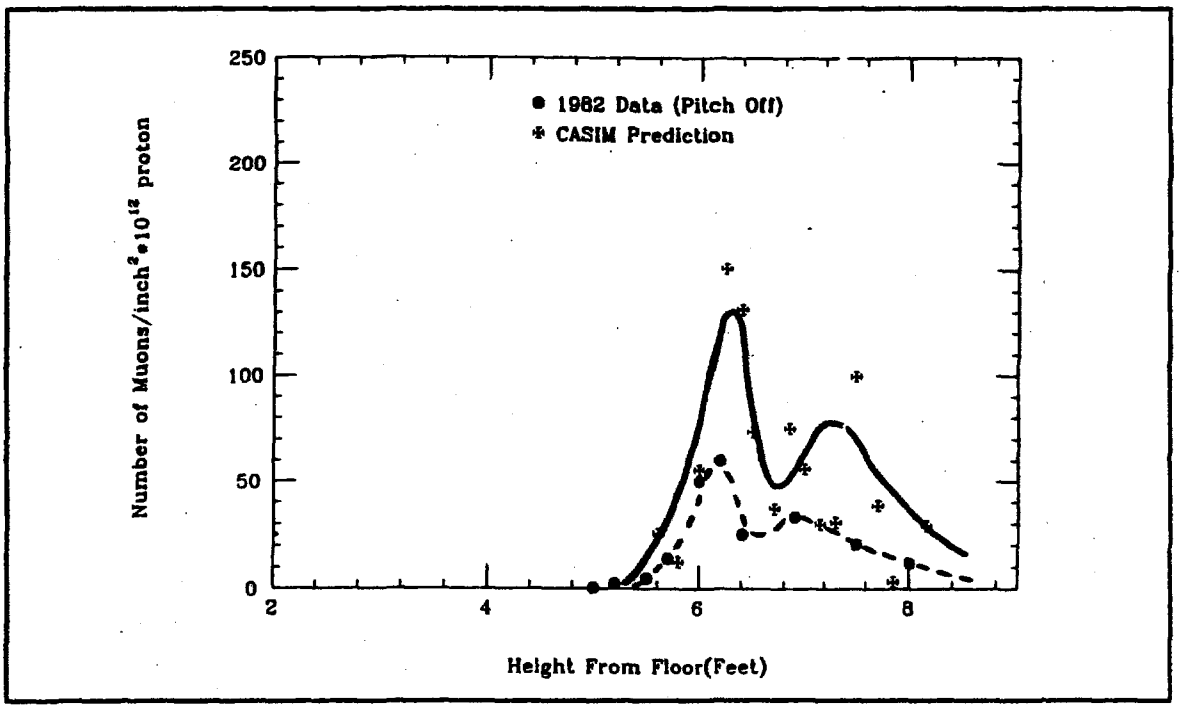

Fig. 4.2.20: Spatial distribution of muons predicted by CASIM for Fermilab E613, compared to measured muon fluxes. Normal beam pitch.

Target and Beam Dump Muons

To calculate the muon flux created by interactions of primary protons, the KAMI secondary beam geometry was simulated in detail, and incorporated into CASIM. The target was taken to be 5 cm of Be and the targeting angle 24 mrad. In order to single out target associated muons, the uninteracted primary beam was not tracked into the beam dump for this simulation. At the statistical level of the simulation, no muons hit within a 1 m radius at the location of the large veto shield. The upper bound on the muon flux into that circle is 10^{-12} muons per incoming proton. The muon flux coming from the beam dump was calculated, using a similar simulation, but with no target and the beam tracked to the beam dump. Figure 4.2.21 shows the radial profile of both target and dump muons at Z=25 m. The rate which is dominated by the beam dump is 10^{-10} per proton.

Defining Collimator Muons

The muon flux produced in the defining collimator affects the collimator design. For the high sensitivity experiments, large beams are required. The openings in both the upstream collimator and the defining collimator must be 12 μstr. If only the defining collimator is changed to create the small ε'/ε beam(s), then most of 10^{10} neutral beam will be dumped there. That is acceptable if the resulting muon flux is sufficiently low. If not, then both collimators will have to be altered to change the beam size.

To estimate the effect, a CASIM run was done in which the secondary neutral beam was tracked through a 12 μstr upstream collimator and dumped in the defining collimator. The resulting muon flux was 5×10^{-8} muons per incoming proton at the nominal 1 m radius circle. Since this rate is comparatively large, both collimators may have to be removable.

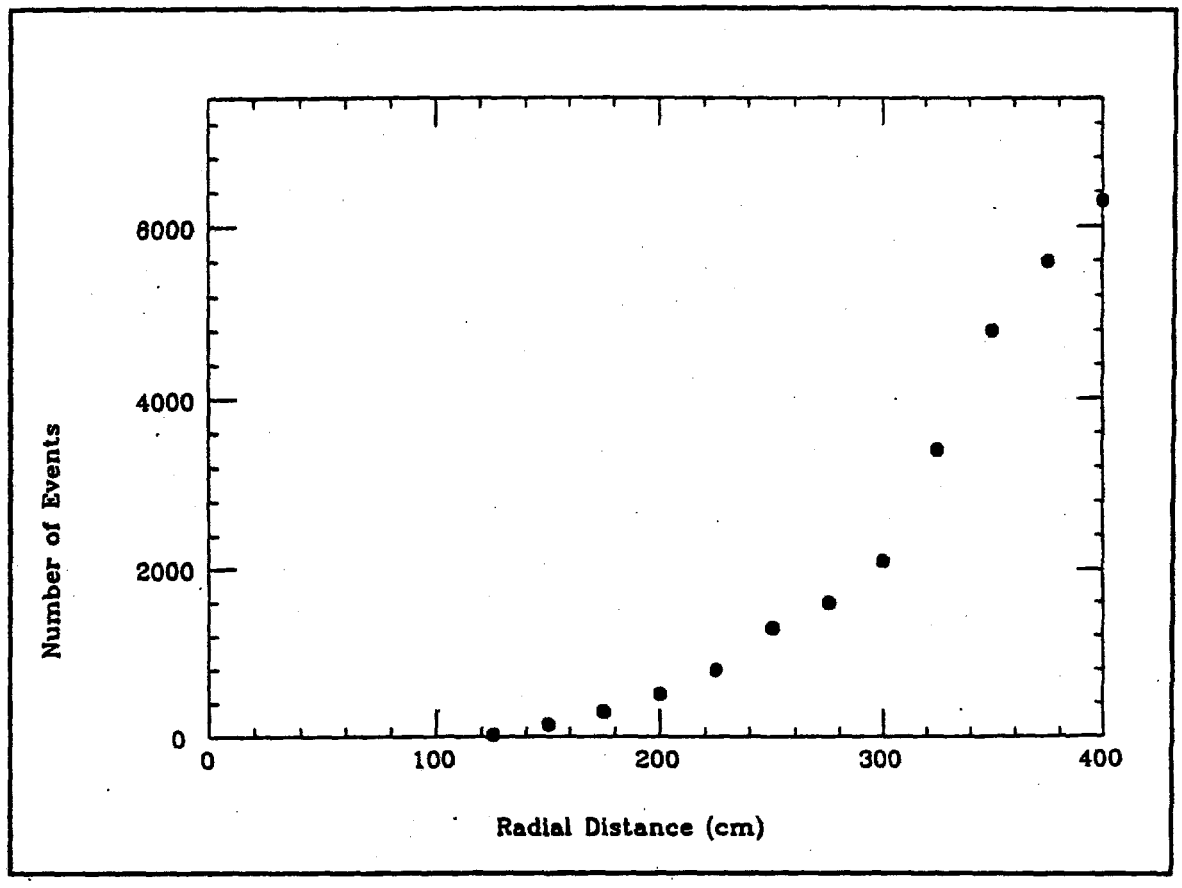

Fig. 4.2.21: Radial distribution at the upstream end of the decay region of muons produced near the kaon target.

Beam Halo Muons

To simulate muons from beam halo, a variant of CASIM was used in which a distribution of muons at the face of the target magnet was taken as input. These muons were then tracked through the system by CASIM. The input muon spectrum was flat in energy from 20 GeV to 100 GeV, with 30% more positive muons than negative. Spatially, the profile was Gaussian with a 50 cm σ, and all tracks were initially directed along the primary beam.

These muons were tracked through the target and dump magnets to the face of the decay pipe. The rate of the muons reaching the 1 m radius circular area was found to be 10^{-1} per incident halo muon. This places a rather stringent requirement on the transport cleanliness of the primary

proton beam. To attain 10^{-7} muon flux on the detector per proton on target, the halo rate must be less than 10^{-6} muons per incident proton. A detailed study of these background muons indicated that they mostly came from the tail of the Gaussian spatial distribution. The dump did not favor a specific energy band. We conclude that most of the muon background due to beam halo can be eliminated by removing the tails of the distribution far upstream from the target. Table 4.2.4 shows the muon flux per proton from each source.

	Target	Beam Dump	Defining Collimator	Beam Halo
μ flux/proton	$< 10^{-12}$	10^{-10}	5×10^{-8}	10^{-7}

Table 4.2.4: Contributions to muon flux at the detector.

4.2.9 K_S BEAM

In order to convert the KAMI facility into a K_S experiment, the beam defining collimators would be removed from the target and dump magnets and the primary beam transmitted to a second hyperon magnet as shown in Fig. 3.5. The proton beam would be brought through the K_L dump magnets just off-axis. The last magnet of the K_L dump would then be used to pitch the proton beam onto the K_S target at a 5-10 mrad angle. This target is located at the entrance to the second hyperon magnet, which would be used to dump the proton beam, sweep away all charged particles, and define the neutral beam. About 5 MHz of muons hit the spectrometer with 10^{12} incident protons. The main muon lobes miss the first chamber by about two meters, and contain an order of magnitude more particles. These particles are quite spread out in position, and will not dominate the rates in the veto counters. The rates from beam halos in the spectrometer can be estimated from the experience of E621 and will be about 6 MHz at the Main Injector. Both these sources are considerably less than the rate of decays of K_S, K_L, and Λ^0's. (See Table 1.1).

4.3 Analysis Magnets

4.3.1 Introduction

Two analysis magnets are preferred for KAMI, located as shown in Figs. 3.1 and 3.2, with the magnetic fields in opposite directions. In order to meet the objectives of the experiment, each magnet is designed to meet the following requirements: momentum kick = 450 MeV/c, field integral uniformity = ±5% over a "good field" aperture 2 m vertical × 3 m horizontal, fringe field < 0.1 T (1 kG) at the detectors. A longitudinal magnet separation of 6 m provides a reasonable compromise between space for apparatus and acceptance.

The magnets shown in Fig. 4.3.1 were found by magnetostatic analysis to meet these requirements while approximately minimizing the sum of the capital and five-year operating costs. Each magnet consists of an iron yoke and rectangular poles with "race-track" coils wrapped around the poles. The coils could be either conventional, i.e. water-cooled copper or aluminum, or superconducting. A preliminary cost estimate with conventional coils gave a total capital cost for two magnets of approximately $8 M and an annual operating cost of about $400 k. It is difficult to estimate the cost of race-track superconducting coils with confidence, but a preliminary cost analysis gave the same capital and operating costs as the conventional case.

Because of these high costs, using the Chicago Cyclotron Magnet (CCM) was considered. This magnet, which is superconducting, is presently located in the New Muon Laboratory (NMUON) at Fermilab. The cost of opening the gap to 2.5 m (an additional 47") for KAMI and moving the magnet downstream (north) in NMUON is estimated to be about $1.2 M. An alternative to moving the magnet is to extend NMUON 25 m to the south and raise the beam height. This is estimated to cost $1.150 M plus the cost of raising the beam height.

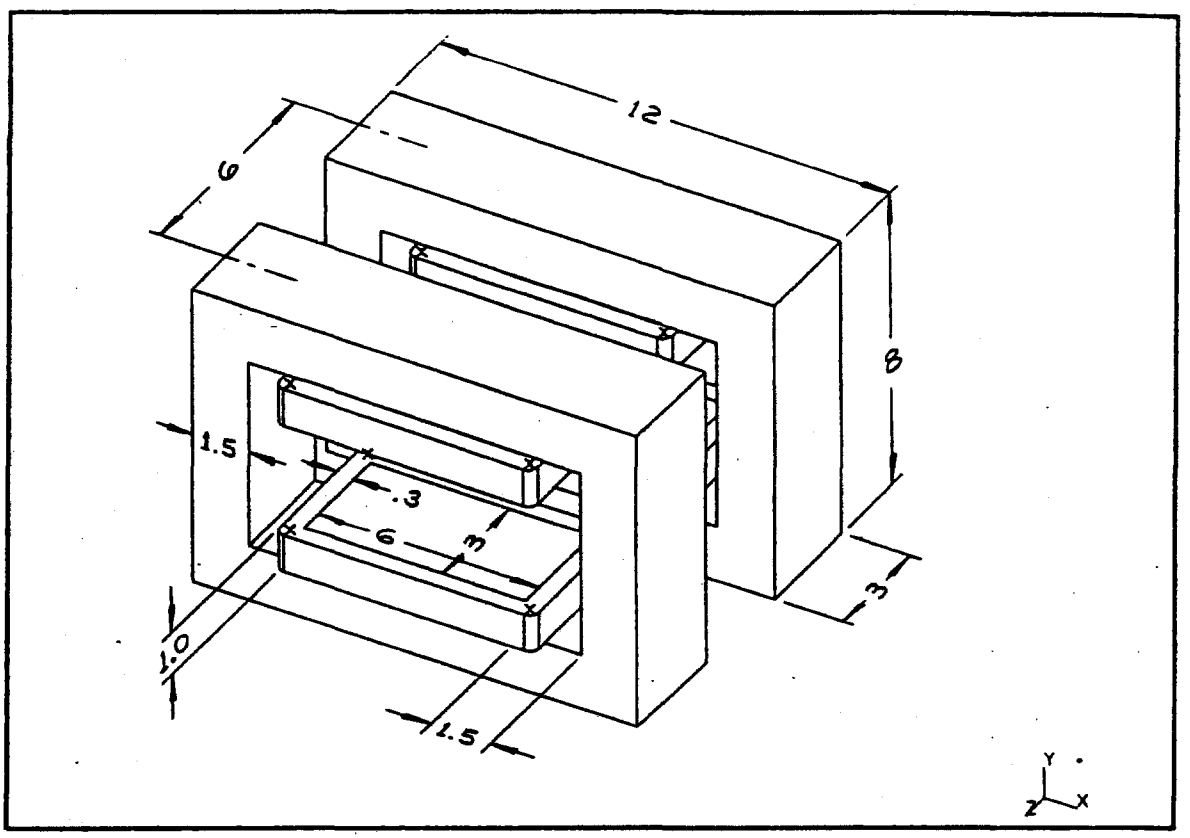

Fig. 4.3.1. Isometric view of KAMI analysis magnets. Dimensions are in meters.

Details of the magnetostatic analysis and the cost estimates for the alternatives are given in the following sections.

4.3.2 Magnetostatic Analysis

The magnetostatic design of the analysis magnets for KAMI was performed with the commercial finite-element program ANSYS (Swanson Analysis Systems, Inc.). The validity of three-dimensional magnetic field calculations performed on ANSYS was verified by calculating the transfer constant (central field divided by excitation in T/A-turn) and the field distribution for a 48D48 and the CCM and comparing the results with measurements. The calculated transfer constant and fields agreed with measured values to better than 5%. Solving a typical 3-d KAMI single magnet problem using both a reduced scaler potential formulation and a vector potential formulation showed that the ampere-turns to achieve a

given central field is 5% higher when using the vector potential. The reduced scaler method was used for the two-magnet problem because it required less computer time. The three components of the magnetic field, B, were calculated by a post processor. The integration limits on the field integral per magnet, $\int B_y dz$, were the position of the chambers C2 and C3 (see Fig. 3.1). The fringe field at these chambers was less than 0.1 T (1000 G).

For the geometry of Fig. 4.3.1 a coil excitation of 0.5 MA-turns gave a field integral of 1.5 T-m, corresponding to a momentum kick of 450 MeV/c. The uniformity of the field integral as a function of x and y over the good field aperture is given in Fig. 4.3.2. The magnitude of the fringe field at the chambers C2/C4 is presented in Fig. 4.3.3. The field in the iron and air at the longitudinal mid-plane of the magnet is shown in Fig. 4.3.4.

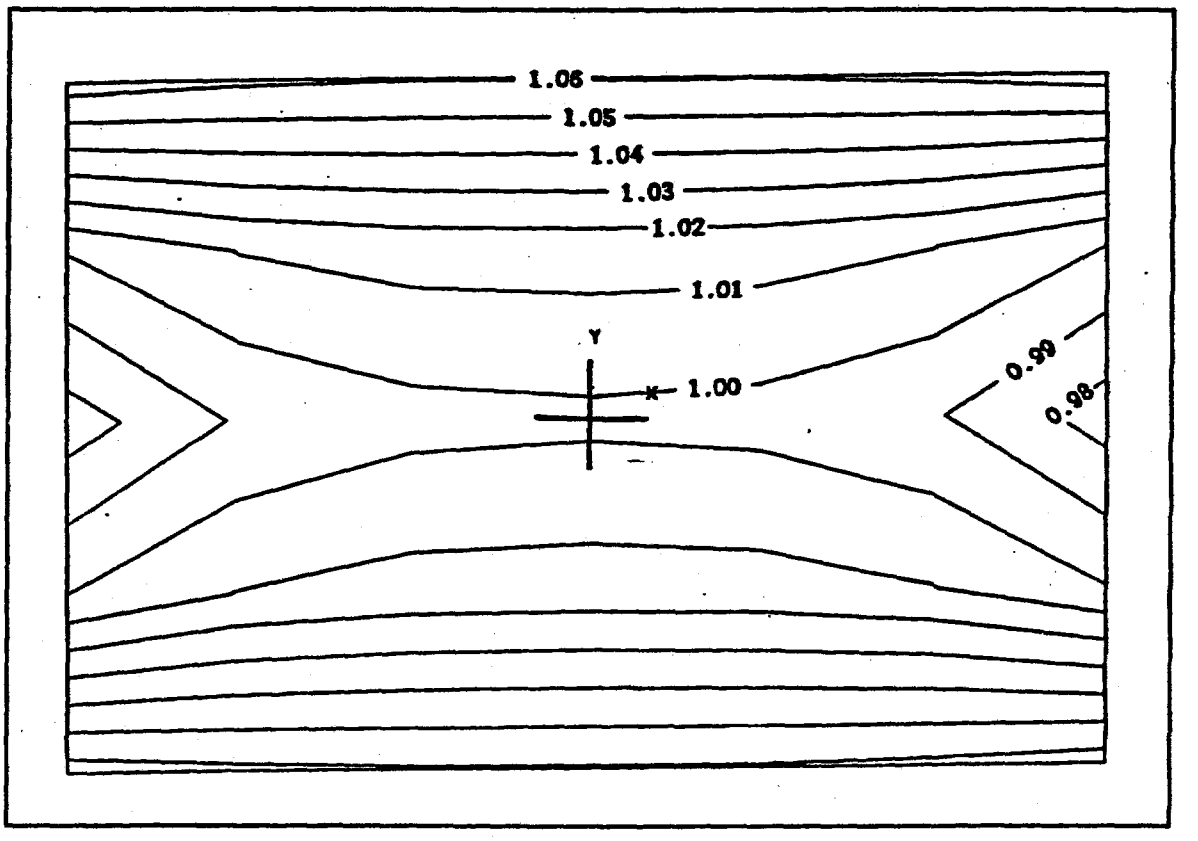

Fig. 4.3.2. Vertical component of the magnetic field, integrated in z from chamber C2 to C3, as a function of x and y over a 2 m high by 3 m wide aperture.

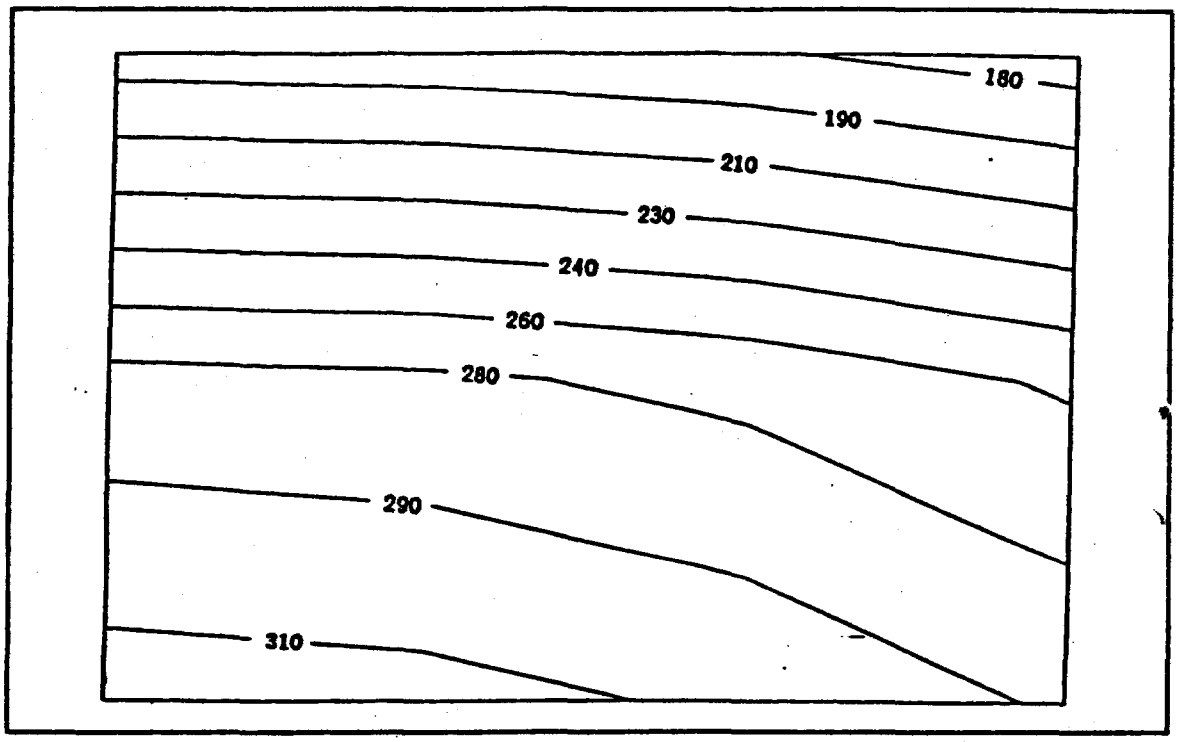

Fig. 4.3.3. Fringe field magnitude as a function of x and y over one quadrant of the aperture at z=43 and 57 m. Units are gauss.

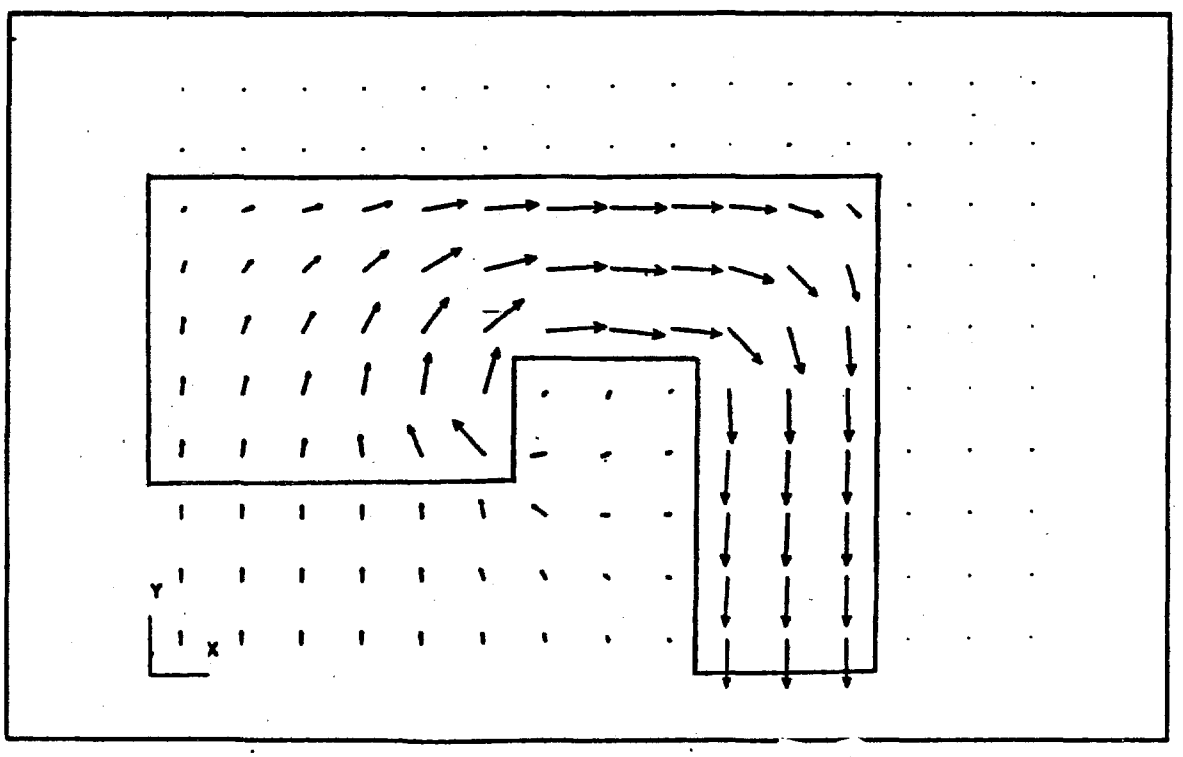

Fig. 4.3.4. Magnitude and direction of the field in the longitudinal mid-plane of each magnet.

4.3.3 Preliminary Cost Estimate - Magnets with Conventional Coils

The capital cost of a magnet system utilizing conventional coils arises from three basic components:

(1) the coils, including the conductor, fixtures and fabrication and insulation

(2) the electrical items, including substations, power supplies, switch gear and heat removal system, and

(3) the steel yoke and flux return legs.

The unit cost of copper coils was estimated from the known costs associated with the procurement of the coils for the analysis magnets for E687 and E706: \$109 k/m^3 of coil + \$100 k. The cost of electrical items was estimated from recent Fermilab purchases: substations at \$100 k/MW + power supplies at \$150 k/MW + switchgear and bus at \$100 k/MW + pumps and cooling at \$100 k/MW = \$450 k/MW. The unit cost of the steel yoke and legs was also estimated from the known cost of the steel for the E687 magnet to be \$1.56 k/tonne (metric) of steel. Neither the cost of the magnet foundations nor the building was part of this estimate.

The electric power required depends on the coil excitation (NI) and the volume of conductor: $P = \rho J^2 V$. The unit operating cost for these conventional magnets is assumed to be only that associated with the cost of electric power: \$500 k/MW-yr. at 100% duty factor.

The five-year total cost of each coil defined as the sum of the capital cost of the coil and electrical equipment and 5-yr. operating cost, is a function only of the width of the coil for a given excitation, pole height, iron length and magnet separation. A coil width of 0.3 m minimizes the 5-yr. total coil cost for the magnets with copper coils shown in Fig. 4.3.1.

The dimensions and cost breakdown of the magnets shown in Fig. 4.3.1 are given in Table 4.3.1 for copper coils, with the coil width chosen

to minimize the total 5-yr. cost. The capital cost for two magnets with copper coils is $8 M and the annual 70% duty factor operating cost is $418 k.

The cost estimates presented above for the conventional two magnet system are preliminary and probably conservative. A few points will clarify this suggestion: 1) The coil designs are based on the coils built for E687 - saddle coils. As the coils on the KAMI magnets are simpler pancake coils, significant savings may accrue. 2) The aperture of the magnets as currently envisioned is quite large - chosen to obtain good field uniformity. A more refined design should allow a reduction in the magnetic volume with resulting cost savings associated with an overall reduction in the scale of the magnets. 3) It should be possible to reduce the cost by using aluminum coils.

Reducing the momentum kick of both magnets to 300 MeV/c (1.0 T-m) reduces the annual operating cost with copper coils from $418 k to $186 k.

4.3.4 Using CCM for KAMI

The CCM (Chicago Cyclotron Magnet) is the 170-inch University of Chicago cyclotron magnet which has been a part of the Fermilab muon spectrometer for many years. It was retrofitted with a pair of superconducting coils in 1981. The magnet was moved from NWA to a new site in the Neutrino Area in 1983 and the New Muon Laboratory (NMUON) subsequently built around it. A standard 600-W cryogenic plant was installed in NMUON to refrigerate CCM and the CERN Vertex Magnet. The associated Mycom helium compressors are located in Lab B. The power cost to operate this plant for CCM alone would be about $125 k/yr.

Dimensions/Constants	Copper Coil	Units
Coil excitation	0.5	MA-turns
Coil/pole height	1	m
Coil width	0.3	m
Pole width	6	m
Pole depth	3	m
Length of average turn	19.2	m
Volume of coil	5.76	m^3
Weight of coil	51.3	tonnes
Power per coil	298	kW
Volume of steel	188	m^3
Weight of steel	1466	tonnes
Costs per Magnet		
Capital cost-coils	1456	$k
Capital cost-electrical	268	$k
Capital cost-steel	2287	$k
Capital cost-subtotal	4011	$k
Annual operating cost, 70% duty factor	209	$k
5-yr. operating cost	1045	$k
Total 5-yr. cost	5056	$k

Table 4.3.1: Estimate of 5-year Cost of Conventional KAMI Magnets. Dimensions and Constants.

The pole diameter of the magnet is 4.32 m, the present gap is 1.3 m. For E665 the magnet runs at a current of 750 A and a central field of 1.3 T. Its present location is approximately 24.4 m (80 feet) north of the south wall of NMUON.

For KAMI the magnet gap would be opened to 2.5 m, an additional 47.25 inches. This will provide a good field height of 2 m and allow space for

the frame of chamber C3. An ANSYS magnetostatic calculation with this gap, at the maximum design current of 825 A, gives a central field of 0.8 T. The maximum fringe field in an x-y plane 3 m from the center of the magnet is about 500 G. The field integral along a diameter at x = y = 0, from z = 47 m to z = 53 m is 4.0 T-m. The variation of the field integral over a 2 m high by 3 m wide aperture is shown in Fig. 4.3.5.

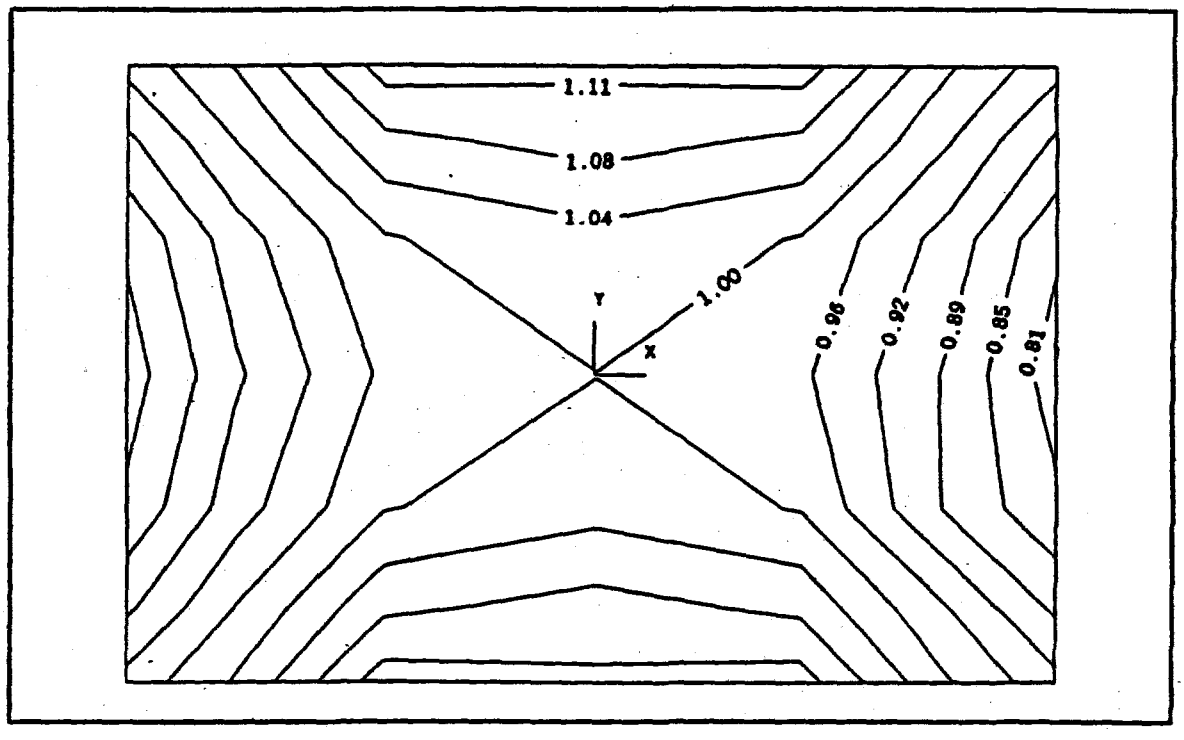

Fig. 4.3.5: Variation of the integrated vertical field in the CCM as a function of x and y, normalized to the value at x=y=0, 4 T-m.

The CCM could be used in the New Muon Lab for KAMI or the magnet and the cryoplant could be moved to a new experimental hall. If NMUON is used for KAMI (Fig. 3.3), the CCM must either be moved north (downstream) at least 25 m (about 80 feet) in order to accommodate upstream KAMI equipment or the south wall of NMUON extended by this amount and the beam height raised. A cost estimate for moving CCM the building was made by the Mechanical and Cryogenics Departments, with assistance from the Construction Engineering Services Section. The CCM weighs about 2000 metric tonnes and requires pilings to bedrock for adequate support. The cost of a new foundation is about $375 k. It will cost

about $355 k for a gantry, handling fixtures and rigging time. Extending the cryogenic lines and opening the gap will cost $220 k. Engineering, design, liaison and inspection will cost $250 k. The total cost is therefore about $1.2 M. The cost of extending NMUON 25 m to the south with a 12 m by 25 m addition was estimated at $1 M, including crane coverage. It will cost about $125 k to open the gap of CCM to 2.5 m. The cost of raising the beamline is not available at this time.

The cost of moving the CCM and cryoplant to a new building has not been estimated.

We point out that it is obviously not possible to run with "opposite magnet polarities" when there is only one magnet. We believe that the requirements on momentum resolution and background rejection can be meet with the CCM but more simulations are required. It will be necessary to run with a measuring plane in the field region and its resolution is important in removing backgrounds from π decay in flight. We are considering scintillating fibers as well as a conventional drift chamber for this plane.

5. THE DETECTOR

In this section, we will give a first order specification of the detector that will address the physics of high precision, high sensitivity kaon decays. At this stage, no detailed design of the elements will be presented but we will be able to give the broad features which will influence the facility and its cost. The costs of the various elements will be estimated in Section 6 of this report.

The detector consists of tracking chambers, electromagnetic calorimetry, particle identification (TRDs for electrons and a range counter for muons), a trigger of several levels, and finally a data acquisition system. These each are described in the following sections.

5.1 Tracking Chambers

5.1.1 General Specifications

For the classes of experiments that we are discussing, excellent tracking and momentum resolution is required; a typical resolution of about 0.2% is needed. The chambers need to operate in a very high singles rate environment with approximately one kaon decay every 30 ns. We will first specify the general requirements for the tracking devices which will be suitable for both the high precision CP violation experiment and high sensitivity rare decay search experiments. These are:

a. minimum material to reduce multiple scattering in the spectrometer, $\leq 2 \times 10^{-3}$ radiation lengths per plane,
b. good position resolution, ≤ 100 μm per plane,
c. fine segmentation, ≤ 5 mm maximum cell size,
d. (off-line) timing resolution ≤ 1 ns,
e. low noise and fast signal (less than 30 ns) for high rate capability (up to 1 MHz per channel),
f. large area coverage up to 3.5 m × 2.5 m.

Drift chambers, straw drift tubes and scintillating fibers are considered to be the possible candidates for the tracking detectors in the spectrometer. For the sake of simplicity in this design report, we will choose drift chambers as an example. We will use a 5 mm hexagon cell (i.e. 2.5 mm drift distance), with offset double layers to resolve the left-right ambiguity in each view for the basic design. To maximize the acceptance for both 2-body and 4-body decay modes, we initially assume that there is no beam hole through the center of the chamber.

The conventional hexagon cell drift chamber is a good choice to have minimum radiation lengths and good position resolution. By choosing fast drift gas, such as CF_4 and a hydrocarbon mixture,[1] one can double the electron drift velocity compared to the commonly used $Ar\text{-}C_2H_6$ (50-50) mixture thereby reducing the maximum charge collection time down to 25 ns at a relatively low gas gain. Low noise, high gain, fast pulse shaping amplifiers and fast TDCs (.5 ns per count) will be used to achieve the desired timing resolution and the high efficiency. Construction of such large area, small drift cell chambers is challenging but should be possible. The alternative is to use small-cell (3 - 5 mm in diameter), thin-walled (25 μm), straw drift tubes which are relatively easier to build in a large area array. The drawback is that they have a small dead region in each cell and added radiation length due to the tube wall thickness. The advantage of the straw drift tubes is the ability to go to a smaller drift cell (1.5 mm drift space) for higher rate capability. In addition, the sense wires are isolated from each other reducing problems associated with broken wires and electrostatic instabilities.

---

1 *Proportional Chamber for Very High Counting Rates Based on Gas Mixtures of CF_4 with Hydrocarbons*, J. Fischer, *et al.*, NIM A238 (1985) 249; *Study of Fast Gases, Resolutions, and Contaminants in the D0 Muon System*, J. M. Butler, *et al.*, Fermilab-Pub-89/222-E (1989).

5.1.2. System Design

The proposed tracking system consists of 5 sets of drift chambers, each having two double-layer orthogonal planes (x and y views). The layout is shown in Fig. 5.1. The first two chambers, separated by 1.5 m, will be placed upstream of the 1st analyzing magnet just after the vacuum decay region. The last two chambers, also separated by 1.5 m, will be placed downstream of the magnet(s). The middle chamber will be located between the two magnets or, in the case of one large analysis magnet as shown in the figure, in its center. With two analyzing magnets, they will run in opposite polarity with momentum kick up to 450 MeV/c each. This configuration gives the least loss in acceptance for both 2-body and 4-body decay modes and the best background rejection for pions which decay in flight as well as a very good momentum measurement. The active area is 2 m (width) by 1.4 m (height) for the 1st chamber and gradually increases to 3.4 m by 2.4 m for the last chamber. Table 5.1.1 shows the active area dimensions for each detector and their z locations. The total number of sense wires in this system is about 9400.

ELEMENT	Z LOCATION [meters from target]	Horizontal Aperture	Vertical Aperture	# of channels
Chamber 1	43.5	2.0	1.4	1360
Chamber 2	45.0	2.2	1.5	1480
1st magnet	47.5	3.0	2.1	
Chamber 3	50.0	2.8	2.0	1920
2nd magnet	52.5	3.0	2.1	
Chamber 4	55.0	3.3	2.3	2240
Chamber 5	56.5	3.4	2.4	2320

Table 5.1.1: Drift Chamber Dimensions and Channels.

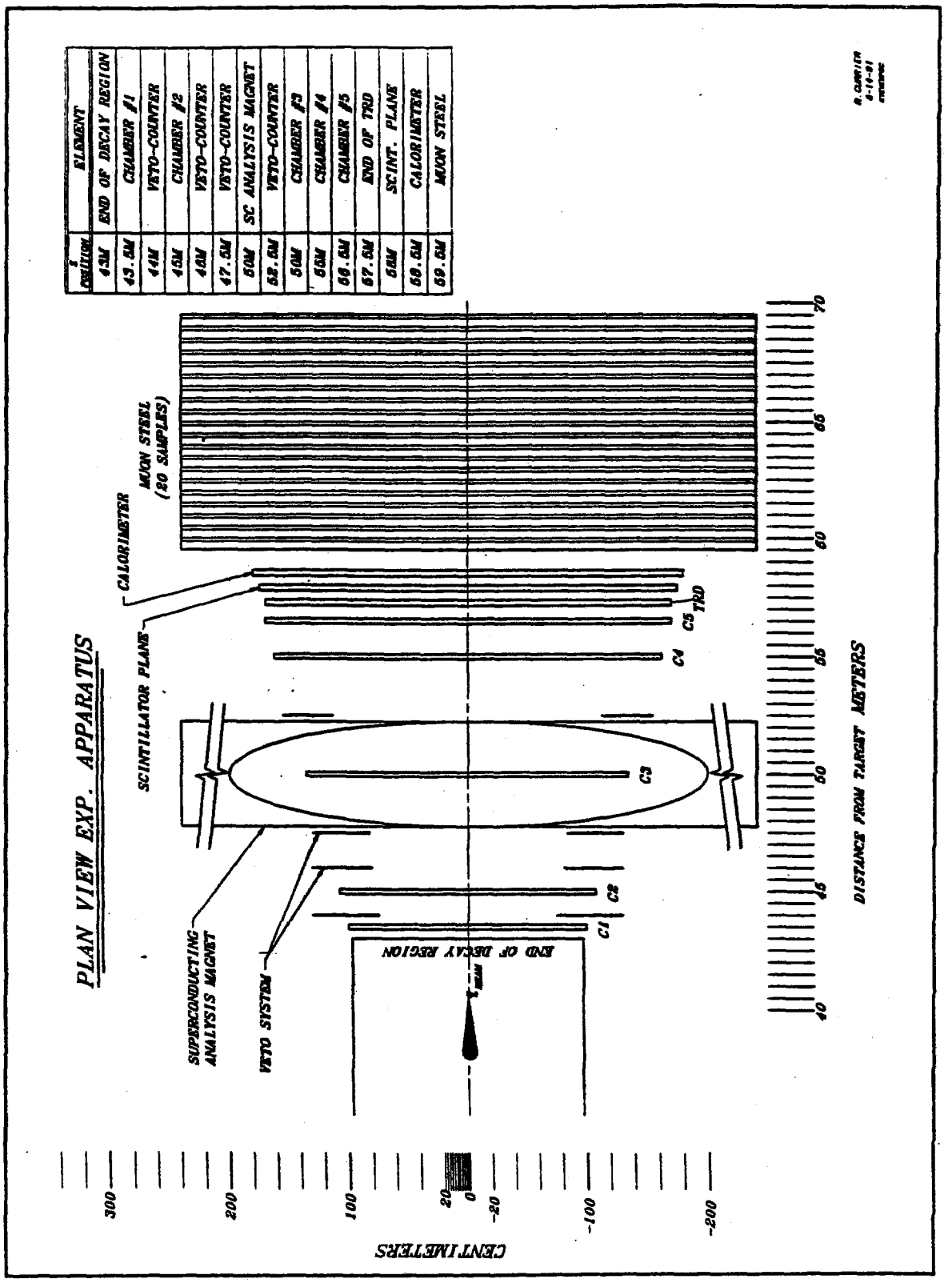

Fig 5.1 Detector layout for K_L decay experiments

In between chambers, large thin-window helium bags should be installed to minimize the multiple scattering of the track. With the use of thin windows on the chamber and Al cathode wires,[2] the total amount of material per chamber can be reduced to less than 2×10^{-3} radiation lengths and 7×10^{-4} interaction lengths. The contribution to the momentum resolution due to multiple scattering in the chambers is estimated to be less than 0.15% and the contribution from position resolution (100 μm) is estimated as 0.033% p for a 200 MeV/c momentum kick in each magnet. This gives a resolution of 0.2% for a 10 GeV/c track. A higher kick in the magnets will further improve the momentum resolution as is needed for the $K_L \rightarrow \mu e$ experiment. The singles rate from K_L decays estimated from a Monte Carlo simulation of the high sensitivity rare decay experiments is about 75 MHz in total for each of the first two chambers and 110 MHz in total for each of the last two chambers. The interaction rate of the neutral beam (up to 3×10^9 hadrons per second) in each chamber is less than 2 MHz which contributes less than 70 kHz per wire in the beam region. The singles rate on the hottest wire in the neutral beam region is then about 1 MHz from all sources. Given the 25 ns resolving time, this should result in an acceptable level of accidental hits. Also, by deadening the middle section of the wires in the beam region, one can reduce the singles rate on these wires by a factor of two while only reducing the acceptance by about 15%.

We have also considered the effects of drift chamber aging[3] ("radiation damage"). The fundamental parameter for discussing the lifetime of a given chamber system is the integral charge collected per length of anode wire. If proper care is exercised in chamber construction and operation, a lifetime (with less than 10% gain loss) of 0.1 C/cm can reasonably be anticipated.[4] In laboratory aging tests, lifetimes one to two orders of magnitude greater[4] than this have been achieved. Using 0.1 C/cm at the highest rate location as our (reasonably conservative) chamber

---

2 BNL $K_L \rightarrow \mu e$ experiment E791 has constructed drift chambers with Al cathode wires to minimize the multiple scattering in their spectrometer.

3 See E. Swallow, KAMI-51, internal note, and references therein.

4 J. Kadyk, "Wire Chamber Aging", NIM A300, 436 (1991) and references therein.

lifetime criterion, we estimate[3] that KAMI drift chambers should operate satisfactorily for well in excess of 10 years.

5.2 Electromagnetic Calorimetry

The experiments outlined in Section 1 require the highest possible precision in electromagnetic calorimetry. For varying reasons, this is true for all four classes of experiments. Also, because of the high rates involved, fast response and substantial immunity to absorbed radiation dose (see Section 5.7) are essential. In this section, we briefly motivate the need for high precision calorimetry and describe an appropriate calorimeter configuration.

We have examined a wide range of calorimetry options[5] in addition to the scintillating crystal array described in this section. Lead glass, lead flouride (PbF_2), scintillating glass, and sampling calorimeters are all incapable of providing the required energy resolution. Scintillating glass is also too slow. A homogeneous liquid argon ionization calorimeter is cumbersome and difficult to build, provides inadequate spatial resolution (because of the long radiation length), is too sensitive to hadrons, and is too slow. A liquid xenon calorimeter is, quite simply, prohibitively expensive ($20 M - $40 M). One using liquid krypton suffers from significant deficiencies in speed, technical uncertainty and complexity, and a somewhat higher cost than scintillating crystals. In the end, the scintillating crystal array emerges as the best option for the KAMI project at this time.[5]

We are still exploring the possibility of using a split layer of crystals with a scintillating fiber plane in-between. Such a configuration may provide superior position resolution[6] (about 0.5 mm) along with the excellent energy resolution of a scintillating crystal calorimeter. Since

---

5 See E. Swallow, KAMI-54, internal note, and references therein.

6 See K. Arisaka, KAMI-52 & 57, internal notes.

larger blocks would be used, the total cost should be comparable to that of the more conventional array under discussion here.

The array that we are considering is shown in Fig. 5.2. It is an array of 70 × 100 crystals having a fiducial region of 2.5 m × 3.6 m. Of the 7000 crystals, it is anticipated that 4100 will be on-hand for the 64 × 64 array needed for E799/832.

5.2.1 ε'/ε

For the measurement of direct CP violation in the 2π mode, one reconstructs 4γ events and compares them with $\pi^+\pi^-$ events. High precision is required for background rejection and for the determination of the energy and distance scales. The following general arguements enable one to set the scale for the required precision.

In E731, the residual background under the $K_L \rightarrow 2\pi^0$ invariant mass plot was about 0.4%, resulting largely from $3\pi^0$ events with two missing photons. For the Main Injector experiment, one wishes to keep the systematic error at the 10^{-5} level which means keeping individual contributions below 3×10^{-6}. This corresponds to a systematic error contribution to the ratio (or double ratio) of about 2×10^{-5}. If the background can be understood to about 20% of itself, this means that we must keep it down to the 10^{-4} level. This requires a factor of about 40 reduction from E731.

In E731, the background arises predominantly from fused gammas. The proposed calorimeter elements will have dimensions of 3.6 cm × 3.6 cm, to be compared with 5.8 cm × 5.8 cm lead-glass blocks in E731. This should result in the reduction of backgrounds from fusion (actually double fusions) by about a factor of 8. The remaining factor of 5 must come from the improved detector resolution.

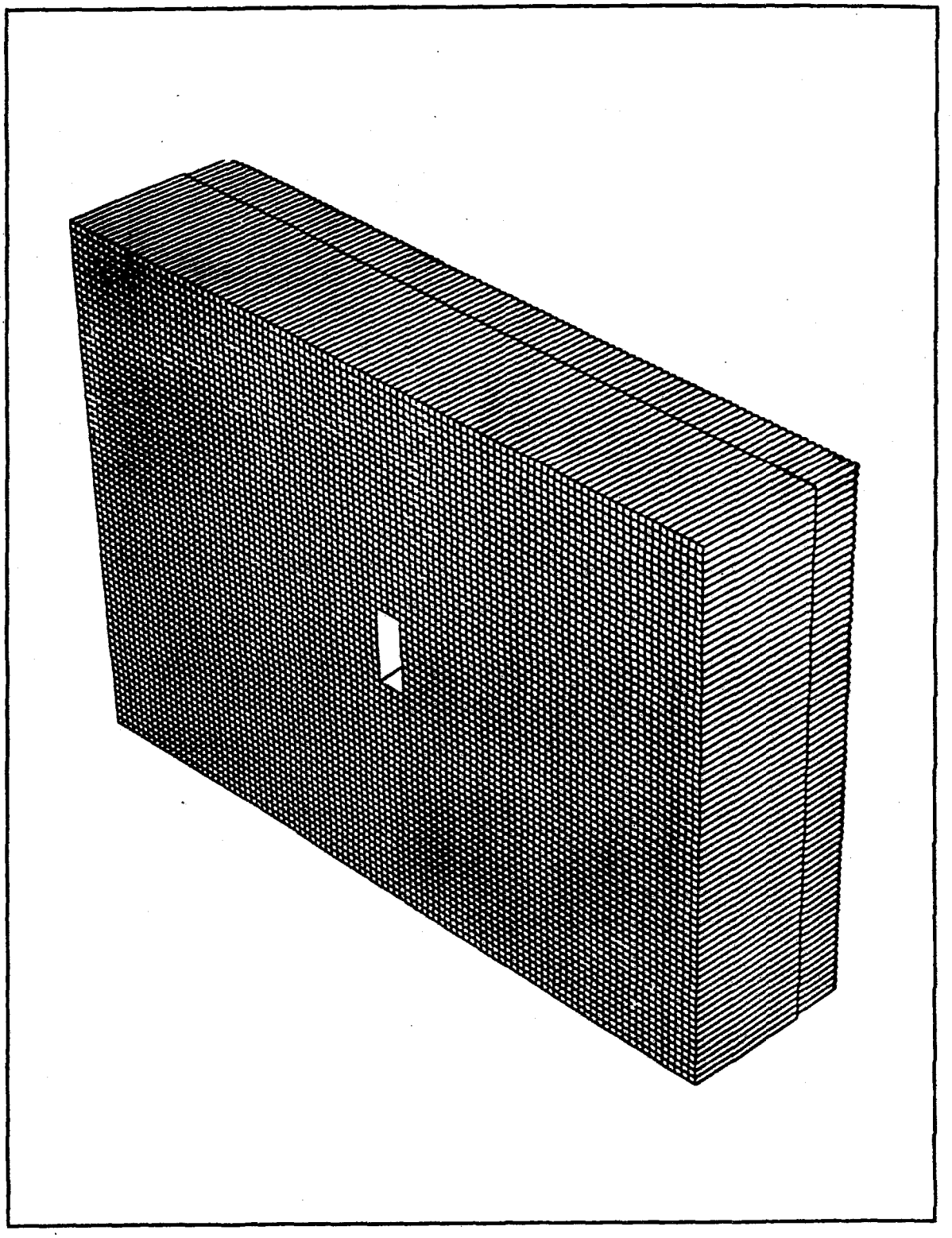

Fig. 5.2: CsI/BaF_2 Crystal Calorimeter.

In E731, the lead glass had the following resolution for photons: $\sigma/E \approx 2.5\% + 5\%/\sqrt{E}$. In addition, the lead glass had a substantial non-linearity which results from two (competing) effects: a well-understood leakage fraction out the back of the blocks which increases slowly with energy and a relatively poorly understood effect from light absorption in the block coupled with the increase in depth of the shower with energy. As a result, the response could be roughly and typically characterized by $E_{(true)} \approx E_{(measured)}^{0.976}$. Since the typical photon energy was about 15 GeV, this corresponds to a resolution of about 3.7%. The non-linearity over the dynamic range, 2 GeV to 60 GeV was then about 8%. We desire to obtain about 0.8% resolution for the typical photon at the Main Injector at an energy of about 4 GeV.

The second reason for improved energy resolution results from the need to compare decays to charged and neutral pions. The (relative) energy scale must be known extremely accurately as it is the energy that gives the Lorentz gamma of the kaon and allows the desired center of mass decay rates to be determined from those measured in the laboratory. Closely coupled with the energy scale is the line-shape: given a photon of known energy, what is the distribution in responses in the calorimeter. In fact, the resolution function and its tails must be well understood to be able to simulate biases in event selection. In E731, the systematic error due to mis-understanding of the energy scale and line shape of the lead glass was estimated to be 0.2%. With the final analysis, this will drop to about 0.05%. It is dominated by uncertainties in the rather substantial non-linearity in the lead-glass response.

The key, then, to better resolution is to improve both the $1/\sqrt{E}$ term and the constant term. The former can be reduced with more light and the latter by making the blocks long enough (at least 25 radiation lengths[7]) and

---

[7] Our EGS simulations indicate that longitudinal shower leakage fluctuations contribute about 0.5% to the constant term for 25 rl blocks, increasing to 1.2 % for 22 rl blocks, and decreasing to 0.3% for 28 rl blocks. A similar pattern is seen in the lower energy (0.1 - 5 GeV) design studies and tests for the CLEO II thallium doped CsI calorimeter. Note that, by design, their *high energy* resolution is limited by leakage

transparent enough. The candidate materials that we discuss below both have enough light output to allow better than $1\%/\sqrt{E}$ behavior, and both can be made transparent enough to reduce the non-linearity by more than a factor of 10 compared to lead-glass. The added bonus of the reduction in non-linearity is that the line-shape becomes more and more Gaussian, greatly facilitating the understanding of the calorimeter response. Studies are still in progress, but it appears that a systematic uncertainty of better than 10^{-4} in the K_S/K_L ratio can be obtained with either of the two materials.

5.2.2 Rare Decay Searches

It is also true that very high precision is demanded in the search for and study of very rare kaon decays, particularly those containing a π^0. The prime example is the $\pi^0 e^+ e^-$ mode already discussed in the physics introduction to this report. There the major background is the mode $K_L \rightarrow e^+e^-\gamma\gamma$ which can be thought of as a Dalitz decay of the K_L with internal radiation. Although the Dalitz decay produces in general low-mass e^+e^- pairs and the radiated photon usually closely follows the direction of one of the electrons, nevertheless this background is substantial relative to the expected CP violating contribution. It is particularly troublesome in that the final state particles are just those in the desired decay, so that particle identification will not be of particular use, and that no particles are lost, so that both the kaon invariant mass and angle with respect to the beam are correctly reconstructed making these kinematic cuts ineffective as well. The only handle one has on the background is the $\gamma\gamma$ invariant mass (aside from making a judicious choice for the region of the Dalitz plot accepted). To keep this background below the 10^{-11} level (roughly the range expected for the standard model signal) will require a calorimeter with typical energy resolution below 1%. For the counterpart K_S interference experiment, high resolution is also necessary for this radiative Dalitz decay (which will contribute mostly in the interference region) and as well for

---

fluctuations. Unlike KAMI, their major requirements included operation in a high magnetic field, compactness, and good resolution at *low* energies. This led them to choose a block length of 16.2 rl. See E. Blucher, *et al.*, NIM A249, 201 (1986).

distinguishing accidental events from the increased rate of hyperon decays close to the target.

It is also clear that for the $\pi^0\mu e$ mode, good resolution is highly desirable. For the $\pi^0\nu\bar{\nu}$ mode, the vertex resolution is a direct function of the energy resolution. In conclusion, for all of the considered experiments, very high precision is desired.

5.2.3 Candidate Materials

We consider the two materials: BaF_2 and CsI. Table 5.2.1 gives the important characteristics of each.

Crystal	Den. gm/cm^3	Rad. len. [cm]	Decay time fast [ns]	Decay time slow	Fast Light yield [pe/GeV]	Fast/Total [0.1 μs/1 μs]	Rads for 10%/25rl loss
BaF_2	4.88	2.1	0.6 @ 220 nm	620 ns	20,000	0.25	≈10 k
CsI(pure)	4.51	1.85	10,36 @ 300 nm	≈2 μs	40,000	0.80	>1 k

Table 5.2.1: Characteristics of BaF_2 and CsI.

The current calorimeter for E731 consists of an 804-block lead glass array where each block has dimension $5.8 \times 5.8 \times 60$ cm^3 with its length parallel to the beam direction. The number of photo-electrons is only 500/GeV which contributes $4.5\%/\sqrt{E}$ to the total electron energy resolution of $1.5\%+5\%/\sqrt{E}$. The low light yield is primarily due to the fact that lead-glass is a Cerenkov radiator, and it will be necessary to use a scintillator to obtain photon statistics good enough for even the next round of Tevatron experiments, let alone for the Main Injector. Both CsI and BaF_2 generate 20000 or more photo-electrons per GeV even after the light yield is compromised to satisfy other requirements such as uniformity of response along the block. This corresponds to $0.7\%/\sqrt{E}$ or better energy resolution from photon statistics only.

As mentioned earlier, another important source of energy resolution is the coupling of longitudinal shower fluctuation to the light absorption within a block. The typical absorption coefficient of lead glass is 3% per radiation length. When this is coupled with longitudinal shower fluctuations of about 1 radiation length (for electrons; for photons, it is even larger), it results in a constant term of about 3% in energy resolution.

With BaF_2, we have studied the uniformity of response along the block with various wrappings and different methods for coupling of the phototube to the block. The absolute absorption length was measured to be 115 cm. However, with a careful teflon wrapping where small sections on both ends are left unwrapped, it was possible to obtain a uniformity consistent with being perfectly flat within the statistical error of about 1% on each point. Also, the response curve is well simulated by a ray tracing Monte Carlo indicating that the understanding of the response is good enough to control the response more or less at will. It is a concern, however, that the resolution may degrade after installation if the response changes (*e.g.*, due to radiation damage).

We have measured the timing resolution of BaF_2 and found it to be 160 ps even without correcting for pulse height. This is due to BaF_2's very fast (0.6 ns decay time) component. As can be seen from Table 5.2.1, BaF_2 also has a slow component; this, however, can be effectively reduced to an acceptable level by a phototube with Cs-Te photocathode or Rb-Te photocathode (a new photocathode material of which we have one prototype sample for evaluation). The fast timing also allows one to use a very narrow gate (20 ns or less). The fast components of CsI are not as fast but probably adequate for the Main Injector. If one adopts the "fly's eye" configuration, BaF_2 blocks could be used near the beam holes where the counting rate is high, with CsI filling the rest of the volume. Since CsI and BaF_2 have very similar radiation lengths and Molière radii, they can be used in combination without substantially complicating the analysis.

The literature on radiation hardness of BaF_2 and CsI is somewhat confusing due primarily to different grades of crystals used for tests. Both materials are probably hard enough for the experiments under

consideration here. In Table 5.2.1, we report the exposure which is expected to result in a 10% light loss over the length of the crystal. In this case, one would see an increase in the constant term of about 0.4%, probably the maximum that could be tolerated. We are presently conducting our own tests on the radiation sensitivity of pure CsI as described in Section 5.7.3. Preliminarily, it appears that pure CsI is considerably more radiation hard than we have indicated in Table 5.2.1. Another desirable feature of these crystals is that they can apparently be "cured" of the radiation damage by exposure to heat or light.

One significant drawback of BaF_2 is that, at present, it is about three times as expensive as CsI. To reduce the calorimeter cost, we have therefore tentatively adopted CsI as the material of choice for the purposes of this report.

5.2.4 Calibration

The calibration of the electromagnetic calorimeter is very important. For the very rare decays, it is desirable to achieve the best possible resolution (for background discrimination); for the high precision experiments (ε'/ε), excellent understanding of the calorimeter response is required.

Currently (E731) calibration is done using a gain monitoring system and several very high statistics event samples. A sample of about a million electrons was taken roughly twice per month by turning the neutral beam into a photon beam and producing pairs with a very thin converter. This sample, which is pure electrons, gives an average of about one thousand events per block. It is more than sufficient to determine gains and non-linearities at one specific time. A monitoring system consisting of a xenon flash lamp and optical fibers allowed us to track the gains of the individual calorimeter channels continuously during periods between these calibration runs. Finally, a sample of about 8 million electrons per week from K_{e3} decays was collected simultaneously with our data. Here the statistics are even greater than in the calibration runs, and there is a wider

range of electron momenta. This appears to be our best source for final calorimeter calibration even though there is a small (<1/3000) non-electron background in the sample. It has the very significant advantage that this sample is collected at exactly the same time and with the same triggering conditions as the signal events. High statistics samples of 3 π^0 and $\pi^+\pi^-\pi^0$ have also been very useful.

We believe that these same techniques will work for the KAMI experiments. Given the bandwidth of the KAMI data acquisition system and a powerful level 3 trigger (see Sections 5.5 and 5.6), it will be possible to collect a calibration sample with over one thousand K_{e3} electrons per block in a couple of hours. Reconfiguring to a photon beam for pair production will not be necessary, thereby saving both time and money. An optical fiber monitoring system with a nitrogen laser for a light source can provide gain tracking. During a one year run, we would also collect more than a billion K_{e3} events along with our data. Even after cleanliness cuts, these would provide one hundred thousand electrons in each of the 7000 crystals, permitting many detailed calibration studies. In addition, we will have the TRDs for particle identification which have the effect of making negligible the background to the calibration samples.

5.3 Particle Identification

Particle identification (particularly electron and muon) is required primarily for background suppression. This section discusses each in term.

5.3.1 Electron Identification by Transition Radiation

The electron identification is a crucial element for several high sensitivity rare decay search experiments in the Main Injector Kaon Facility. The non-destructive nature of transition radiation detector (TRD) particle ID systems makes them complementary to calorimetric π/e

rejection, which can deliver a combined π/e rejection factor of 10^{-4} or better in the momentum range 1-50 GeV.[8] Unfortunately, the basic design features of existing large area TRDs make them unusable in very high rate environments. The reason is that to achieve the desired π/e rejection, the conventional TRD x-ray radiator is usually filled with a stack of several hundred thin (15-20 μm) polypropylene films, or an equivalent mat of thin polypropylene fibers. The total radiator volume of several modules typically corresponds to 5% of a radiation length, and the x-ray detecting wire chamber is about 1.5 cm thick of xenon in which the charge collection times are typically on the order of 1 μs. Therefore, in order for TRDs to function in a high rate environment, it is desirable to minimize the total amount of material, and it is essential to reduce the charge collection time.

A fine sampling TRD system suggested by R. Tschirhart[9] could solve the above problems. The system consists of 30 modules, where each module has 50 polypropylene foils (or the fiber mat equivalent) followed by a double layer, thin-walled (25 μm), straw tubes with 3-4 mm diameter. This is shown in Fig. 5.3. Only the positions of sense wires over threshold are read out, with the threshold typically set at 5 keV so that a relatively simple discrimination system is adequate to detect the x-ray signals. The small diameter straw tube with a fast drift gas mixture of 80%:10%:10% $Xe:CF_4:C_2H_2$ can reduce the charge collection time to 30 ns.[10] Such a system will greatly improve the high rate capability. Also significantly less radiator material is required in a fine sampled TRD system to achieve the same π/e rejection as a conventional TRD system because there is less radiator material in each module to absorb the x-rays. Two possible problems exist with a tube based chamber system. One is the nonuniform x-ray absorption in the tube wall and the other is the varying x-ray detection

---

8 *Electron Identification up to 100 GeV by Means of Transition Radiation*, H.-J. Butt *et al.*, NIM A252 483 (1986); *Transition Radiation Detectors and Particle Identification*, B. Dolgoshein, NIM A252, 137 (1986).

9 "A Large Area Fast TRD for the 1990's", R. Tschirhart in the *Proceedings of the Symposium on Particle Identification at High Luminosity Hadron Colliders*, Fermilab, 609 (1989).

10 *Xe-Containing Fast Gas Mixtures for Gas-Filled Detectors*, L. G. Christophorou, *et al.*, NIM 171, 491 (1980).

efficiency, both as a function of impact parameter. However, a Monte Carlo simulation of a 30-module tube-based system with threshold readout shows no significant dependence of π/e rejection on track impact parameter. A prototype test of such a fine sampling TRD system will be needed to prove it's capability.

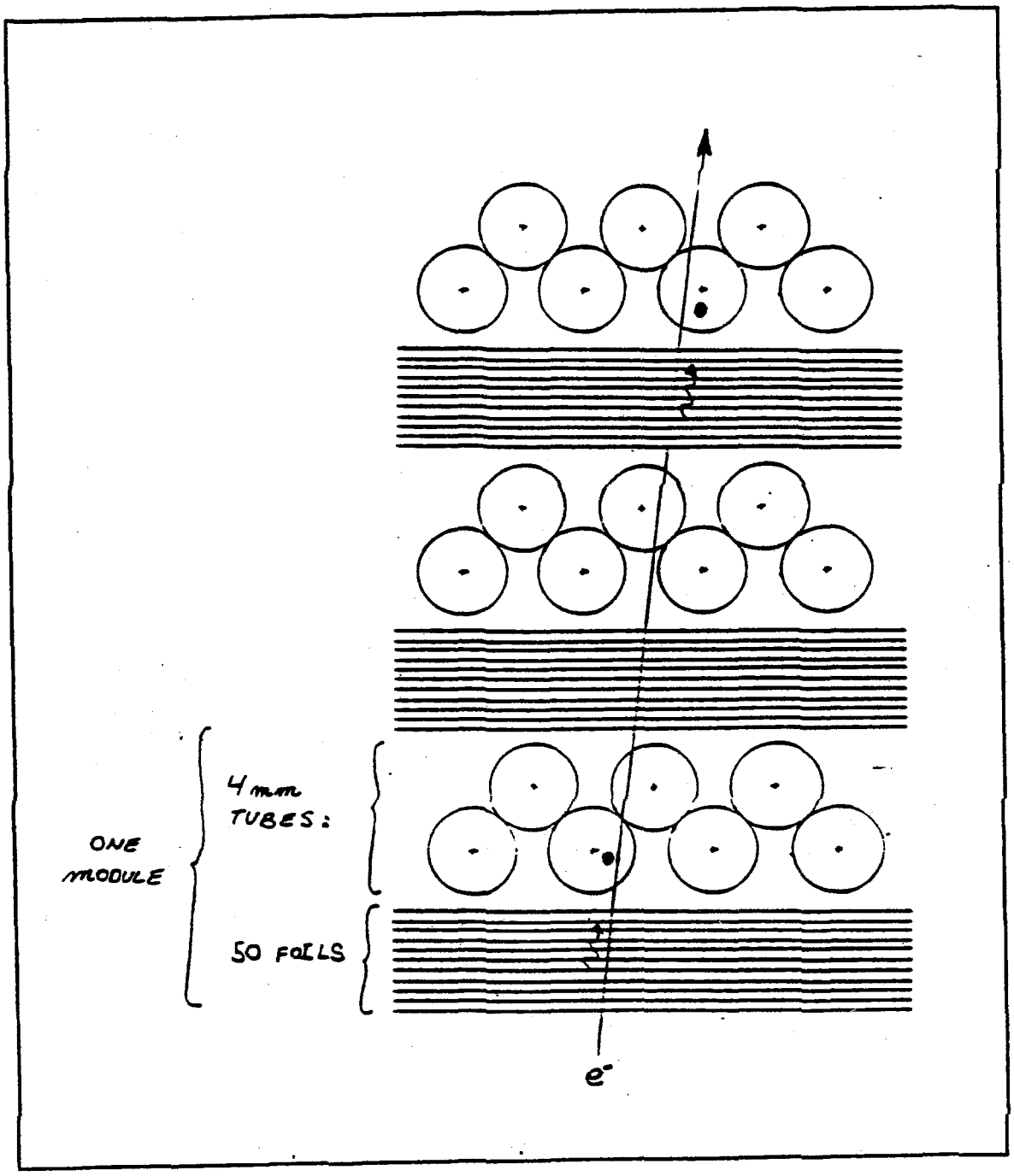

Fig. 5.3: Schematic of sampling TRD module.

5.3.2 Muon Identification

The muon identification system is most critical for the lepton flavor violating searches. It is of use in eliminating the two primary sources of background in this measurement. One source is K_{e3} decays in which the pion decays in the spectrometer. Most of these events have a μe invariant mass well below the kaon mass and are easily eliminated kinematically. When the neutrino momentum is close to zero and the pion decays after the momentum measurement, the "μe" invariant mass can be within 8 MeV/c^2 of the kaon mass. Extreme tails in the momentum (and hence mass) resolution due for example, to pattern recognition errors or large angle scatters, will result in background at some level which is difficult to estimate. An additional source of such background is from decays within the magnetic spectrometer. In such cases, the momentum could be badly measured. The redundant momentum measurement eliminates most such events, but at very low sensitivities, it is difficult to calculate backgrounds due to such decays plus pattern recognition or other errors.

The muon identification system is useful in adding to the kinematic background suppression. Approximately 75% of pion decays result in a muon with momentum less than 90% of that of the pion. Hence, by measuring the range and eliminating events with muon energy less than 90% of the measured particle momentum, 75% of this source of background could be eliminated.

The second generic background is due to K_{e3} decays in which both of the particles are misidentified. Due to the incorrect mass assignments, a small fraction of such events can reconstruct with an invariant mass at or above the kaon mass. The kinematic suppression is about 10^{-6}. To achieve a background below 10^{-13}, an additional factor of 10^{-7} is necessary. At these levels, the misidentification will likely result from accidental overlaps of a lepton from a second decay with the track measured in the spectrometer. We have not calculated these probabilities, but feel that the additional requirement that the muon range be consistent with the measured momentum will be necessary.

The muon detector envisaged would consist of sufficient material to range 12 GeV muons. Roughly 10 m of steel would be required. It would be in layers of increasing thickness going from the front to the back of the range finder, with particle detectors between the layers. Thickness would be chosen to correspond to an incremental range of 10% of the original momentum of a muon stopping at that point. Twenty three layers are required. Each layer is roughly 3.4×5.0 m^2. A total of 1500 tons of steel is required and for this we are considering the existing steel in the muon lab.

A possible choice for the detectors would be drift tubes, with an x and a y measuring plane at each layer. With a 1 cm cell, this would require about 40,000 channels, assuming both the x and the y channels were split at the center to minimize channel rates. The relatively small cell size is used to minimize the livetime (with Argon-CF_4 gas, the maximum drift time in the cell would be about 50 ns.) Another possibility would be proportional wire chambers, with similar or even smaller resolving times. In order to minimize the electronics channel count, a number of wires could be ganged together before the readout. The modularity could be varied depending on the rate. We estimate that about 5000 channels of readout would be required. The readout would be relatively simple, with only latches on the ganged channels.

To cleanly eliminate pion punch through and to provide a good starting point for a tracking procedure in the range finder, the front end would be equipped with 4 (2x and 2y) planes of segmented scintillation counters with thin steel plates between them. In addition, to improve the rejection of background due to out of time tracks, we would use a few planes of scintillation counters in the array. Thus, the device would have 8 planes of scintillators, with a total of 140 m^2 by 2 cm thick of scintillator. Using 5 cm wide channels, and phototubes at each end, it uses about 1300 phototubes. The readout would require 1300 channels of TDCs, and the trigger electronics would require about 350 channels of meantimers. In addition, we would measure the pulse-height on the four upstream-most planes, requiring 650 channels of ADC.

5.4 Gamma Veto

For the experiments under consideration here, it is important that gammas escaping from the aperture of the calorimeter be seen with high efficiency. In the case of ε'/ε, this is to reduce the background from $3\pi^0$ decays. There are backgrounds for the rare decay searches involving pile-up of more than one decay within the detector resolving time. The signature of extra particles is very helpful in reducing this effect. But clearly the most stringent requirement will be for the $\pi^0\nu\bar{\nu}$ mode where it is necessary to detect a photon in the range of 30 to 700 MeV with an inefficiency of less than 10^{-3}. Much of the following discussion therefore seeks to show in general terms how this most stringent requirement may be met. We then describe a veto system suitable for beginning the experimental program and for initiating the evolution of this more powerful device.

5.4.1 Design Considerations

A total of at least 15 radiation lengths is needed to convert a single photon from the $K_L \rightarrow 2\pi^0$ decay with sufficiently small inefficiency. The proportion of scintillator, as well as the extent of sampling in this veto system, is determined by the study of photonuclear interaction processes which result in photon detection inefficiency. For reasons of cost, we consider a sampling veto; then the major consideration is the inability to see an interaction in the passive part of the detector.

5.4.1.1 Photonuclear Inefficiencies

At energies below a few hundred MeV, a photon sometimes interacts with a nucleus and produces slow protons, pions and neutrons. Of these, neutral pions are detected with very high efficiency, but the slow charged pions, protons and neutrons are harder to detect. For the purposes of the veto design, these processes were studied quantitatively in the following

manner. First, using a Monte Carlo program called PICA[11], the products of a photonuclear interaction were generated for a photon of given energy in the given medium. From the energy of daughters, dE/dx and range (inelastic vs. proton recoil cross-sections in case of neutrons), it was decided whether the occurrence of the interaction could be detected or not. Repeating the procedure over the energy range of interest (30 to 700 MeV), the detection inefficiency curve due to the process was computed and is shown in Fig. 5.4. The ratio of the photonuclear to Coulomb interaction cross-section was obtained from the literature.

The next step was to introduce the inefficiency curve into a $2\pi^0$ background Monte Carlo for $\pi^0\nu\bar{\nu}$. The inefficiency was exaggerated by a scale factor of 60 in order to reduce the computation time. Out of three million generated $2\pi^0$ background decays, 70 events with double failure in the veto system passed all the $\pi^0\nu\bar{\nu}$ analysis cuts, corresponding to a single-event background at 6.5×10^{-12}.

5.4.1.2 Proton Detection

The proton to electron light yield ratio in plastic scintillator is 1:4 at 4 MeV. Hence, one should be able to see a proton that is above 4 MeV when it gets to the scintillator. In lead the proton dE/dx can be represented as 650 *ln(2.6E)/E MeV/cm. It is assumed that a proton produced in lead is seen if its "effective range" is greater than the half thickness (times $2^{1/2}$ for random direction) of the lead. Thus a 25 MeV proton made in a photonuclear interaction in the lead can go 1.1 mm towards the scintillator. These considerations determine the thicknesses of the passive material which averages 2mm.

5.4.1.3 Pion Detection

The dE/dx for 0.7 MeV π^{+-} in scintillator is the same as that for a 4 MeV proton. Thus we assume that one can see a 1 MeV π^{+-} in plastic scintillator. In lead, the π^{+-} "range" is approximately 5.5 mm at 25 MeV.

---

[11] T. Gabriel and R. Alsmiller, *Phys. Rev.* **182**, 1035 (1969).

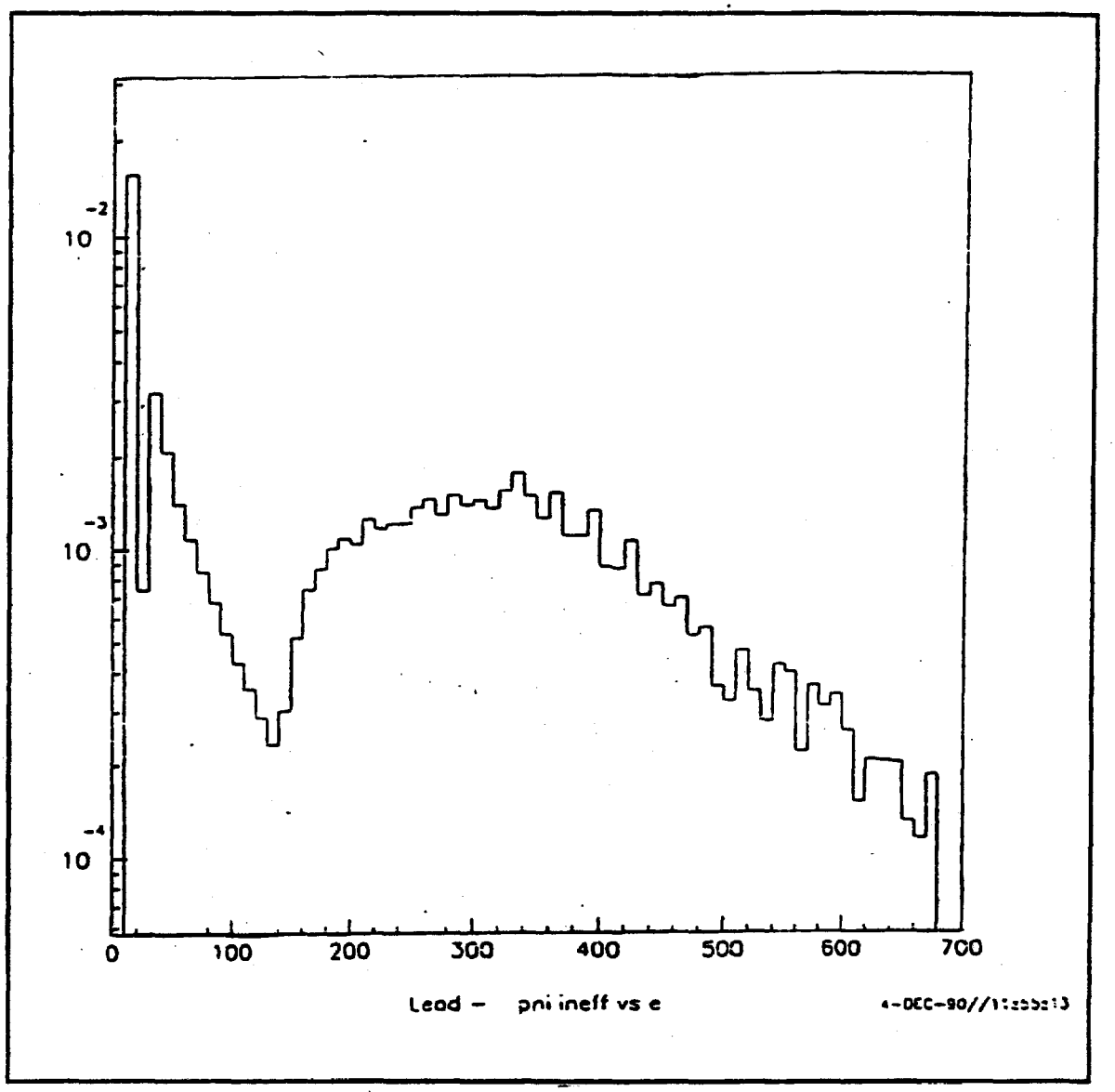

Fig. 5.4: Photonuclear inefficiency vs. energy.

5.4.1.4 Neutron Detection

Neutrons are somewhat more problematic. Short of very violent nuclear reactions, they can be seen most effectively by proton recoil in plastic scintillator. Typically, a neutron is produced in a photonuclear interaction inside, for example, lead. In order to be seen, it has to travel through part of the lead layer, then suffer a proton recoil in the scintillator

and transfer at least 4 MeV to the proton. Recoils off the Carbon in the scintillator can be ignored since the cross-section is 30% lower than that for a proton, peaks forward, and the neutron can lose at the most 30% of its momentum to the Carbon. The neutron detection efficiency in the veto system is computed on a radiation-length weighted basis assuming that the neutron is not detected if it suffers inelastic interaction in the passive part of the system, or is below 8 MeV, or escapes the system without a proton recoil. The thickness of material encountered by the neutron is corrected for geometrical factors. In the end, a neutrons efficiency of about 50% can be achieved.

The thickness of the lead layers in such a veto system is decided on the basis of maximum neutron detection efficiency for a fixed sampling by a given total thickness of scintillator. The general trend is that the inner layers need to be thin, and get thicker progressively. This is so because a thick passive layer in the beginning would tend to "eat up" neutrons. Also, backward going neutrons tend to be lost if they don't get to see enough scintillator. Deeper inside the veto system, the photon flux is significantly reduced so increased inefficiency does not matter as much any more. A neutron efficiency of 50% is obtained for 8 samples by a total of 35 cm of scintillator. The lead then provides the total radiation lengths necessary to convert photons. The values used for cross-sections were all for 25 MeV neutrons which is a reasonably good approximation.

In the PICA program, the nucleus is often left with a significant amount of energy after the absorbing the photon. Photons which then result from nuclear de-excitation will increase the detection probability. The same is true when a neutron that is produced in a photonuclear interaction has an inelastic interaction with the nucleus of the passive material in the veto. Thus the efficiency may actually be somewhat higher than calculated.

5.4.2 Chosen Configuration

We have chosen a phased approach for the veto system. For experiments prior to the $\pi^0\nu\bar{\nu}$ search, our primary veto configuration will be an expanded version of that planned for E799/832. It consists of a set of highly segmented annular lead-scintillator detectors[12] located at carefully chosen locations along the beam line (see Figs. 3.1-3.3). This will enable us to re-use the detectors constructed for the Tevatron experiments, a considerable initial saving in cost and effort for KAMI. The segmentation of these detectors provides position information as well as energy information thus allowing us to analyze and understand background sources in the KAMI environment. Such information will be important for background suppression during the early part of the experimental program and will be crucial for developing the hermetic veto system required for the $\pi^0\nu\bar{\nu}$ search. The small upstream section of the decay volume will be instrumented with a cylindrical prototype for this hermetic veto system.

Figure 5.5 shows a schematic view of one of the annular ring counters for the decay region. Scintillating tile and fiber construction enables us to have the sensitive volume of the detector in isolated vacuum for a low detection threshold while operating the phototubes and bases outside the vacuum.

For the $\pi^0\nu\bar{\nu}$ search, a hermetic veto system would be required. As analyzed above, a basic configuration would have plastic scintillator with lead/steel layers inside the vacuum and a liquid scintillator/lead volume surrounding the vacuum tank. We estimate the additional cost of this system at $2-3M. Though further analysis based upon prototype studies and operational experience from the early part of the KAMI program is needed in order to develop a more detailed design for this advanced veto system, the discussion above shows that the goal of 10^3 single photon rejection is not unreasonable.

---

[12] See discussions by K. Arisaka, *et al.* in KAMI-52, 55, 56, 58, internal notes.

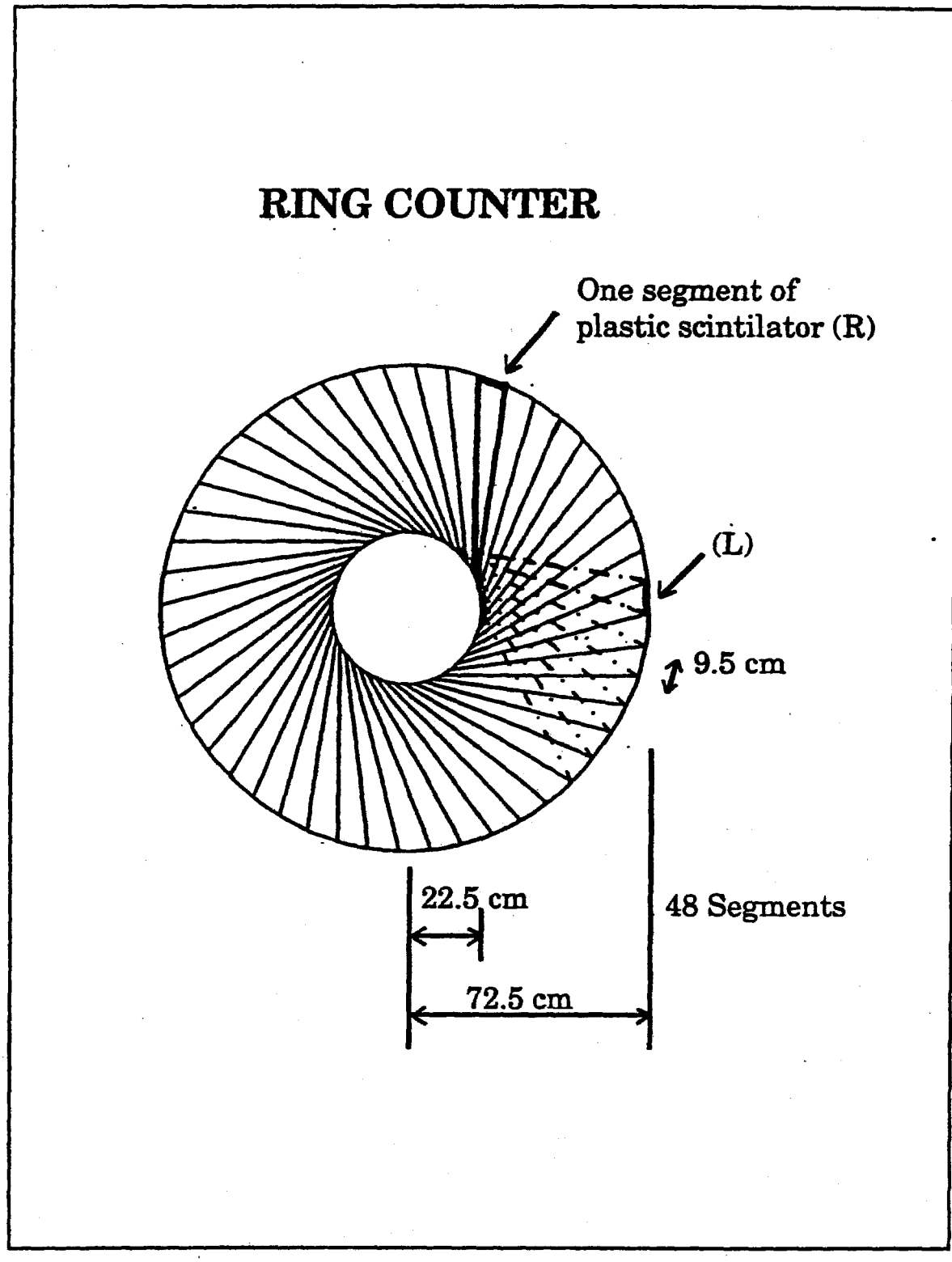

Fig 5.5: Schematic view of a ring veto counter.

5.5 Triggers

Here we will estimate the trigger rates for the high statistics ε'/ε experiment, the rare "direct" CP-violation experiments ($K_L \rightarrow \pi^0 e^+ e^-$ and $K_L \rightarrow \pi^0 \nu\bar{\nu}$) as well as the lepton flavour violation experiments ($K_L \rightarrow \mu e$ and $K_L \rightarrow \pi^0 \mu e$). In each case, the goal is that of reducing a raw kaon decay rate to levels acceptable for "tape" storage. Here, "tape" implies that the details of how the data is to be preserved are still open to discussion. (See Section 5.6.5)

5.5.1 ε'/ε Experiment

We first consider the rates in the ε'/ε experiment. Tables 5.5.1 and 5.5.2 indicate the raw rates for both K_L and K_S decays to neutral and charged final states together with the rate reduction at various stages of the trigger. These rates were estimated by Monte Carlo simulations of the various decay modes with their contributions summed at each stage[13]. The trigger devices employed are relatively standard.

Dead times associated with the various levels of triggering appear to be manageable. The active regenerator provides fast (<10 ns) pulses which effectively eliminate the vast majority of events with charged particles made in inelastic interactions. The total energy signal in the calorimeter is available within 100 ns of the event. Similarly, the gamma veto is a very fast signal. The 2 track requirement in the charged trigger is made with scintillation counters. The veto from the TRD system might take on the order of 500 ns, and the 4-cluster trigger from the calorimeter can probably be done within 1 to 2 μs. The look-up table for rejecting invalid charged mode patterns is fast enough to be done in about 200 ns, while the track processor might take about 10 μs.

---

[13] See T. Yamanaka, KAMI-59, internal note.

RATE	K_L	K_S
Raw decays, interactions	600k	3400k
Total E in cal.; no hit in regenerator	420k	26k
gamma veto	410k	24k
4-clusters, neutral	20k	6k
Level 3 Mass	3k	2k
(Good events)	(0.36k)	(0.84k)

Table 5.5.1: $2\pi^0$ triggers per spill for ε'/ε experiment.

RATE	K_L	K_S
Raw decays, interactions	600k	3400k
No regenerator hit; gamma veto; 2 tracks; no muon	420k	24k
TRD	180k	12k
Look-up table; track processor	26k	8k
Level 3 Mass	2.5k	4.5k
(Good events)	(0.87k)	(2.5k)

Table 5.5.2: $\pi^+\pi^-$ triggers per spill for ε'/ε experiment.

The total trigger rate, including some calibration events, for the ε'/ε experiment is shown in Table 5.5.3.

Total neutral trigger rate	5k
Total charged trigger rate	7k
Total calibration trigger rate	1k
GRAND TOTAL	13k

Table 5.5.3: Total Triggers per spill, ε'/ε.

5.5.2 High Rate Experiments

The triggering challenge in such experiments is to reduce the raw kaon decay rate of 33 MHz down to a few kHz for "tape" writing. Fast processors are required to reduce the rate to an acceptable level. The raw trigger rate is dominated by K_{e3}, $K_{\mu 3}$, $3\pi^0$ and $\pi^+\pi^-\pi^0$ decays.

Trigger rates for $K_L \rightarrow \pi^0 e^+ e^-$, $K_L \rightarrow \pi^0 \mu e$ and $K_L \rightarrow \mu e$ were estimated[14] from Monte Carlo simulations of the primary K_L decay modes. Tables 5.5.4 and 5.5.5 summarize the trigger rates and the rate reductions at the various stages.

Mode	Rate	Dominated by
$K_L \rightarrow \pi^0 ee$		
raw decays	33 MHz	
E_{Total} > 10 GeV	14 MHz	$3\pi^0$
gamma veto	13 MHz	$3\pi^0$
2-track, no μ	4.1 MHz	K_{e3}, $\pi^+\pi^-\pi^0$
TRD (e)	1.1 MHz	K_{e3}
Hits in chamber 1	320 kHz	K_{e3}
4-cluster	14 kHz	$\pi^+\pi^-\pi^0$
level 3	3 kHz	
$K_L \rightarrow \pi^0 \mu e$		
raw decays	33 MHz	
E_{Total} >10 GeV	14 MHz	$3\pi^0$
gamma veto	13 MHz	$3\pi^0$
2-track, 1 μ	310 kHz	$K_{\mu 3}$
TRD (e)	150 kHz	K_{e3} with π decay
Hits in chamber 1	56 kHz	K_{e3} with π decay
4-cluster	4.4 kHz	$\pi^+\pi^-\pi^0$ with π decay
level 3	1 kHz	

Table 5.5.4: Estimated trigger rates for $K_L \rightarrow \pi^0 ee$ *and* $K_L \rightarrow \pi^0 \mu e$.

[14] See T. Yamanaka, KAMI-59, internal note.

Mode	Rate	Dominated by
$K_L \to \mu e$		
raw decays	33 MHz	
2-track, 1-μ, gamma veto	10 MHz	$K_{\mu 3}, K_{e3}$
range out μ p_μ<7 GeV	7 MHz	$K_{\mu 3}, K_{e3}$
TRD (e)	1 MHz	$K_{\mu 3}, K_{e3}$
look-up table p<7 GeV	300 kHz	$K_{\mu 3}, K_{e3}$
1-cluster, E/p (e)	100 kHz	K_{e3}
level 3 mass, p_t^2	2 kHz	

Table 5.5.5: Estimated trigger rate for $K_L \to \mu e$.

Since it is imagined that all of the high rate searches will be run simultaneously, we list in Table 5.5.6 the total trigger rate for the high rate experiment.

$K_L \to \pi^0 \mu e$ *trigger rate*	1 kHz
$K_L \to \mu e$ *trigger rate*	2 kHz
$K_L \to \pi^0 ee$ *trigger rate*	3 kHz
TOTAL HIGH RATE TRIGGER RATE	6 kHz

Table 5.5.6: High Rate Triggers, Total.

We next turn to the π^0 + "nothing" experiment. Here we rely very heavily upon the gamma veto to reduce the trigger rate to an acceptable level as is shown in Table 5.5.7.

Mode	Rate	Dominated by
$K_L \rightarrow \pi^0 \nu\bar{\nu}$		
raw decays	10 MHz	
E_{Total} in calorimeter	1.6 MHz	
no-track	370 kHz	$3\pi^0$
gamma veto	3.7 kHz	$3\pi^0$
2-cluster	1.8 kHz	$3\pi^0$, $2\pi^0$
level 3	1 k Hz	$3\pi^0$, $2\pi^0$

Table 5.5.7: Estimated trigger rate for $K_L \rightarrow \pi^0 \nu\bar{\nu}$.

Finally, we give a similar breakdown for the K_S experiment in Table 5.5.8.

Mode	Rate	Dominated by
$K_S \rightarrow \pi^0 ee$		
raw decays	15 MHz	
two track, E_T in calorimeter	640 kHz	Λ decays
TRD	90 kHz	
4-cluster	25 kHz	
level 3 mass, p_t^2	4 kHz	

Table 5.5.8: K_S Trigger rate.

We conclude that although reduction of the trigger rate is challenging, there is no serious obstacle to achieving a low enough rate to be written to storage media as we discuss in the next section of this report.

5.6 The DAQ System and Off-line Computing

5.6.1 Introduction

In this section, we discuss the conceptual design of the data acquisition (DAQ) system for the Main Injector kaon experiments. The DAQ involves gathering the raw data from the detectors (drift chambers, scintillators, TRDs, vetoes, calorimeter...), making further (*Level 3*) decisions to select any interesting events and saving them to an appropriate storage medium ("tape"). The first level of discussion pertains to the number of channels in the experiment and the number expected to contain information for one event. This establishes the size of the event. Then the event rate is considered at each stage of the trigger (see Section 5.5). *Level 0* trigger is defined as the fastest and most simple possible trigger, to be used to strobe data from chambers, counters and calorimeter into registers, TDCs, ADCs and flash ADCs for further processing. The *Level 1 and Level 2* trigger will then use the fastest available data to perform more sophisticated partial event reconstruction and selection, such as cluster finding in the calorimeter, track finding in the spectrometer, particle ID, track momentum and *E/p* etc. The final level of trigger (*Level 3*) will involve on-line real-time computing to fully reconstruct the entire event. These considerations of the trigger rates and the sizes of events lead to estimates of the band width of the DAQ system at any particular level.

Lower Bounds on the DAQ band width

One may try to set the scale of the DAQ band-width based on the number of events expected in the experiments we have discussed. Such an estimate is based simply on the number of events in the final trigger level as discussed in Section 5.5.

In the ε'/ε experiment, from the estimated trigger rate in Table 5.5.3, one expects 13k events/spill in 3 sec for tape writing. If each event contains 2k Bytes, then the bandwidth is 13k × 2k / 3 sec = 9 MByte/sec!

In the rare decay and lepton flavour violation experiments, the number of events is about 6k/spill (see Table 5.5.6), so the bandwidth needed is roughly the same.

5.6.2 Detector Channels

There are about 10k drift chamber TDCs, 50k TRD latches, 6k muon channels (latches, ADCs and mean timers), 30k calorimeter channels (ADCs, flash ADCs and TDCs), and about 7K photon veto channels (latches, ADCs, and TDCs). In addition, there will be another 1K channels of scintillator for the *Level 0* trigger and general monitoring.

5.6.3 Event Sizes

We now try to estimate the size of an event. The $2\pi^0$ events are expected to include about 500 channels of calorimeter (ADCs, flash ADCs and TDCs), if one uses sparse readout. Other additional channels will be required for monitoring and checking as well as some accidentals. We estimate the equivalent of 700 channels, each with addressing, pulse height, and time information which requires 24 bits (3 Bytes) per channel. Therefore, a typical $2\pi^0$ event might consist of 2100 Bytes (2.1 kB).

A minimal charged event would consist of two tracks through the full spectrometer. That would yield 40 hits in the chambers, 5 hits in the TRD, and assorted other scintillator hits. 50 hits at 3 Bytes/hit implies 150 Bytes/event for the drift chamber system. In addition, there will be calorimeter/muon detector information. We estimate 200 channels for this additional information (or 600 Bytes). However, the rates are high, and the gate widths required for the drift chambers will be of order 30 nsec, so some accidentals are expected. It is more appropriate to assume that a typical charged event would have 300 Bytes of information from drift chamber system plus monitoring and checking or a total of 600 Bytes of information. With the 600 Bytes from the muon/calorimeter, this yields an event size of 1200 Bytes or more for charged events.

5.6.4 The Readout System

The typical front end readout rate is on the order of 100 kHz from the estimated trigger rates. Assume that the average event size is 2 kBytes. Then the DAQ bandwidth at the front end would be of the order 1×10^5 events/sec $\times$ 2000 Bytes / event = 200M Bytes/sec. The front end readout must be *highly parallel* and *very fast*. It will therefore be necessary to provide fast dual port or FIFO memories for each of the elements of the charged particle spectrometer, and to provide several layers of buffering on the calorimeter. Either a Fastbus or VME based system with fast digitization time in TDCs and ADCs will be considered as the front end readout system.

In order to form a *Level 1* trigger, it will also be necessary to provide fast access to the information from the detector. In the electromagnetic calorimeter, this information is provided by flash ADCs on each channel. The flash ADCs read out separately from the main ADCs and are used in a cluster finding trigger processor. Similarly, PWC type readout must be taken from the drift chambers. Time resolution may be improved in the *Level 1* charged mode trigger by using *mean timers* between ambiguity resolving planes to determine the time of the track. This tighter timing may provide a significant reduction of accidentals. The fast information can then be used to form a track finding trigger.

These "fast access" data must also be preserved for off- line analysis in order to study triggering. Fast buffering for *Level 1* data must also be provided in the DAQ.

Essentially the same information used in the *Level 1* trigger is used in the *Level 2* trigger in which track and cluster matching, particle ID, *E/p* and other kinematical quantities can be reconstructed. The event buffering can be reduced somewhat at this level because of the reduced rate. It may be possible to start event building here at the subsystem level. Both *Level 1 and Level 2* triggers are specialized high speed processors which will make use the existing on-going effort and experience of the Cluster Finder and Track Processor for the Tevatron experiments E731/773/799.

Events which satisfy the *Level 2* trigger must be built up and transmitted as complete events to the *Level 3* processors. One method currently being considered for event building is using a very high speed buss that interconnects the outputs of the *Level 1+2* buffers with *Level 3* input buffers. There would be a number of *Level 3* input buffers equal to the number of processing elements to be used in the *Level 3* trigger. The *Level 3* buffers would be filled in either a "round-robin" or on an "as available" basis. Either method can be constructed so as to allow for the addition and/or removal of processors as needs change or for repair.

The *Level 3* trigger is really a farm of on-line processors. At the present time, one can buy computing for between $100 and $250/MIP. 2000 MIPS are needed to do a real time reconstruction of the events. At this level, only fully reconstructed events plus background and test events will survive. For most experiments, the resulting event rate should be of the order of the rates quoted in the "lower bound" discussion above.

5.6.5 "Tape"

Two of the schemes that are are currently in use to save large samples of events at high rates are:

1) Farms of 8 mm drives, and
2) Honeywell VLDS (Very Large Data Store).

The first of these schemes is currently in use in a number of experiments and provides a bandwidth improvement over the existing 8 mm drives (about 200 kHz) of a factor of 10 to 30 depending on the number of drives used. 8 mm drives with twice the density and therefore twice the bandwidth are currently coming onto the market. A system with 25 of these double density drives would provide a bandwidth of order 10 MHz, which is quite adequate.

The Honeywell VLDS (Very Large Data Store) is similar to the 8 mm technology, but uses VHS video cassettes. It has the advantage that it can write data at up to 4 MHz. The capacity of a tape is about 5.2 GByte.

Therefore, three drives could handle the full bandwidth.

The VLDS drives cost about $20 k each. At least four would be required as we must also have off-line access to the data. The cost/drive of the 8 mm drives is $1860. (Oct '90)

We conclude that, even with today's technology, an adequate data acquisition system can be assembled at a reasonable cost.

5.6.6 Off-line Computing

As discussed above, we will require about 2000 MIPS of on-line computational power during data taking to reduce our data to tape to an acceptable level. This system could be so configured that, when the experiment is not running, the system can be used for off-line analysis. We foresee that some of the "first-pass" DST production could be done on this system. As is traditional at Fermilab, we envision that further analysis of these DSTs will use the Fermilab Central Computing Facility as well as various university facilities.

To obtain a more quantitative estimate of our off-line computing needs, we have reviewed our E731 usage. For KAMI we assume a 50-fold increase in raw data volume and (to be conservative) no increase in computational cleverness. Creation of the first-pass DSTs would then require about 10k MIPS-months; *e.g.*, 5 months of dedicated use of a 2000 MIPS system. Analysis of the DSTs would require another 5k to 10k MIPS-months. The Monte Carlo study of acceptance, backgrounds, and systematics would consume another 5k to 20k MIPS-months. This yields a total estimate for on-line computing of between 20k and 40k MIPS-months for each class of experiment. This would imply the need for majority access to an off-line system somewhat larger than that envisioned for on-line use.

5.7 Radiation Damage

Given the high rates expected in KAMI experiments, it is important to make sure that the detector can stand the level of radiation to which it will be exposed. The most critical element is the electromagnetic calorimeter, which is treated here. The issue of drift chamber aging is discussed in Section 5.1.2.

In this investigation, we have drawn on our experience with radiation exposure and damage to the lead glass calorimeter used in Tevatron E731. In E731 running at 10^{12} incident protons per spill, the calorimeter experienced an average radiation dose of about 25 rads per week in each of the 24 lead glass blocks bordering the beam holes. Most of the accidental activity, and hence radiation damage, in the lead glass array occurred in the region between the two beams and near the vacuum beam. It arose from (elastic) interactions in a Be absorber (and Pb gamma filter) placed in the neutral beam downstream of the initial collimator. GEANT simulations[15] reproduce the general radiation pattern and indicate that the size of the effect is quite sensitive to the location of the absorber/filter and the alignment of subsequent collimators. These investigations are continuing. This background can be eliminated by running without an absorber, or it can be very greatly reduced by placing the absorber upstream of the initial collimator.

Neutron interactions in the regenerator (for ε'/ε) and K_L decays should then be the dominant sources of radiation damage at the Main Injector. These have been investigated with Monte Carlo simulations as discussed in the following sections.

---

[15] See W. Slater, KAMI-57, internal note.

5.7.1 E731 Simulation

A simplified version of the E731 Monte Carlo was used to model K_L decays. For this estimate, only $K_L \rightarrow \pi e \nu$ and $K_L \rightarrow 3\pi^0$ were considered. Showers were not generated in the calorimeter; if the electron or gamma pointed at a given block, then it was assumed that that block contained all of the energy. For the entire E731 run of about 30 weeks with 3×10^9 K_L decays, this estimate gives 1 rad per edge block. So the conclusion is that K_L decays produced <0.05 rads per week, much less than the observed 25 rads per week as expected.

Radiation damage from neutron interactions in the E731 regenerator was modeled using GEANT. The program was run for 50 and 100 GeV neutron energies. Figure 5.6 shows the neutron flux and flux times momentum versus momentum. Folding in the calculated neutron momentum spectrum including absorber effects gives 0.1 to 1 rads per week for an edge block. A range is quoted because of the limited statistics due to the large amount of computer time needed. Thus the radiation damage from hadron interactions in the regenerator was also small as expected.

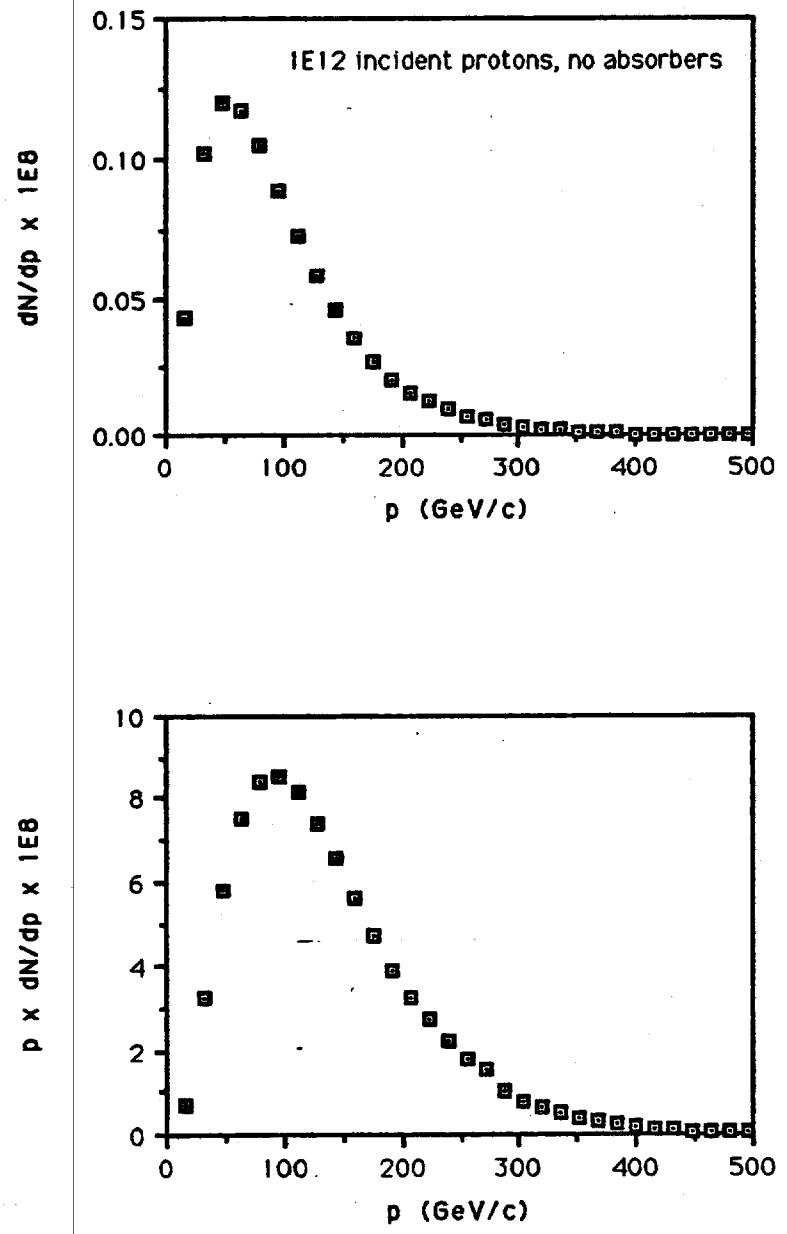

Fig 5.6: Neutrons from 800 GeV/c Protons.

5.7.2 KAMI Simulation

To determine radiation damage during the high rate experiments, K_L decays were modeled in the detector assuming a CsI calorimeter with a 12 μstr. beam hole. With 3×10^{13} protons every 3 seconds and 100 hours of running per week this gives 1.7×10^{13} K_L decays. A CsI block 3.3 cm × 3.3 cm × 44.4 cm on the edge of the beam hole gets 700 rads per week. The dependence on radius is shown in Fig. 5.7.

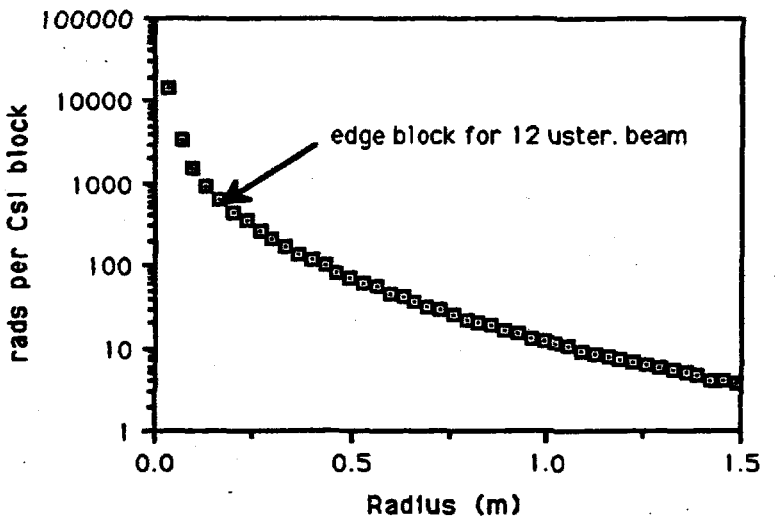

Fig. 5.7: Radiation damage from KL decays - 1 week run.

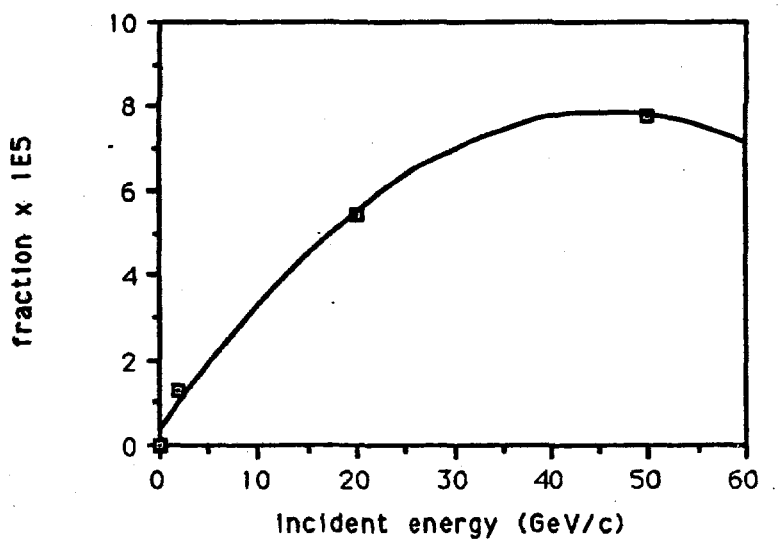

Fig. 5.8: Fraction of energy per edge block from neutron interaction.

To determine damage during the ε'/ε experiment, neutron interactions were modeled using GEANT; a 10% interaction length scintillator regenerator placed at 28 m from the target and a 1 μstr beam were assumed. Calculations were done for 3×10^{13} incident protons every 3 seconds and 100 hours per week. The fraction of incident neutron energy deposited in an edge block is plotted versus energy in Fig. 5.8. The neutron spectrum used is shown in Fig. 5.9. The resulting radiation damage in one edge block was about 70 rads per week.

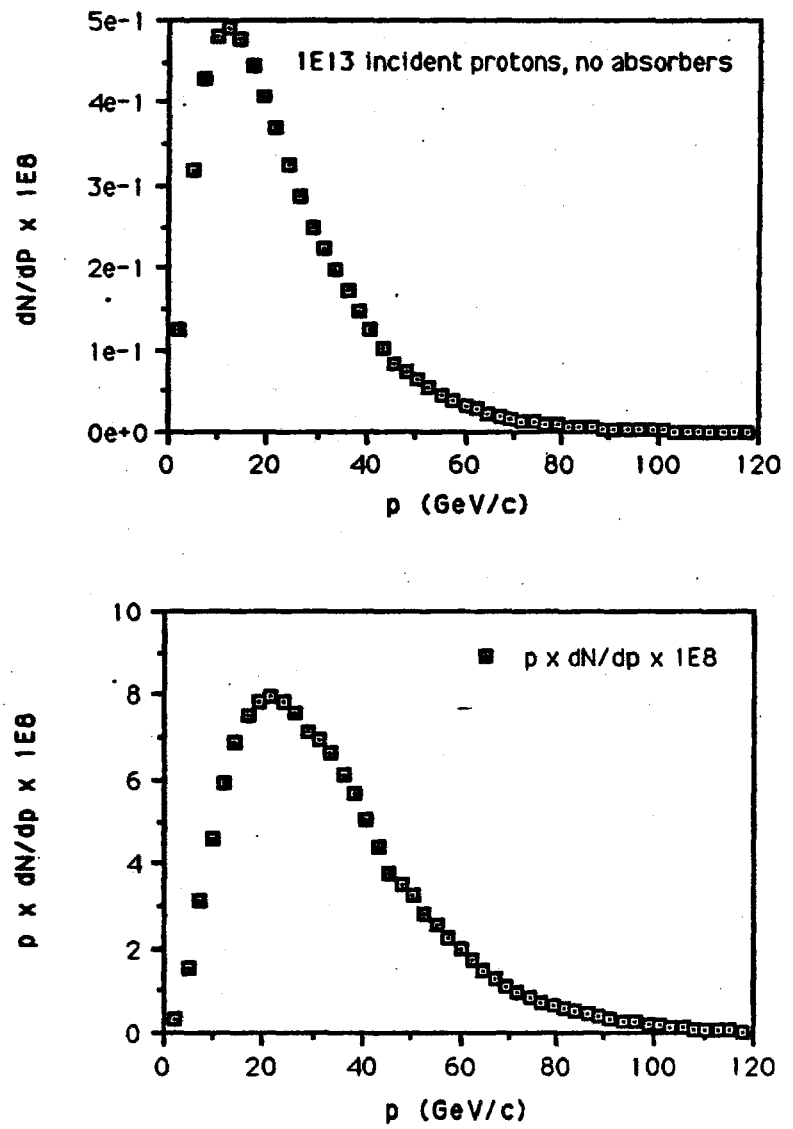

Fig 5.9: Neutrons from 120 GeV/c Protons.

5.7.3 Ongoing CsI Tests

We are in the process of testing pure CsI for radiation sensitivity. We have exposed one crystal from Horiba (20 cm long and of similar cross-section to those planned for KAMI) to increasing doses of gamma radiation from a intense ^{60}Co source at Argonne National Laboratory. (For lead glass, a given dose of low energy gamma rays is generally found to cause somewhat more radiation damage than an equal dose from high energy hadrons.[16]) With a dose of about 20,000 rads, we have observed no measurable change in the transparency of the crystal: the light absorption across the 20 cm length is less than 2%. Since we could tolerate as much as 5% over this same length, it appears that this material is as hard as is required for the KAMI program, including the very intense rare decay search mode.

We do note, however, that there is an apparent overall decrease in light output at about the 30% level after the 20 krad exposure. From selective exposures of part of the crystal, it appears that this is a surface effect which degrades light coupling to the photomultiplier tube, not a volume effect. It thus poses no significant problem even if the radiation dose is distributed non-uniformly throughout the block, as is likely in actual operation. At this level the loss of photostatistics has almost no impact on the resolution.

In any case, we plan to continue these tests, both with ^{60}Co gamma rays and with high energy hadrons, on several crystals.

---

[16] See, for example, K. Kirsebom and R. Sollie, NIM A245, 351 (1986).

6. COSTS

In this Section, we will give our best estimates of the costs associated with carrying out the physics program that we have presented. We include the costs associated with the siting of the facility, the technical components of the facility (the primary beam elements, the secondary beam elements, and the analysis magnets) as well as of the detector. We also include 5 year operating costs of major secondary beam subsystems and the analysis magnets.

The estimates are intended to give the general scope of this project. Many of them are firmly based upon existing devices or can be extrapolated with reliability; however, it is impossible for a reliable estimate to be given for each element and in some cases which we spell out in the discussion, we have only been able to make our best guess.

6.1 Civil Construction Costs

Table 6.1.1 displays our cost estimates for KAMI civil construction. As we have done elsewhere, we have assumed siting in NMUON in order to have a definite costing model (see Sections 2 and 4). This model calls for an experimental hall extension, addition of dirt over existing primary beam enclosures, steel shielding at Batavia and Eola Roads, and appropriate beam pipe and enclosure extensions. We treat the building extension and shielding upgrades as "existing" because they are needed for the Tevatron kaon program (E799/832). Analogous work would be required for other siting choices, though specific costs would certainly be different.

Table 6.1.1: Estimated Civil Construction Costs

Item	Component	Unit	Unit Cost ($)	# Units	Cost ($k)	Exist ($k)	New ($k)
Experimental Hall Extension							
	40' x 80' Bldg. Addition	sq. ft.	250	3200	800	800	
	20 Ton Crane	unit	225,000	1	225	225	
Subtotal					1,025	1,025	
Shielding Upgrade							
	Dirt over enclosure	cu. yd.	7	45400	318	318	
	Steel at Batavia, Eola	ton	500	1105	553	553	
Subtotal					871	871	
Switchyard Primary							
	Berm Pipe	ft.	250	690	173		173
	G1 tunnel extension	ft.	3,000	35	105		105
Subtotal					278		278
Total Civil Construction					2,174	1,896	278

6.2 Primary Beam (Technical) Costs

Estimates for primary beam technical costs are shown in Table 6.2.1. We treat part of the instrumentation as "existing" because it represents needed improvements in primary beam diagnostics for the Tevatron kaon physics program (E799/832). Again, to make definite estimates, we use siting in NMUON as a working model. If another area is chosen, details of the cost estimates will be different.

Table 6.2.1 Estimated Primary Beam (Technical) Costs

Item	Component	Unit	Unit Cost ($)	# Units	Cost ($k)	Exist ($k)	New ($k)
Beam Elements							
	EPB Dipoles	magnet	45,000	8	360		360
	3Q60 Quads	magnet	35,000	4	140		140
	Trim Dipoles	magnet	16,000	6	96		96
	225 kW Power Supplies	unit	25,000	4	100		100
	150 kW Power Supplies	unit	80,000	6	480		480
	10 kW Power Supplies	unit	9,000	6	54		54
	Vacuum System	unit	75,000	1	75		75
	Rigging	unit	80,000	1	80		80
Subtotal					1,385		1,385
Beam Instrumentation							
	BPMs	unit	4,600	20	92	23	69
	LMs	unit	1,200	20	24	12	12
	SWICs	unit	9,000	4	36	27	9
	Precision Wire Scanner	unit	25,000	1	25		25
Subtotal					177	62	115
Total Primary Beam Costs					1,562	62	1,500

6.3 Secondary Beam Costs

In Table 6.3.1 we give a breakdown of the estimated costs for each of the major secondary beam components. Whenever possible, estimates have been made by scaling from previous relevant construction. In particular, many unit costs for the two new secondary beam magnets have been scaled from the expense history for the 1984-1985 construction of the E687 analysis magnet. An inflation factor of $(1.05)^6 = 1.34$ was applied whenever no more direct cost escalation indicator was available. Reference design parameters for the magnets were obtained from performance information for the E497 hyperon magnet.

Vacuum system estimates are based on experience with the E731 vacuum system combined with other installations employing significantly higher vacuum levels. Mechanical cost estimates (for the target assembly, tapered channel, etc.) were prepared with the assistance of the Research Division Mechanical Department.

Table 6.3.1: Secondary Beam Cost Estimates

ITEM	COMPONENT	UNIT	UNIT COST ($)	REF.	# of UNITS	COST ($k)
Target Magnet						
	Magnet Steel	tonne	1,400		400	560.0
	Clean & Install	tonne	132		400	52.8
	Misc. Parts	tonne	24		400	9.6
	Coil Copper	tonne	5,500	1	37	203.5
	Bend & Braze	tonne	1,760		37	65.1
	Shot Blast	tonne	154		37	5.7
	Insulation Fixtures	tonne	406		37	15.0
	Insulate	tonne	4,490		37	166.1
	Handling Fixture	unit	12,000		1	12.0
	Coil Clamps	unit	14,000		1	14.0
	Pole Steel	tonne	2,200		12	26.4
	Machine Pole	unit	10,000		1	10.0
	Insert Pb	tonne	2,200		29	63.8
	Machine Pb	unit	20,000		1	20.0
	Tapered Channel	unit	50,000		1	50.0
	Channel Cooling	unit	10,000		1	10.0
	Power Supply	k W	450	2	325	146.3
Subtotal						1,430.3
Dump Magnet						
	Magnet Steel	tonne	1,400		625	875.0
	Clean & Install	tonne	132		625	82.5
	Misc. Parts	tonne	24		625	15.0
	Coil Copper	tonne	5,500	1	15	82.5
	Bend & Braze	tonne	1,760		15	26.4
	Shot Blast	tonne	154		15	2.3
	Insulation Fixtures	tonne	406		15	6.1

ITEM	COMPONENT	UNIT	UNIT COST ($)	REF.	# UNITS	COST ($k)
	Insulate	tonne	4,490		15	67.4
	Handling Fixture	unit	12,000		1	12.0
	Coil Clamp	unit	14,000		1	14.0
	Dump Copper	tonne	6,600		14	92.4
	Machine Copper	unit	10,000		1	10.0
	Dump Cooling	unit	10,000		1	10.0
	Insert Pb	tonne	2,200		59	129.8
	Machine Pb	unit	10,000		1	10.0
	Power Supply	k W	450	2	150	67.5
Subtotal						**1,502.9**
Sweeping Magnet(s)						
	BM-109					0.0
	BM-109					0.0
	Power Supply	k W	450	2	500	225.0
Subtotal						**225.0**
Vacuum System						
	Pipe, Flanges, Windows, etc.	unit	400,000		1	400.0
	Pumps	unit	60,000		8	480.0
Subtotal						**880.0**
Other						
	Target Assembly	unit	8,000		1	8.0
	Target Drive	unit	4,000		1	4.0
	Defining Collimator	unit	30,000		1	30.0
	Install Shielding	unit	200,000		1	200.0
Subtotal						**242.0**

ITEM	COMPONENT	UNIT	UNIT COST ($)	REF.	# UNITS	COST ($k)
Total Capital Costs						**4,280.2**
5-yr Operating Cost						
	Target Magnet Power	kW yr	500	3	813	406.3
	Dump Magnet Power	kW yr	500	3	375	187.5
	Sweeping Magnets Power	kW yr	500	3	1250	625.0
	Vacuum System	yr	20,000		5	100.0
Total 5-yr Operating Cost						**1,318.8**
Total Construction & 5-yr Operation						**5,599.0**

1 Copper conductor price as quoted for Main Injector magnets.

2 This is estimated as for analysis magnets in Section 4.3.3.

3 This assumes that magnets are in operation 50% of the time.

6.4 Analysis Magnet Costs

Section 4.3 details our analysis magnet options and the cost estimate bases for them. Here we simply summarize the total estimated costs for the three alternatives. We have assumed 70% operation for conventional analysis magnets and 100% for the superconducting CCM.

Table 6.4.1: Cost Estimate Summary for Analysis Magnet(s)

Alternative	Capital Cost ($k)	Annual Operating Cost ($k)	5-year Total Cost ($M)
Two magnets, copper coils	8,000	418	10.1
CCM, move and open gap	1,200	125	1.825
CCM, open gap and extend building.	125 1,025	125	0.750 1.025

We have used the third alternative to make our total project cost estimates. The building extension is included as civil construction in Section 6.1.

6.5 Detector Costs

Here we give the breakdown of the costs of each of the major detector items. Aside from the cost of scintillator, which will be bought commercially, the major expense is in electronics. For the electronic components, we have used the costs of existing commercial items although it is likely that by using our own designs, substantial cost reductions will be seen. Also, volume discounts are not assumed except for the scintillator. Assembly costs such as for chamber wiring, etc. are not included, but machining costs such as for chamber frames are meant to be included.

We give both total costs and the new costs, based upon some "existing" equipment. Here we have taken for existing both some items that are already built (*e.g.* the TRD gas system) as well as some items that are anticipated to be built for the Tevatron Kaon program, E799/832 (*e.g.* part of the EM calorimeter).

These assumptions and the cost bases are made clear in the references to the following Table 6.5.1 which gives the estimated detector costs. We have benefited from the experience and effort of Stephen Pordes in preparing this Table.

Table 6.5.1: Estimate of KAMI Detector Costs

Detector	Element	Unit	Cost/ Unit [$]	Ref	# of Units	Total Cost [K$]	Exist [K$]	New [K$]
Wire Chambers								
	2m × 3m 5mm cell drift chambers	chamber	15,000	1	5	75		75
	amp/disc	channel	12	2	10,000	120		120
	0.5 ns TDCs	channel	50	3	10,000	500		500
	trigger processor	system	400,000	4	1	400	100	300
	cables	16 channels	50	5	625	32		32
	crate/cntrlr	crate	10,000	6	5	50		50
	stands	chamber	2,000	1	5	10		10
	gas system	system	20,000	1	1	20		20
	LVPS	each	1,000	38	10	10		10
	HVPS	per pair	800	39	10	8		8
Subtotal						1,225	100	1,125
EM Calorimeter								
	CsI, $3.6 \times 3.6 \times 45 cm^3$	channel	1000	7	7,000	7,000	4,000	3,000
	PMTs, bases	channel	200	8	7,000	1,400	800	600
	ADCs, 15 bit eq.	channel	45	9	7,000	315	170	145
	8 bit flash ADCs 4 samples	channel	30	10	7,000	210	120	90
	1 ns TDCs	channel	50	3	7,000	350	200	150
	crate/cntlr	crate	10,000	6	10	100	70	30
	trig. processor	system	1,500,000	11	1	1,500	850	650
	delay cables	channel	108	12	7,000	756	432	324

Detector	Element	Unit	Cost/ Unit [$]	Ref	# of Units	Total Cost [K$]	Exist [K$]	New [K$]
	trig. cables	channel	10	13	7,000	70	40	30
	HV supplies	256 ch.	25,000	14	28	700	400	300
	HV cables	channel	12	15	7,000	84	48	36
	Monitor fibers	bundle	1,000	1	310	310	180	130
	Monitor laser	unit	8,000	1	1	8	8	-
	Monitor hardware	unit	7,000	1	1	7	4	3
	Climate control & support	system	20,000	16	1	20	20	
Subtotal						12,830	7,342	5,488
TRDs								
	modules	tube	3	17	40,000	120		120
	amp/disc.	channel	12	2	40,000	480		480
	latches	channel	30	18	8,000	240		240
	cables	16 channels	50	5	2,500	125		125
	supports	module	500	1	30	15		15
	crates	unit	10,000	6	4	40		40
	gas system	system	50,000	19	1	50	40	10
	LVPS	each	1,000	38	40	40		40
	HVPS	per pair	800	39	20	16		16
Subtotal						1,126	40	1,086
Veto Systems								
	Scintillator	kg	88	20	3,200	282	150	132
	Scint. fibers	m	0.5	21	44,000	22	12	10
	Lead sheet	tonne	2,000	21	74	148	55	93
	PMTs, bases	unit	300	21	1250	375	155	220
	Regenerator system	unit	267,000	22	1	260	210	50

Detector	Element	Unit	Cost/ Unit [$]	Ref	# of Units	Total Cost [K$]	Exist [K$]	New [K$]
	HV supplies	256 channels	25,000	14	5	125	100	25
	discrim.	channel	12	2	1250	15	6	9
	latches	channel	30	23	1250	38	16	22
	ADCs	channel	50	9	1250	63	27	36
	1ns TDCs	channel	50	3	1250	63	27	36
	signal cables	channel	20	27	1250	25	11	14
	HV cables	channel	12	15	1250	15	6	9
	crate/cntrlr	unit	10,000	6	4	40	20	20
	stands	unit	2,000	24	4	8		8
	vacuum tank	module	5,000	24	10	50	50	
	mech. supports	module	10,000	21	14	140	110	30
Subtotal						1,669	955	714
Muon System								
	drift tubes	unit	3	17	40,000	120		120
	amp/disc	unit	12	2	40,000	480		480
	latches	channel	30	18	5,000	150		150
	cables	16 channels	50	5	312	15		15
	LVPS	each	1,000	38	40	40		40
	HVPS	per pair	800	39	20	16		16
	5×2×250 scintillator	cm^2 2 cm thick	0.18	25	1.625×10^6	285		285
	PMTs,bases	unit	150	26	1300	195		195
	HV supplies	256 channel	25,000	14	6	150		150
	ADCs	channel	50	9	650	32.5		32.5
	signal cables	channel	20	27	1300	26		26
	HV cables	channel	12	15	1300	15.6		15.6
	Mean timers	channel	50	28	350	17.5		17.5
	crate/cntrlr	unit	10,000	6	3	30		30
	Stands	plane	100	1	20	2		2

Detector	Element	Unit	Cost/ Unit [$]	Ref	# of Units	Total Cost [K$]	Exist [K$]	New [K$]
	Steel	ton	500	40	1500	750		750
	Gas system	system	1,000	1	1	1		1
Subtotal						**2,326**		**2,326**
Scintillator Trigger								
	1cm × 5cm × 2m scintillator	cm^2 1cm thick	0.15	25	2.5×10^5	38		38
	PMTs/Bases	unit	400	29	250	100		100
	HV supplies	256 channels	25,000	14	1	25		25
	signal cables	unit	20	27	250	5		5
	delay cables	unit	55	30	250	13.8		13.8
	HV cables	unit	12	15	250	2.5		2.5
	ADCs	unit	50	9	250	12.5		12.5
	Discriminator	16 channels	1,700	41	16	27		27
Subtotal						**224**		**224**
Trigger								
	crates	unit	2,000	31	2	4		4
	modules	unit	2,000	32	40	80		80
	cables	unit	10	33	80	0.8		0.8
Subtotal						**85**		**85**
DAQ								
	40 MIPS processors	unit	10,000	34	50	500		500
	exabyte drives	unit	2,000	35	50	100		100
	disks	unit	1,500	36	50	75		75
	networking, software,racks	system		37		125		125

Detector	Element	Unit	Cost/ Unit [$]	Ref	# of Units	Total Cost [K$]	Exist [K$]	New [K$]
Subtotal						800		800
Total						20,285	8,437	11,848

1 Based upon experience in E731.

2 Nanometric Amp/Disc N-277.

3 Cost based on LRS 1879 96 channel Fastbus TDC.

4 Modification and expansion of the E773 track processor constructed at the University of Chicago.

5 50' of 17 pair twist'n flat with 3M cable ends.

6 Fastbus crate, Fermilab F.S.C.C.

7 Based upon preliminary discussions with suppliers and with prices quoted to other experiments. It is assumed that a major part of the calorimeter is in place for the 1994 Fixed Target run.

8 Preliminary estimate of low-gain 6 stage 1 1/8" phototube/base combination.

9 LRS 1885 96 channel Fastbus ADC.

10 100 ns samples are sufficient so that bandwidth is not critical.

11 Based upon the costs of the E731 cluster finder constructed at the University of Chicago.

12 Delay cables are 150' of double shielded coax with BNC connectors (RG214) @ $0.72/ft.

13 Trigger cables are short lemo cables used to connect trigger logic.

14 LRS 1440 256 channel supply.

15 2 SHV connectors and 30' RG-58 cables commercially assembled.

16 From experience; cost is high because of climate control.

17 Straw tubes can cost between $0.50 and $10.00 per tube, depending upon wall thickness. The cost of the complex gas manifold is included.

18 Nanometric Latch N-278. Ganged readout in groups of 5 deep.

19 Based on cost of Xenon recirculating system built for E773/E799.

20 Based on quotation from Kuraray International Corporation.

21 Based on costs from construction of E799 preconverter at UCLA.

22 Assumes reuse of P832 regenerator system; new cost is for modifications.

23 Nanometric Latch N-278.

[24] Extrapolated from E731 veto counter mounting experience.

[25] Based upon the cost of Bicron scintillator for E-711 calorimeter (50% of single sheet cost).

[26] Using a 10 stage PMT.

[27] 200' of RG-58 with BNC connectors.

[28] Guess for this item.

[29] 12-stage PMT.

[30] 200' RG-8 with BNC connectors, assembled commercially.

[31] A guess that final trigger logic will take 2 CAMAC crates.

[32] Typical CAMAC module cost.

[33] Two ribbon cables per module.

[34] Assumes a reduction of 50% on present prices.

[35] Current cost of this 8 mm drive.

[36] Current cost of 600 mb disks.

[37] Estimate by I. Gaines.

[38] 100 amp Lambda Power Supply.

[39] Fermilab standard chamber high voltage power supply.

[40] Cost of steel.

[41] LRS Camac disc.

6.6 Cost Estimate Summary

We here compile the estimated cost totals for the major subsystems in the KAMI facility together with allocations for EDIA and contingencies. Table 6.6.1 includes items which are needed for the KAMI program only, while Table 6.6.2 contains those items which are common to KAMI and Tevatron kaon physics program (E799/832). In Table 6.6.3 we show the combined cost estimates. We calculate EDIA (15%) and contingency (20%) for all capital costs.

Table 6.6.1: Cost Estimate Summary for Items Needed Only for the KAMI Program

Item	Cost Estimate		EDIA	Contingency	Total
	Capital ($M)	Operating (5 year) ($M)	($M)	($M)	($M)
Civil Construction	0.28		0.04	0.06	0.38
Primary Beam	1.50		0.23	0.30	2.03
Secondary Beam	4.28	1.32	0.64	0.86	7.10
Analysis Magnet	0.13	0.65	0.02	0.03	0.83
Detector Systems	11.85		1.78	2.37	16.00
Total	18.04	1.97	2.71	3.62	26.34

Table 6.6.2: Cost Estimate Summary for Tevatron Program Items which are also Needed for the KAMI Project.

Item	Cost Estimate		EDIA	Contingency	Total
	Capital ($M)	Operating (5 year) ($M)	($M)	($M)	($M)
Civil Construction	1.90		0.28	0.38	2.56
Primary Beam	0.06		0.01	0.01	0.08
Secondary Beam					
Analysis Magnet					
Detector Systems	8.44		1.27	1.69	11.40
Total	10.40		1.56	2.08	14.04

Table 6.6.3: Combined KAMI Cost Estimate Summary

Item	Cost Estimate		EDIA	Contingency	Total
	Capital ($M)	Operating (5 year) ($M)	($M)	($M)	($M)
Civil Construction	2.18		0.32	0.44	2.94
Primary Beam	1.56		0.24	0.31	2.11
Secondary Beam	4.28	1.32	0.64	0.86	7.10
Analysis Magnet	0.13	0.65	0.02	0.03	0.83
Detector Systems	20.29		3.05	4.06	27.40
Total	28.44	1.97	4.27	5.70	40.38

The total cost would be somewhat greater if the CCM is not available for KAMI. In this case the capital costs would be about $8 M greater to cover the construction of the two new analysis magnets.

Labor costs for activities like fabrication and assembly have been included in many, but not all, of the estimates (*e.g.*, civil construction, secondary beam magnets, production target, and analysis magnets). Engineering and design costs have generally not been included beyond the blanket EDIA allowance. A systematic analysis of manpower needs and resources is presently under way.

7. SCHEDULING

In this section we consider the timing of the construction of the facility together with the detector. For the most part, this will be limited by the available funding.

We assume that the Main Injector's funding will begin in FY92 and that it's profile will extend over a period of four years, *i.e.* stretched out about one year longer than originally planned. Thus, we would expect that we could begin data taking in early 1996.

For the purpose of drafting a definite scenario, we also assume the following concerning the physics to be addressed in each run.

1. In the 1994 fixed-target run at the Tevatron, E799/832 (rare decays and ε'/ε) will be executed. These measurements will be made in the new detector hall and beam line and with the required new equipment. It is assumed for the cost estimates that the experiments are sited in the NMUON area.

2. For the first 1.5 yrs. of operation, the physics focus of the KAMI program will be on a further measurement of ε'/ε (high precision).

3. For the next 1.5 yrs. of operation, the physics focus will be on rare decays (high rate).

4. For the next 1.5 yrs. of operation, the physics focus will be on the $\pi^0\nu\bar{\nu}$ experiment (hermetic).

5. For the next 1.5 yrs. of operation, the physics focus will be on K_S decays.

Clearly the actual sequencing of runs can, and probably will, be modified in response to the nature of our results and the general development of the field.

We consider that this scenario adequately provides for realization of the KAMI program's exciting physics potential including allowance for the impact of demands from the NUMI program and Tevatron operation. A wide variety of practical beam sharing modes will be available as discussed in Section 4.4.1. In Section 1, we assumed a conservative 35% operating efficiency when defining a data taking year; NUMI has been similarly conservative. Here, in addition, we have allowed 1.5 calendar years for each KAMI data taking year. Together these ensure that we are not "double-counting" Main Injector protons.

In the following table, we show the estimated year-by-year funding needed for this program. Indicated separately are over-lapping costs associated with the E799/832 Tevatron program. Costs of detector elements which are not needed on "day 1" have been assigned to the later fiscal years.

We note first that items which are assigned to the Tevatron program are clearly needed for E799/832 and the funding profile reflects this need. The costs assigned to E799/832 are not meant to be inclusive: a complete analysis of the requirements for E799/832 is currently being prepared. However, it is possible that some of the components assigned exclusively to the KAMI project (*e.g.*, the beam dump magnet) would be of use in the Tevatron program if funding could be available early enough.

All of the costs shown include EDIA and contingency as discussed in Section 6.6 and are in $M FY90.

8. RESEARCH and DEVELOPMENT

In order to meet the goal of starting to do physics as soon as beam is available from the Main Injector, a number of areas must receive immediate and on-going research and development support. Here we summarize and reemphasize a number of these.

Of course, to develop detailed plans for siting and staging, the programmatic choice of location of the KAMI facility must be made. This should be made with the Tevatron program in mind in order to make the best possible use of resources that may be common to both programs.

Some specific areas that require continuing and/or new efforts are discussed briefly below. To carry out these projects, the on-going participation of people from Fermilab as well as other institutions will be required. Financial support for prototyping and technical support will also be required in the near term. Longer range planning for the R&D effort is under way.

8.1 Primary Beam

The detailed design of the primary beam in such a way as to prevent a muon halo buildup is critical. The μ/p ratio must be kept less than 1.0×10^{-7}: hopefully much less!

The positional stability of the proton beam on target is a critical issue for the ε'/ε experiment. Techniques must be developed to control the beam position to the required accuracy. Instrumentation to monitor the beam position must also be developed. See Sections 4.1.5 and 4.1.7.

8.2 Target Area

More design effort is required to understand the radiation dose the target and dump magnets will receive, how modifications of the design might make dealing with these problems easier, and how to build coils with minimal sensitivity to radiation damage.

Target cooling investigations must be performed to ensure reliable operation and positional stability.

In light of heightened EH&S concerns, a continuing study of radiation safety issues is essential as the KAMI design matures. Preliminary simulations of the muon flux in the NMUON counting room area performed with CASIM predict a radiation dose of about 1 mrem per hour. More detailed shielding studies are now underway. Systematic projections for site boundary levels, personnel area levels and air activation will be required at each stage of design development. Shielding requirements for the primary beam must be specified in greater detail. A procedure for extracting and storing highly radioactive beam dump inserts must be developed.

8.3 Spectrometer Magnets

The design presented for the conventional magnets is still preliminary. As discussed in Section 4.3, there is still considerable room for optimization of the design vis-a-vis the cost. In addition, other configurations of the magnet are under consideration.

Fundamental to the magnet design is of course the momentum measurement. In order to know the mean momentum to the order of 0.03%, it will be necessary to know the field (integrals) to 0.01% or better. This requires both a measurement of B to that accuracy, and a measurement of where the field is measured so that dB/dx * (error in x) is also less than

0.01%. Improvements in the magnet measurement techniques that allow for measurements to these accuracies may be used as a basis for reducing the requirements on field uniformity and thus on magnet cost. Track position measurement must of course also be made to the same accuracy.

8.4 Detector R&D

The KAMI program aggressively challenges the current state of detector technology. The problem of doing precision sensitive experiments in a high rate environment will provide a challenge to the experimenters. A number of items in particular require prototyping and and testing in order to assure excellent detector performance when the beam is available.

8.4.1 Vacuum and Veto System

For the $K_L \rightarrow \pi^0 \nu\bar{\nu}$ experiment, the vacuum and veto requirements are particularly demanding. Much has been learned about the vacuum system requirements. Additional studies are under way to understand outgassing rates and to better understand the pumping requirements. More needs to be done. As outgassing rates are understood and controlled, for example, the pumping needs and therefore costs of the system may be reduced. Also, the radiation hardness of the possible window materials needs to be determined.

The hermetic veto system that must work inside the vacuum system needs continuing design work as well as prototyping. At the level of veto efficiency required, calculations are not enough! Operational experience with the veto system for the earlier experiments will be crucial in developing a final design. The impact of the ultimate veto system on the vacuum system will need reevaluation when a full design is available.

8.4.2 Tracking Chambers

The current sensitivities are limited by the estimated rate handling limits of the drift chambers. It is therefore important to confirm that the large chambers contemplated in fact work at the rates quoted.

Even better, if it is possible to run at higher K decay rates, the neutral beam can be opened up for the rare decay modes and even lower branching ratios may be probed.

8.4.3 TRD

Large TRDs of the type discussed in Section 5.3.1 have in fact not yet been run in an experiment. It is therefore important that a prototype of this type of TRD be built and run as soon as possible. It is particularly important to understand possible correlations between misidentifications made by the TRD and EM calorimeter in determining the presence of an electron.

8.4.4 Electromagnetic Calorimetry

Work is under way to better understand CsI and BaF_2 crystals. This effort must continue. The construction of larger subsystems to confirm the resolution as a function of energy, and to understand more clearly effects related to radiation damage and "curing" has begun. See Sections 5.2 and 5.7.3.

8.4.5 DAQ

This is a very dynamic field. The choices available commercially are large; and growing in both the areas of computation and in data storage. It therefore seems appropriate to 'keep one's options open' as long as possible.

On the other hand, the front end problems are formidable! Large amounts of data must be moved and stored very quickly. It will therefore be necessary to start on the design of the front end very soon. It would be preferable to use as much of the DAQ system as possible in evaluating prototypes of the detectors (see above). The system integration at this level is also very important. The problems associated with very high speed busses to move the data from the detector to the first level of storage need design efforts with goals of reliability and low cost but yet very high band-widths.

A time frame in which decisions must be made should be established. As noted above, one would like to keep the options open as long as possible to make as much use as possible of improving technology and falling prices (per unit of through-put). It must also be kept in mind that the DAQ system must interface with the rest of the experiment and decisions critical to the overall system must not be delayed. Of course there must be time for the development and testing of software to go with the DAQ system. If there is any possibility of using 'non-standard' components, the lead time for learning to interface and use those non-standard components may be quite long.

9. SUMMARY

In this report we have envisioned an exciting series of neutral kaon experiments made possible by the unique combination of energy, intensity, and time structure which characterize the slow extracted beam from the Fermilab Main Injector. The greater levels of precision in probing CP violation (ε'/ε, $K_L \rightarrow \pi^0 e^+ e^-$, $K_L \rightarrow \pi^0 \nu\bar{\nu}$, $K_S \rightarrow \pi^0 e^+ e^-$) and of sensitivity in testing lepton flavour conservation ($K_L \rightarrow \mu e$, $K_L \rightarrow \pi^0 \mu e$) achievable in these experiments will provide stringent tests of the Standard Model and important windows on potential new physics. These experiments will contribute greatly to the vitality of the Fermilab physics program during the second half of this decade.

If programmatic considerations permit maximum use of pre-existing facilities and equipment, including items to be used in the next generation of Tevatron kaon experiments (E799/832), the Total Project Cost (TPC) is estimated to be $26.34 M. This TPC includes a Total Estimated Cost (TEC) of $20.01 M plus $6.33 M for EDIA and contingency. Including the overlapping costs from the Tevatron kaon physics program yields a TEC of $30.41 M and a TPC of $40.38 M. (Note that the TEC and TPC include $1.97 M for 5-year operating costs of major secondary beam systems and the Chicago Cyclotron Magnet.) If the Chicago Cyclotron Magnet is not available for KAMI, and it is necessary to construct new analyzing magnets, an additional capital cost of up to $8 M would be incurred.

Our analyses indicate that these experiments, while challenging, can be carried out with a combination of current technology and reasonable extrapolations thereon. The schedule developed in this report is aimed at being ready to start work on physics as soon as the Main Injector can deliver beam. In this connection, we have also sought to identify those areas in which further investigation and design need to go forward in a timely fashion.

APPENDIX A: CHARGED KAONS at KAMI

The primary focus of the KAMI group at Fermilab is the physics of neutral kaons. This conceptual design report details the possible evolution of a program of neutral kaon experiments lasting into the next decade. It is recognized, however, that experiments of interest in the distant future cannot be predicted with certainty, as they depend on the results obtained by experiments in the intervening years. One possible future direction for the program is experiments with charged kaons. While this subject has not been examined in any detail by the KAMI group, we have designed the neutral beam so that at least one charged beam option is available as a simple modification of the neutral beam elements. In this appendix we provide a brief overview of some of the currently interesting topics in charged kaon physics, describe the modifications necessary to convert the neutral beam into a charged beam, and specify the first order properties of this charged beam. We emphasize that no attempt has been made to actually design charged kaon experiments at this point.

A.1 KAMI Charged Kaon Beam

In order to convert the KAMI neutral beam into a charged beam, two modifications are required. The first is to replace the tapered neutral beam-defining channel in the target sweeping magnet with a curved channel. The technique of using a curved "hyperon channel" in a high field magnet to produce a charged beam in a short distance has been used at Fermilab before.[1] Figure A.1 shows the basic geometry of such a beam.

---

[1] FERMILAB TM-964, "Design For a Short Charged Secondary Beam," Thomas R. Cardello, 1 March, 1980.

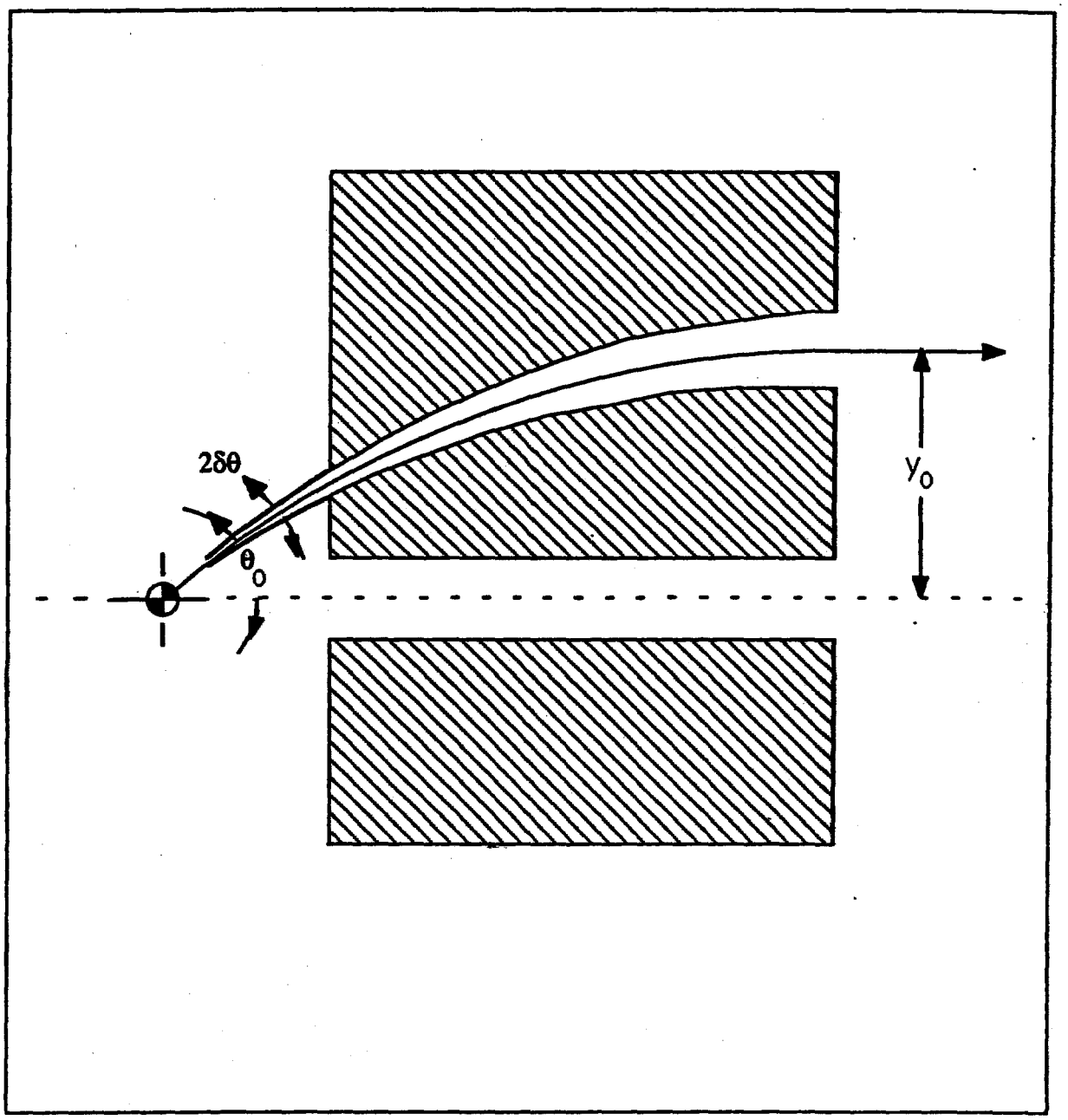

Figure A.1: Basic geometry of the curved channel for a KAMI charged beam.

The second modification is to the beam dump magnet. In the standard mode, the neutral beam passes above the beam dump through a region of high field. For charged beam applications, the sweeping field of the beam dump magnet would deflect the beam. In order to remedy this problem, the Pb spacers that fill the magnet gap to the left and right of the neutral beam (see Fig. 4.2.11) would be replaced by iron, effectively shorting out the magnetic field in the beam region while preserving the muon sweeping field in the beam dump region. This will only work if the iron is not driven into saturation, so the sweeping field is less than for the neutral beam case. The muon flux on the detector in this configuration has been estimated using CASIM to be about 3×10^{-5} per incident proton. This may limit the proton flux on target to the 10^{12} range, but substantial kaon fluxes are still available.

In order to estimate the particle yield for the beam we make the approximation that

$$\text{yield} = \int dp \int d\Omega \frac{d^2N}{dpd\Omega} \cong \frac{d^2N}{dpd\Omega}(p_0,\theta_0)\,\Delta p\Delta\Omega$$

where we use the Malensek parameterization for $d^2N/dpd\Omega(p_0,\theta_0)$. The transmission phase space, $\Delta p\Delta\Omega$, is given by

$$\Delta p\Delta\Omega = 16\ p_t\delta\theta_x(\delta\theta_y/\theta_0)^2.$$

Using these approximations, Fig. A.2 shows the kaon and pion rates and the rate of kaon decays in the decay volume for a curved channel which has a 28% momentum bite, at a 20 mrad production angle. The plot is normalized to the maximum proton intensity, 3×10^{13} protons per second. The momentum bite is chosen to be the largest that would allow the charged beam to pass through the normal beam holes in the calorimeter.

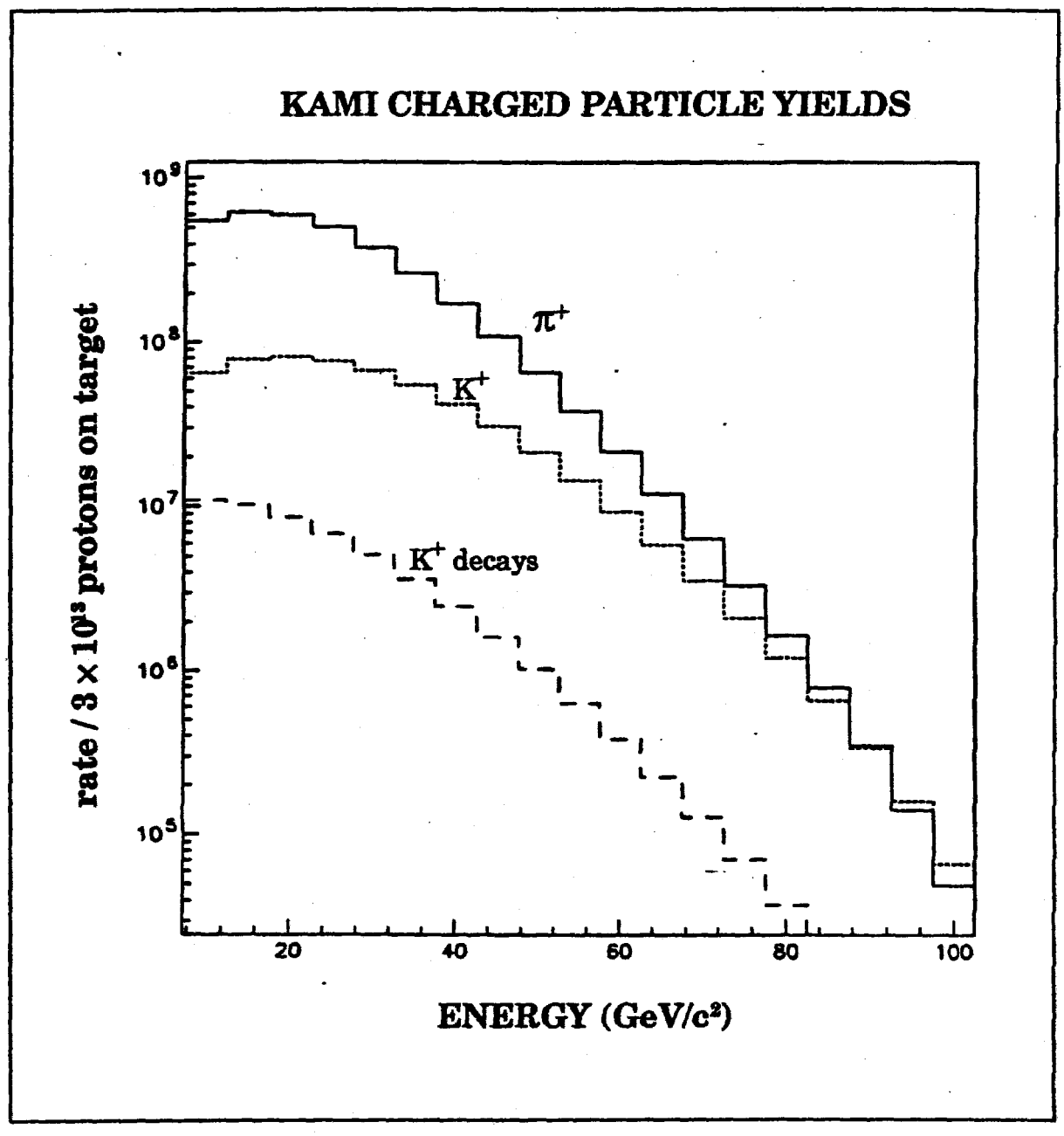

Figure A.2: KAMI charged beam fluxes.

A.2 Charged Kaon Physics and Sensitivity

As in the neutral beam case, there are two classes of experiments that might be done with the KAMI high flux charged kaon beam, rare decays and high precision measurements. Among the many possible rare decays, we consider two important examples: $K^+ \rightarrow \pi^+ +$ "nothing" and $K^+ \rightarrow \pi^+\mu^+e^-$. As an example high precision measurement, we consider a difference in the slope parameters of $K^+ \rightarrow \pi^+\pi^+\pi^-$ and $K^- \rightarrow \pi^-\pi^-\pi^+$, which would be a signature of direct CP violation.

A.2.1 Search for $K^+ \rightarrow \pi^+ +$ "nothing"

Within the Standard Model, $K^+ \rightarrow \pi^+ +$ "nothing" proceeds through the second order weak interaction since first order is suppressed by the GIM mechanism. This reaction is a clean test of the theory because the neutrino pair ("nothing") does not couple to the photon. Estimates of the branching ratio using recent constraints on the KM angles and on the top quark mass give a range of 1 to 4×10^{-10} for three neutrino families. It is important to notice that this decay is virtually free of the hadronic-related theoretical uncertainties. Thus, if the top mass is known, then the KM matrix element $|V_{td}|$ could be determined unambiguously. Any deviation from the Standard Model prediction would therefore signal new physics. Note that the physics addressed here is quite different from that involved in the analogous neutral decay (see Section 1).

The current best branching ratio limit ($< 5 \times 10^{-9}$) comes from BNL. KAMI offers the intensity for orders of magnitude improvement in statistics. Some background studies have already been done and published in the Main Injector Workshop Proceedings.

A.2.2 Search for and $K^+ \rightarrow \pi^+ \mu^+ e^-$

This decay is forbidden in the Standard Model and thus is sensitive to new physics. If the ultimate unified theory includes a heavy neutral flavor changing boson ϕ, then a sensitivity of 10^{-12} probes a mass m_ϕ well beyond the SSC:

$$BR(K^+ \rightarrow \pi^+ \mu^+ e^-) = 10^{-12} (150 \text{ TeV}/m_\phi)^4 (g_\phi/g_W)^4.$$

Such flavor violations probe the weak points of the Standard Model, *i.e.* the nature of symmetry breaking and the origin of family structure. The potential sensitivity is available to make a meaningful contribution or perhaps a major discovery. The current best limit ($<2.1 \times 10^{-11}$) comes from the last round of BNL experiments. The high flux of KAMI could make a significant improvement in statistics. The background will need more detailed study, but it seems that with the advantages of full kinematic constraint and enough particle identification in the detector, a sensitivity below 10^{-12} could be within reach.

A.2.3 Direct CP violation in $K^+ \rightarrow \pi^+ \pi^+ \pi^-$ and $K^- \rightarrow \pi^- \pi^- \pi^+$

Measurement of ε' through neutral kaon 2π decay is not the only way to probe direct CP violation. Another method is to compare the decay of K^+ and K^- into three charged pions. If CP commutes with the weak Hamiltonian, then both decays are identical. With just CPT invariance, however, the decays may be different because final state strong interactions couple to the modes $K^+ \rightarrow \pi^+ \pi^0 \pi^0$ and $K^- \rightarrow \pi^+ \pi^0 \pi^0$. In the three body decays, CP violation can cause a difference in the density of the Dalitz plots. If $a^+(a^-)$ is the slope parameter describing the density variation across the Dalitz plot for the $K^+(K^-)$ decay, then a nonzero value for $d=(a^+-a^-)/(a^++a^-)$ provides a signature for direct CP violation. Within the Standard Model, $|d|$ could be as small as 5 $|\varepsilon'|$. Previous measurements (Particle Data Group) made in the 70's yield $a^+ = -0.2154 \pm 0.0035$, and $a^- = -0.217 \pm 0.007$. These errors are statistically dominated by a total of three million observed decays, and could be improved enormously. Statistics would not be the limiting factor in making such a measurement at KAMI.